# HIGHWAY RESEARCH RECORD

## Number 103

# Bridges and Structures

## 8 Reports

Presented at the
44th ANNUAL MEETING
January 11-15, 1965

SUBJECT CLASSIFICATION
27 Bridge Design

HIGHWAY RESEARCH BOARD
of the
Division of Engineering and Industrial Research
National Academy of Sciences—National Research Council
Washington, D. C.
1965

# *Department of Design*

W. B. Drake, Chairman
Assistant State Highway Engineer, Kentucky Department of Highways
Lexington

## BRIDGE DIVISION

J. N. Clary, Chairman
Bridge Engineer, Virginia Department of Highways
Richmond

## COMMITTEE ON BRIDGE DESIGN

(As of December 31, 1964)

Vernon J. Burns, Chairman
Deputy Chief Engineer (Design)
New York State Department of Public Works
Albany

W. C. Anderson, Chief, Research and Development Engineer, The Union Metal Manufacturing Company, Canton, Ohio
Arthur L. Elliott, Bridge Engineer, California Division of Highways, Sacramento
T. R. Higgins, Director of Engineering and Research, American Institute of Steel Construction, New York, New York
John J. Hogan, Consulting Structural Engineer, Portland Cement Association, New York, New York
Nelson C. Jones, Engineer of Bridge and Road Design, Michigan State Highway Department, Lansing
Adrian Pauw, Professor of Civil Engineering, University of Missouri, Columbia
Sidney L. Poleynard, Bridge Design Engineer, Louisiana Department of Highways, Baton Rouge
Charles F. Scheffey, Chief, Structural Division, Office of Research and Development, U. S. Bureau of Public Roads, Washington, D. C.
C. P. Siess, Professor of Civil Engineering, University of Illinois, Urbana
J. R. Stemler, Manager, Highway Products and Structural Section, Sales Development Division, Aluminum Company of America, New Kensington, Pennsylvania
Ivan M. Viest, Structural Engineer, Sales Engineering Division, Bethlehem Steel Corporation, Bethlehem, Pennsylvania
H. N. Wilcox, Bridge Engineer, Bridge Division, Office of Engineering, U. S. Bureau of Public Roads, Washington, D. C.

## COMMITTEE ON STEEL SUPERSTRUCTURES

(As of December 31, 1964)

M. N. Quade, Chairman
Consulting Engineer, Parsons, Brinckerhoff, Quade and Douglas
New York, New York

Frederick H. Dill, Assistant to Vice President, Engineering, American Bridge Division, Pittsburgh, Pennsylvania
Arthur L. Elliott, Bridge Engineer, California Division of Highways, Sacramento
Carl H. Gronquist, Partner, Steinman, Boynton, Gronquist and London, New York, New York

T. R. Higgins, Director of Engineering and Research, American Institute of Steel Construction, New York, New York
William H. Munse, Jr., Department of Civil Engineering, University of Illinois, Urbana
Sidney L. Poleynard, Bridge Design Engineer, Louisiana Department of Highways, Baton Rouge
A. A. Toprac, Professor of Civil Engineering, University of Texas, Austin
Ivan M. Viest, Structural Engineer, Sales Engineering Division, Bethlehem Steel Corporation, Bethlehem, Pennsylvania

## COMMITTEE ON CONCRETE SUPERSTRUCTURES

(As of December 31, 1964)

W. E. Baumann, Chairman
Engineer of Bridge and Traffic Structures
Illinois Division of Highways
Springfield

Raymond Archibald, Otis, Oregon
James W. Baldwin, Associate Professor of Civil Engineering, University of Missouri, Columbia
Carl E. Ekberg, Head, Department of Civil Engineering, Iowa State University, Ames
E. S. Elcock, Bridge Engineer, State Highway Commission of Kansas, Topeka
Phil M. Ferguson, Department of Civil Engineering, University of Texas, Austin
R. S. Fountain, United States Steel Corporation, Pittsburgh, Pennsylvania
John J. Hogan, Consulting Structural Engineer, Portland Cement Association, New York, New York
C. L. Hulsbos, Professor of Civil Engineering, Fritz Engineering Laboratory, Lehigh University, Bethlehem, Pennsylvania
T. W. Jennings, Assistant State Highway Engineer (Structures), Florida State Road Department, Tallahassee
W. T. Robertson, Bridge Design Engineer, Washington Department of Highways, Olympia

## COMMITTEE ON FIELD TESTING OF BRIDGES

(As of December 31, 1964)

LeRoy T. Oehler, Chairman
Supervisor, Physical Research Section
Research Laboratory Division, Michigan State Highway Department
Lansing

Vernon J. Burns, Deputy Chief Engineer (Design), New York State Department of Public Works, Albany
J. M. Hayes, Professor of Structural Engineering, School of Civil Engineering, Purdue University, Lafayette, Indiana
J. J. Kozak, Supervising Bridge Engineer - Special Studies, California Division of Highways, Sacramento
W. H. Munse, Jr., Department of Civil Engineering, University of Illinois, Urbana
C. P. Siess, Professor of Civil Engineering, University of Illinois, Urbana
Robert F. Varney, Bridge Engineer, Bridge Research Branch, Structural Research Division, Office of Research and Development, U. S. Bureau of Public Roads, Washington, D. C.
Ivan M. Viest, Structural Engineer, Sales Engineering Division, Bethlehem Steel Corporation, Bethlehem, Pennsylvania

# Foreword

The eight papers in this Record offer the reader with an interest in the design of highway structures some interesting new concepts and information.

The first paper reports on research concerning the use of non-solid sign backgrounds as a means of diminishing wind forces on large signs and lowering the structural requirements of the signs' support structures. Among other things, it was found that certain louvered plates greatly reduce wind effect and, with proper mounting, do not appreciably reduce visibility.

Another paper outlines, on the basis of tests for thermal stresses in a composite highway bridge in Virginia, a simple formula which may find application in future standard design procedures. The formula relates thermal stress at the bottom of the girder to temperature difference between top and bottom of the slab and the depth of the floor system.

Fatigue testing of prestressed concrete I-beams was studied at Lehigh University to determine the load-deflection response after the initial cracking of the concrete. The third paper discusses the results and indicates that the fatigue of the web reinforcement was more critical than the fatigue of the prestressing strands.

An experimental study of the influence of substructure designs on the dynamic load responses in composite steel-and-concrete bridge decks is reported on in another paper. The results indicate that superstructure vibrations can be meliorated to some extent by the use of more rigid substructure. In such cases, heavy bulky piers would be favored over the weaker, more slender piers.

Composite steel-and-concrete bridge deck units made with inverted steel T-beams were prefabricated and tested at the University of Texas to evaluate the resistance of such floors to punching shear failure under highway loadings. The results are reported on in this Record, as are the findings of an investigation of the fatigue strength of stud shear connectors. The results of the latter study are compared with AASHO standard allowable stress values and the author suggests that the factors of safety required by AASHO might be revised and liberalized.

Another paper reports on tests of stud shear connectors in composite girders. The author concludes that design of welded stud shear connectors can be based on the range of stress in fatigue.

The final paper in this Record presents the results of structural analysis of arch-type bridge trusses with inclined hangers. The authors explain their "deformation method" of analysis and a computer program for use in the design of a Langer girder bridge.

# Contents

# Wind Tunnel Investigation of Nonsolid Sign Backgrounds

DANNY R. TIDWELL and CHARLES H. SAMSON, JR.,
Texas Transportation Institute, Texas A and M University

The needs of modern highway systems dictate large sign backgrounds to convey essential information to the motorist. Large signs mean high wind loadings, which in turn lead to large and relatively massive support structures. A feasibility study was made of six types of nonsolid backgrounds, with a solid background as control. Specimens, 2 by 1.5 ft, were tested at 50, 75, and 100 mph in a 7- by 10-ft subsonic wind tunnel at angles of wind incidence (rotation about vertical axis) of 15, 30, 45, 60, 75, and 90 deg. Results indicate that a louvered background offers promise from the standpoints of reduction of wind loadings and of satisfactory visibility characteristics.

•THE PURPOSE of this research was to investigate the feasibility of using nonsolid sign backgrounds. Large sign backgrounds are often required on modern highway systems to convey essential information to the motorist. Large sign backgrounds result in high wind loadings which, in turn, lead to relatively large sign-support structures. With increased size, sign-support structures generally present greater collision hazards to the motorist.

It is emphasized that only six selected nonsolid backgrounds were considered. It was not intended to make an exhaustive study, but rather to determine if nonsolid backgrounds offer the possibility of producing a substantial reduction in wind loads on the sign structures.

## TESTING FACILITIES

The 7- by 10-ft subsonic wind tunnel at Texas A and M University was used in the experimental work. Figure 1 shows an external view of the wind tunnel. Specimens were tested at velocities of 50, 75, and 100 mph. They were oriented at angles of incidence (rotation about vertical axis) of 0, 15, 30, 45, 60, 75, and 90 deg with respect to the direction of wind in the tunnel. Figure 2 is a drawing of a test specimen subjected to the wind force. The side, normal, and lift forces are components of the wind force. The moment refers to the twisting moment about the vertical axis.

Figure 3 shows one of the test specimens mounted in the tunnel. The method of mounting the sign on X-bracing may be seen.

## TEST SPECIMENS

All specimens were 2.0 ft wide and 1.5 ft high. Sign backgrounds investigated were the following:

1. Solid plate (100 percent solid)[a]—used as a basis of comparison for other specimens, of 0.081-in. thick aluminum (Fig. 4).

[a]The term percent solid as used here refers to the percentage of solidity as viewed along a normal to the plane of the sign.

Paper sponsored by Committee on Bridge Design.

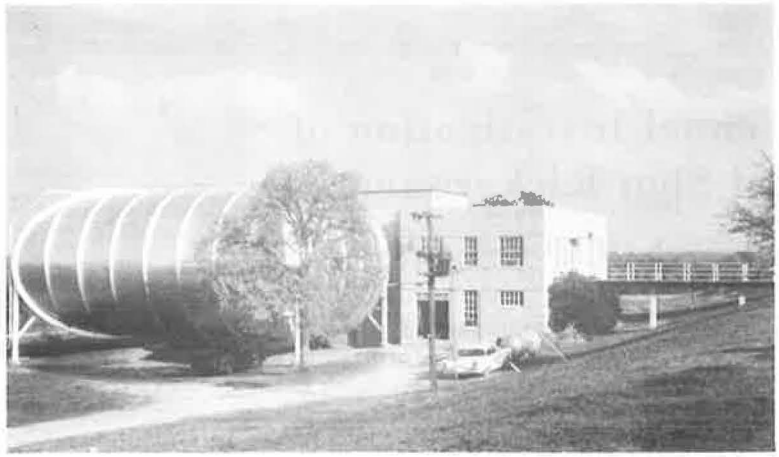

Figure 1. Wind tunnel facility.

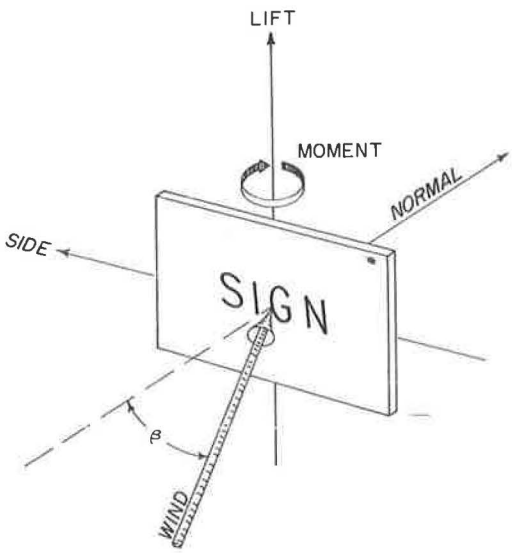


Figure 2. Forces acting on sign.

Figure 3. Test specimen mounted in wind tunnel.

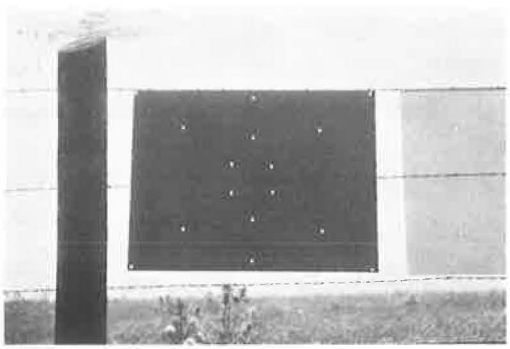

Figure 4. Solid plate, 100 percent solid.

2. Perforated plate (62.5 percent solid)—0.031-in. thick steel with 32.3 holes/sq in., each hole 0.125 in. in diameter (Fig. 5).

3. Perforated plate (93.8 percent solid)—0.250-in. thick fiberboard plate with 1 hole/sq in., each hole 0.281 in. in diameter (Fig. 6).

4. Expanded metal (39.2 percent solid)—original 0.046-in. thick steel sheet flattened, with openings of 1-in. major diagonal and 0.325-in. minor diagonal (Fig. 7).

5. Honeycomb (2.4 percent solid)—1-in. thick aluminum with regular hexagonal cells having 0.188-in. diagonals and 0.0004-in. wall thickness (Fig. 8).

6. Honeycomb (4.0 percent solid)—1.9-in. thick paper-based material with

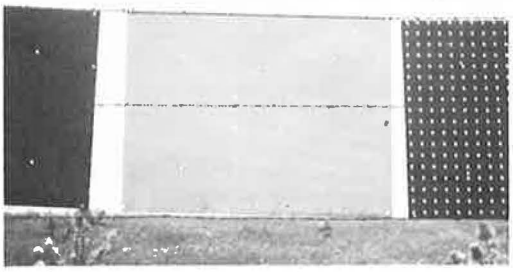

Figure 5. Perforated plate, 62.5 percent solid.

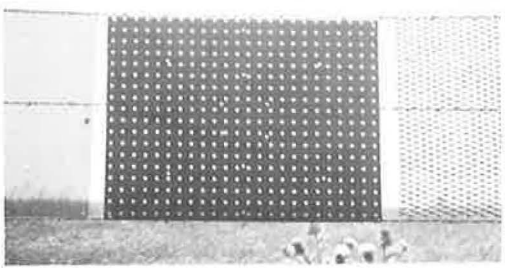

Figure 6. Perforated plate, 93.8 percent solid.

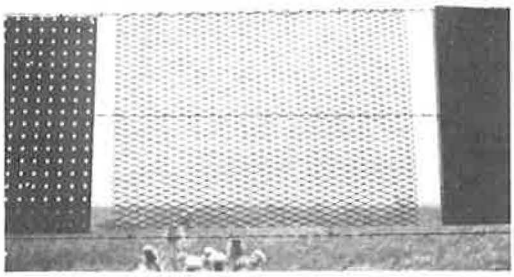

Figure 7. Expanded metal, 39.2 percent solid.

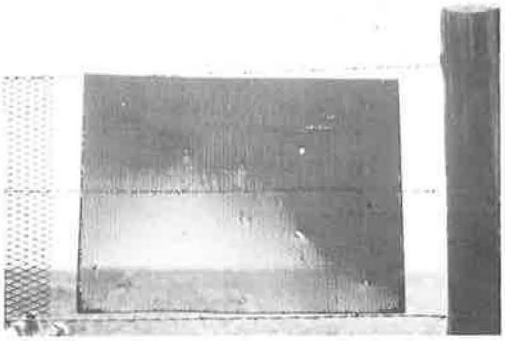

Figure 8. Honeycomb, 2.4 percent solid.

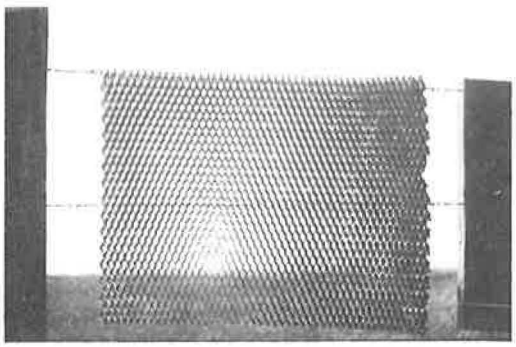

Figure 9. Honeycomb, 4.0 percent solid.

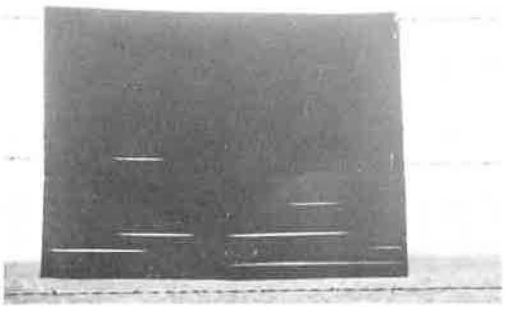

Figure 10. Louvers, 100 percent solid.

elongated hexagonal cells having 0.20-in. short side, 0.45-in. long side, 0.90-in. long diagonal, and 0.009-in. single wall thickness (Fig. 9).

7. Louvers (100 percent solid) — 1.73-in. overall thickness; each louver 2.0 in. deep, 0.052 in. thick, and spaced at 1-in. intervals at an angle of 30 deg with the horizontal (Fig. 10).

TABLE 1

WIND TUNNEL RESULTS—SOLID PLATE
(100 Percent Solid)

| Velocity (mph) | Angle (deg) | Side Force (lb) | Normal Force (lb) | Resultant Force (lb) | Moment (ft-lb) |
|---|---|---|---|---|---|
| 50.0 | 0.0 | 0.0 | 24.8 | 24.8 | 0.0 |
| 50.0 | 15.0 | 0.1 | 25.3 | 25.3 | -1.4 |
| 50.0 | 30.0 | -0.3 | 24.5 | 24.5 | -2.7 |
| 50.0 | 45.0 | -0.2 | 23.8 | 23.8 | -3.2 |
| 50.0 | 60.0 | -0.8 | 24.5 | 24.5 | -7.5 |
| 50.0 | 75.0 | 0.0 | 10.0 | 10.0 | -3.5 |
| 50.0 | 90.0 | 0.3 | 0.4 | 0.5 | 1.9 |
| 75.0 | 0.0 | 0.2 | 57.2 | 57.2 | 0.3 |
| 75.0 | 15.0 | 0.2 | 55.6 | 55.6 | -3.1 |
| 75.0 | 30.0 | -0.3 | 53.3 | 53.3 | -5.6 |
| 75.0 | 45.0 | -0.6 | 50.4 | 50.4 | -6.6 |
| 75.0 | 60.0 | -2.4 | 55.9 | 56.0 | -16.8 |
| 75.0 | 75.0 | -1.3 | 23.6 | 23.6 | -8.0 |
| 75.0 | 90.0 | 0.3 | 1.0 | 1.0 | 3.9 |
| 100.0 | 0.0 | -0.1 | 103.1 | 103.1 | 0.3 |
| 100.0 | 15.0 | -0.1 | 97.2 | 97.2 | -5.6 |
| 100.0 | 30.0 | -1.0 | 92.0 | 92.0 | -9.8 |
| 100.0 | 45.0 | -2.5 | 87.2 | 87.2 | -12.1 |
| 100.0 | 60.0 | -4.2 | 100.6 | 100.7 | -30.1 |
| 100.0 | 75.0 | -1.7 | 42.6 | 42.7 | -14.3 |
| 100.0 | 90.0 | 0.7 | 2.4 | 2.5 | 6.5 |

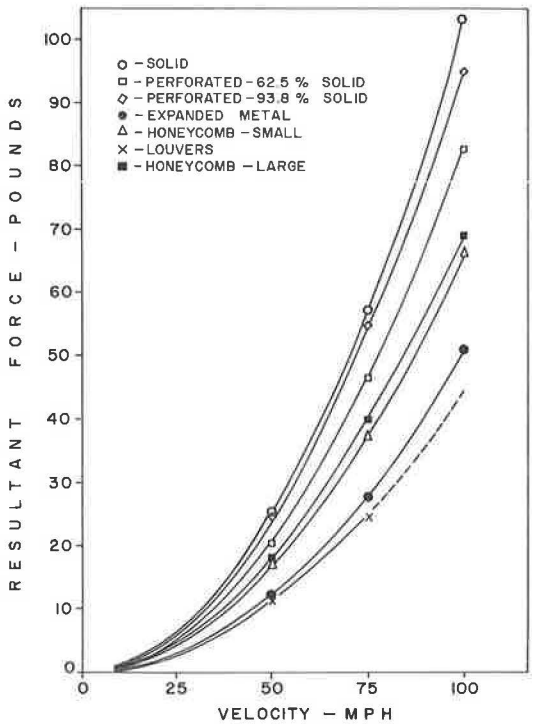


Figure 11. Variation of maximum force with velocity.

The picture of the louvered panel (Fig. 10) was taken after wind tunnel testing. A structural failure at the welds occurred during the 100-mph test, and no data were obtained for this run. Figure 4 reveals the slight imperfections remaining after the panel was reassembled for the purpose of making the photograph.

Some of the pictures of sign backgrounds show the mounting holes for attaching to the X-bracing. Specimens shown in Figures 4 through 10 were suspended from a fence wire.

## RESULTS

Tables 1 through 7 provide the data acquired from the wind tunnel tests. For each angle of incidence ($\beta$ in Fig. 2) of 0, 15, 30, 45, 60, 75, and 90 deg, data were recorded for side force, normal force, resultant force, and moment (twist about vertical axis).

Figure 11 shows a plot of maximum resultant force vs velocity for each sign background. For the louvered panel, the curve is extrapolated to 100 mph as indicated by the dashed line. Figure 12 shows a plot of maxi-

TABLE 2

WIND TUNNEL RESULTS–PERFORATED PLATE
(62.5 Percent Solid)

| Velocity (mph) | Angle (deg) | Side Force (lb) | Normal Force (lb) | Resultant Force (lb) | Moment (ft-lb) |
|---|---|---|---|---|---|
| 50.0 | 0.0 | 0.1 | 20.6 | 20.6 | -0.0 |
| 50.0 | 15.0 | 0.4 | 19.6 | 19.6 | -0.7 |
| 50.0 | 30.0 | 0.8 | 18.0 | 18.1 | -1.5 |
| 50.0 | 45.0 | 1.6 | 15.2 | 15.3 | -1.8 |
| 50.0 | 60.0 | 1.8 | 10.3 | 10.4 | -0.8 |
| 50.0 | 75.0 | 1.4 | 4.0 | 4.2 | -0.3 |
| 50.0 | 90.0 | 0.4 | 0.1 | 0.4 | 0.6 |
| 75.0 | 0.0 | 0.2 | 46.4 | 46.4 | 0.1 |
| 75.0 | 15.0 | 0.1 | 42.2 | 42.2 | -1.7 |
| 75.0 | 30.0 | 1.4 | 40.6 | 40.6 | -3.6 |
| 75.0 | 45.0 | 3.1 | 35.0 | 35.1 | -4.5 |
| 75.0 | 60.0 | 3.3 | 23.7 | 24.0 | -3.6 |
| 75.0 | 75.0 | 1.8 | 9.9 | 10.0 | -1.0 |
| 75.0 | 90.0 | 0.8 | 0.4 | 0.9 | 1.0 |
| 100.0 | 0.0 | 0.4 | 82.4 | 82.4 | 0.2 |
| 100.0 | 15.0 | 1.3 | 79.7 | 79.7 | -3.3 |
| 100.0 | 30.0 | 3.0 | 71.5 | 71.6 | -6.1 |
| 100.0 | 45.0 | 4.4 | 61.7 | 61.9 | -8.2 |
| 100.0 | 60.0 | 4.7 | 42.1 | 42.4 | -4.9 |
| 100.0 | 75.0 | 3.4 | 18.4 | 18.7 | -2.0 |
| 100.0 | 90.0 | 0.8 | 1.0 | 1.3 | 1.6 |

TABLE 3

WIND TUNNEL RESULTS–PERFORATED PLATE
(93.8 Percent Solid)

| Velocity (mph) | Angle (deg) | Side Force (lb) | Normal Force (lb) | Resultant Force (lb) | Moment (ft-lb) |
|---|---|---|---|---|---|
| 50.0 | 0.0 | 0.2 | 19.1 | 19.1 | 0.0 |
| 50.0 | 15.0 | 0.5 | 24.4 | 24.4 | -1.1 |
| 50.0 | 30.0 | -0.3 | 20.8 | 20.8 | -2.1 |
| 50.0 | 45.0 | 0.4 | 19.6 | 19.6 | -4.3 |
| 50.0 | 60.0 | 0.3 | 18.3 | 18.3 | -3.4 |
| 50.0 | 75.0 | 0.3 | 8.1 | 8.1 | -2.1 |
| 50.0 | 90.0 | 0.6 | -0.0 | 0.6 | 1.5 |
| 75.0 | 0.0 | 0.3 | 54.5 | 54.5 | 0.6 |
| 75.0 | 15.0 | 0.7 | 54.2 | 54.2 | -2.7 |
| 75.0 | 30.0 | -0.1 | 47.6 | 47.6 | -4.0 |
| 75.0 | 45.0 | -0.7 | 42.9 | 42.9 | -6.1 |
| 75.0 | 60.0 | 0.8 | 41.5 | 41.5 | -7.0 |
| 75.0 | 75.0 | 0.1 | 19.1 | 19.1 | -5.2 |
| 75.0 | 90.0 | 1.0 | 0.3 | 1.0 | 3.3 |
| 100.0 | 0.0 | 0.4 | 94.7 | 94.7 | 0.6 |
| 100.0 | 15.0 | 0.7 | 93.1 | 93.1 | -4.7 |
| 100.0 | 30.0 | -0.1 | 85.9 | 85.9 | -8.6 |
| 100.0 | 45.0 | -0.0 | 78.0 | 78.0 | -12.7 |
| 100.0 | 60.0 | 1.3 | 73.0 | 73.0 | -12.5 |
| 100.0 | 75.0 | 0.6 | 35.1 | 35.1 | -9.4 |
| 100.0 | 90.0 | 1.8 | 0.9 | 2.0 | 6.1 |

TABLE 4

WIND TUNNEL RESULTS—EXPANDED METAL
(39.2 Percent Solid)

| Velocity (mph) | Angle (deg) | Side Force (lb) | Normal Force (lb) | Resultant Force (lb) | Moment (ft-lb) |
|---|---|---|---|---|---|
| 50.0 | 0.0 | 0.2 | 12.2 | 12.2 | -0.3 |
| 50.0 | 15.0 | 0.1 | 12.1 | 12.1 | -0.6 |
| 50.0 | 30.0 | 0.0 | 10.7 | 10.7 | -0.8 |
| 50.0 | 45.0 | 0.1 | 8.2 | 8.2 | -0.8 |
| 50.0 | 60.0 | 0.7 | 5.2 | 5.2 | -0.0 |
| 50.0 | 75.0 | 0.5 | 2.4 | 2.4 | -0.0 |
| 50.0 | 90.0 | 0.3 | 0.0 | 0.3 | 0.2 |
| 75.0 | 0.0 | 0.5 | 27.7 | 27.7 | -0.4 |
| 75.0 | 15.0 | -0.0 | 27.1 | 27.1 | -1.6 |
| 75.0 | 30.0 | -0.0 | 24.8 | 24.8 | -2.0 |
| 75.0 | 45.0 | 0.4 | 19.3 | 19.3 | -1.6 |
| 75.0 | 60.0 | 0.9 | 12.0 | 12.1 | -0.9 |
| 75.0 | 75.0 | 0.4 | 6.1 | 6.1 | -0.0 |
| 75.0 | 90.0 | 0.1 | 0.2 | 0.2 | 0.6 |
| 100.0 | 0.0 | 0.9 | 50.8 | 50.8 | 0.0 |
| 100.0 | 15.0 | 0.4 | 50.4 | 50.4 | -2.9 |
| 100.0 | 30.0 | 0.2 | 45.9 | 45.9 | -4.0 |
| 100.0 | 45.0 | 0.4 | 35.3 | 35.3 | -3.4 |
| 100.0 | 60.0 | 1.2 | 21.7 | 21.7 | -1.6 |
| 100.0 | 75.0 | 0.9 | 11.1 | 11.1 | -0.4 |
| 100.0 | 90.0 | 0.1 | 0.6 | 0.7 | 0.8 |

TABLE 5

WIND TUNNEL RESULTS—HONEYCOMB
(2.4 Percent Solid)

| Velocity (mph) | Angle (deg) | Side Force (lb) | Normal Force (lb) | Resultant Force (lb) | Moment (ft-lb) |
|---|---|---|---|---|---|
| 50.0 | 0.0 | 0.4 | 4.3 | 4.3 | 0.0 |
| 50.0 | 15.0 | 10.7 | 4.5 | 11.6 | 1.9 |
| 50.0 | 30.0 | 16.5 | 3.9 | 16.9 | 2.9 |
| 50.0 | 45.0 | 15.2 | 2.1 | 15.3 | 2.6 |
| 50.0 | 60.0 | 10.7 | 1.4 | 10.8 | 0.7 |
| 50.0 | 75.0 | 4.5 | 0.5 | 4.5 | 1.1 |
| 50.0 | 90.0 | 2.1 | 0.5 | 2.2 | 0.6 |
| 75.0 | 0.0 | 0.5 | 8.1 | 8.1 | 0.4 |
| 75.0 | 15.0 | 22.8 | 8.0 | 24.1 | 4.3 |
| 75.0 | 30.0 | 36.1 | 7.0 | 36.8 | 6.4 |
| 75.0 | 45.0 | 34.9 | 5.1 | 35.3 | 7.7 |
| 75.0 | 60.0 | 23.3 | 2.9 | 23.5 | 4.5 |
| 75.0 | 75.0 | 9.4 | 1.5 | 9.5 | 2.4 |
| 75.0 | 90.0 | 2.5 | 1.1 | 2.8 | 0.6 |
| 100.0 | 0.0 | 0.2 | 14.6 | 14.6 | 0.4 |
| 100.0 | 15.0 | 41.6 | 14.2 | 44.0 | 7.4 |
| 100.0 | 30.0 | 64.8 | 12.1 | 65.9 | 11.3 |
| 100.0 | 45.0 | 62.9 | 8.9 | 63.5 | 11.1 |
| 100.0 | 60.0 | 40.6 | 4.7 | 40.9 | 8.0 |
| 100.0 | 75.0 | 16.2 | 2.4 | 16.4 | 4.1 |
| 100.0 | 90.0 | 4.9 | 2.8 | 5.6 | 1.2 |

TABLE 6

WIND TUNNEL RESULTS–HONEYCOMB
(4.0 Percent Solid)

| Velocity (mph) | Angle (deg) | Side Force (lb) | Normal Force (lb) | Resultant Force (lb) | Moment (ft-lb) |
|---|---|---|---|---|---|
| 50.0 | 0.0 | 0.4 | 3.8 | 3.8 | 0.4 |
| 50.0 | 15.0 | 11.9 | 3.1 | 12.2 | 2.6 |
| 50.0 | 30.0 | 17.7 | 2.4 | 17.9 | 4.0 |
| 50.0 | 45.0 | 16.6 | 0.7 | 16.6 | 4.7 |
| 50.0 | 60.0 | 11.8 | 0.1 | 11.8 | 2.9 |
| 50.0 | 75.0 | 4.8 | -0.2 | 4.8 | 1.5 |
| 50.0 | 90.0 | 2.2 | 0.4 | 2.2 | 0.4 |
| 75.0 | 0.0 | 1.1 | 8.6 | 8.6 | 0.4 |
| 75.0 | 15.0 | 26.7 | 8.2 | 27.9 | 6.4 |
| 75.0 | 30.0 | 39.2 | 6.0 | 39.6 | 9.4 |
| 75.0 | 45.0 | 36.0 | 2.3 | 36.1 | 8.9 |
| 75.0 | 60.0 | 24.0 | 0.1 | 24.0 | 6.3 |
| 75.0 | 75.0 | 8.8 | -0.2 | 8.8 | 2.9 |
| 75.0 | 90.0 | 1.8 | 1.1 | 2.1 | 1.0 |
| 100.0 | 0.0 | 1.8 | 18.2 | 18.3 | 1.4 |
| 100.0 | 15.0 | 46.9 | 17.1 | 49.9 | 12.5 |
| 100.0 | 30.0 | 67.7 | 11.9 | 68.7 | 16.8 |
| 100.0 | 45.0 | 62.6 | 5.7 | 62.8 | 15.6 |
| 100.0 | 60.0 | 43.3 | 1.1 | 43.3 | 11.1 |
| 100.0 | 75.0 | 16.2 | 0.1 | 16.2 | 4.9 |
| 100.0 | 90.0 | 15.3 | 2.6 | 15.5 | 2.0 |

TABLE 7

WIND TUNNEL RESULTS–LOUVERS
(100 Percent Solid)

| Velocity (mph) | Angle (deg) | Side Force (lb) | Normal Force (lb) | Resultant Force (lb) | Moment (ft-lb) |
|---|---|---|---|---|---|
| 50.0 | 0.0 | -0.3 | 10.9 | 11.0 | -0.3 |
| 50.0 | 15.0 | 2.4 | 11.0 | 11.3 | -0.2 |
| 50.0 | 30.0 | 4.1 | 9.3 | 10.1 | 0.2 |
| 50.0 | 45.0 | 2.7 | 4.3 | 5.1 | -0.1 |
| 50.0 | 60.0 | 3.4 | 3.2 | 4.7 | 0.8 |
| 50.0 | 75.0 | 2.8 | 1.4 | 3.1 | 1.1 |
| 50.0 | 90.0 | 1.6 | 0.5 | 1.7 | 0.3 |
| 75.0 | N.D. | – | – | – | – |
| 75.0 | 15.0 | 4.7 | 24.0 | 24.4 | 0.1 |
| 75.0 | 30.0 | 7.8 | 19.7 | 21.2 | 0.9 |
| 75.0 | 45.0 | 8.0 | 12.9 | 15.2 | 1.5 |
| 75.0 | 60.0 | 6.4 | 7.4 | 9.8 | 2.1 |
| 75.0 | 75.0 | 5.7 | 3.5 | 6.7 | 2.6 |
| 75.0 | 90.0 | -0.2 | 1.0 | 1.0 | 1.0 |
| 100.0 | 0.0 | – | – | – | – |
| 100.0 | 15.0 | – | – | – | – |
| 100.0 | 30.0 | – | – | – | – |
| 100.0 | 45.0 | – | – | – | – |
| 100.0 | 60.0 | – | – | – | – |
| 100.0 | 75.0 | – | – | – | – |
| 100.0 | 90.0 | – | – | – | – |

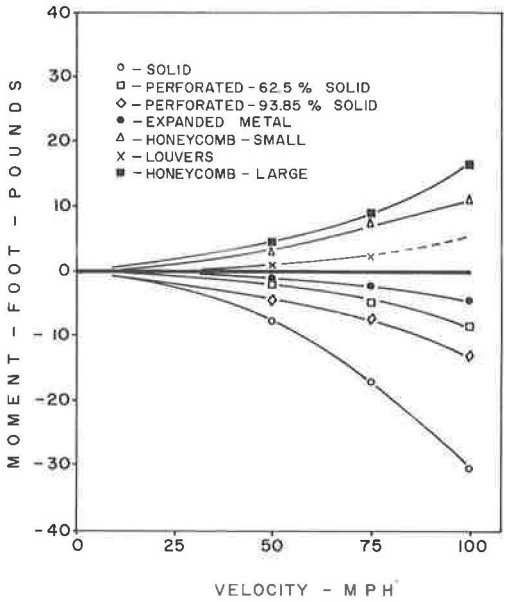


Figure 12. Variation of maximum moment with velocity.

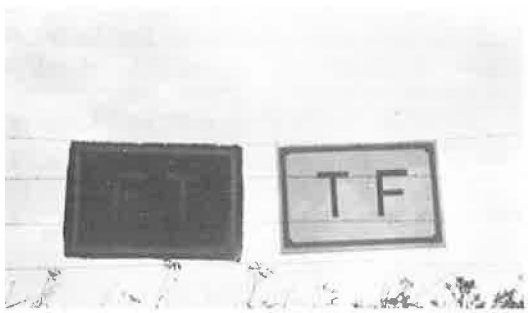


Figure 13. Visibility observations.

TABLE 8

REDUCTION IN MAXIMUM FORCE AND MOMENT AT 100 MPH

| Sign Backgrounds | Reduction (%) | |
|---|---|---|
| | Force | Moment |
| Louvers[a] | 57 | 83 |
| Expanded metal | 51 | 87 |
| Honeycomb, 2.4% solid | 36 | 63 |
| Honeycomb, 4.0% solid | 33 | 44 |
| Perforated plate, 62.5% solid | 20 | 73 |
| Perforated plate, 93.8% solid | 8 | 58 |

[a] Based on extrapolated data.

mum moment vs velocity for each sign background. Data for plotting the curves of Figures 11 and 12 are taken from Tables 1 through 7.

Table 8 provides comparisons of percent reduction in maximum forces and in maximum moment for the sign backgrounds. In each case, the solid background is used as the basis of comparison.

The X-bracing on which the sign backgrounds were mounted resulted in some interference effect on the nonsolid backgrounds. Consequently, some inherent inaccuracies of this nature exist in the data. However, these inaccuracies are small.

## CONCLUSIONS

From the results of the investigation, it is concluded that the use of nonsolid sign backgrounds appears feasible. However, other factors not evaluated in this research need to be weighed before a preference of one type of sign background over another can be established. For example, the matter of cost needs consideration. The cost of sign supports would probably be reduced as a result of reduced wind loadings. However, additional complexity of manufacturing and mounting might well lead to a total cost in excess of that for the solid background sign structure.

Visibility also merits consideration. Although no organized research was performed with respect to visibility characteristics, a few observations were made, two of which are shown in Figure 13. On the right, suspended from a fence wire, is a sign background constructed from the perforated plate having 0.125-in. holes. On the left is a background constructed from the aluminum honeycomb. Visibility would be an important factor in considering the use of nonsolid backgrounds.

The louvered background offers the greatest percent reduction in wind force, as well as the possibility of providing a solid appearance through a proper design of louvers.

The writers wish again to call attention to the fact that this research was not intended to be comprehensive. Obviously, only a few of the many possibilities with respect to shape of openings, dimensions, positioning of louvers, etc., have been considered.

## ACKNOWLEDGMENT

The authors wish to acknowledge the facilities provided for this research by the Texas Engineering Experiment Station at Texas A and M University.

# Simplified Design Check of Thermal Stresses in Composite Highway Bridges

WILLIAM ZUK, Professor of Architecture, University of Virginia, and
Consultant to the Virginia Council of Highway Investigation and Research

A simple formula intended for use as a design check of thermal stresses in simply supported composite highway bridges is described. It is based on a series of field tests of various bridges ranging in span from 47 ft 3 in. to 71 ft 5 in. The formula relates the thermal stress at the bottom of the girder to the temperature difference between the top and bottom of the slab and the depth of the bridge.

• ALTHOUGH a small body of literature exists on thermal stresses in composite beam construction (defined as a flexural member consisting of a steel beam with a concrete slab firmly attached to its top) the quantitative analysis contained in such literature is generally too complex to be of direct use to bridge designers (see Refs. 1 and 2 for all related references). The few existing specifications contained in the construction codes of various organizations are little better. Germany's code (DIN 1078, 1958) for temperature effects in composite construction is as follows:

A. Indeterminate structure: a straight line variation of $\pm 15°$ C shall be assumed between the top of concrete slab and bottom of steel girder.
B. Statically determinate structures: the thermal effect shall be allowed for by an additional shrinkage of $10 \times 10^{-5}$. These stresses shall be combined with live load stresses as follows: (a) Full live load + half temperature difference. (b) Full temperature variation and live load reduced by 1% per meter of span to 40 meters span, then constant 40% reduction.
C. Shearing forces due to temperature difference may be distributed as a triangular shearing force diagram at the end of the girder with a length equal to the effective slab width. (In association with this shearing force the code also specifies the use of heavy end anchorages tieing the slab and beam together at their interface.)

Austria, Sweden, and Japan are the only other countries with a thermal stress provision in their codes, and these codes are all essentially based on the German code. The United States has no direct provision, although Section 1.2.15 of the 1961 AASHO Standard Specifications for Highway Bridges states: "Provision shall be made for stresses or movements resulting from variations in temperature."

Obviously, none of the existing codes gives the designer any direct information on how to convert temperatures to stresses, on which all elastic design is based. For this reason, a series of field tests were conducted by the Virginia Council of Highway Investigation and Research in cooperation with the U. S. Bureau of Public Roads in 1964 to determine, if possible, a simple method to predict thermal stresses.

## FIELD STUDIES

Six simple span composite bridges (all at least 2 yr old) were selected for testing. They ranged from 47 ft 3 in. to 71 ft 5 in. in span, as indicated in Table 1, and all had

Paper sponsored by Committee on Bridge Design.

TABLE 1

COMPOSITE BRIDGES INVESTIGATED

| Va. Bridge | Avg. Slab Thickness (in.) | Girder Spacing (ft) | Girder Size | Bridge Span C. to C. (ft) |
|---|---|---|---|---|
| On Rt. 671 over Rt. 11-A at Lexington | 8 | 8 5/12 | 24 WF 100 with 10- × 3/4-in. lower cover plate | 47 1/4 |
| On Rt. 635 over Pedlar River at Pedlar Mills | 7 1/2 | 7 2/3 | 33 WF 141 | 51 5/12 |
| On Rt. 252 over Hays Creek at Brownsburg | 7 3/4 | 7 2/3 | 36 WF 160 | 56 |
| On Rt. 256 over South River at Grottoes | 7 1/2 | 8 1/6 | 36 WF 150 with 10 1/2- × 5/8-in. lower cover plate | 61 1/4 |
| On Rt. 250 over South River at Waynesboro | 7 | 6 1/2 | 36 WF 150 with 11- × 3/4-in. lower cover plate | 69 |
| On Rt. 257 over Dry River near Dayton | 7 3/4 | 7 2/3 | 36 WF 170 with 10 1/2- × 9/16-in. and 9- × 3/8-in. lower cover plates | 71 5/12 |

conventional Lubrite plate bearings. On each bridge an interior girder was instrumented for strain reading by a 10-in. Whittemore gage at the upper and lower flanges. (Facia girders were not instrumented in this series of tests as they are subject to unusual temperature conditions caused by solar radiation on the lower flanges and are generally over-designed.) Numerous strain readings were periodically taken under dry, zero live-load conditions. Because of its age, the concrete was assumed to be in a post-shrinkage state. The Whittemore gage was calibrated by an invar bar before each set of readings. Simultaneously with the strain readings, temperatures at the top of the slab and at the upper and lower flanges of the girder were also taken with a quick response surface thermometer. An infrared thermometer, which proved greatly superior to the surface thermometer, was used in the latter portion of the studies.

From these data and the following equation, thermal stresses at the measured positions in the girder could be obtained:

$$f = eE - cET \tag{1}$$

where

f = thermal stress in girder;
e = measured strain;
E = modulus of elasticity ($30 \times 10^6$ psi);
c = coefficient of expansion ($6.5 \times 10^{-6}$/°F); and
T = temperature change.

Except for regions close to the end of the girder, thermal stresses are essentially constant along the length of the beam.

For comparative purposes, temperature changes, T, were related to conditions early in the morning, when the entire bridge was almost at a uniform temperature state.

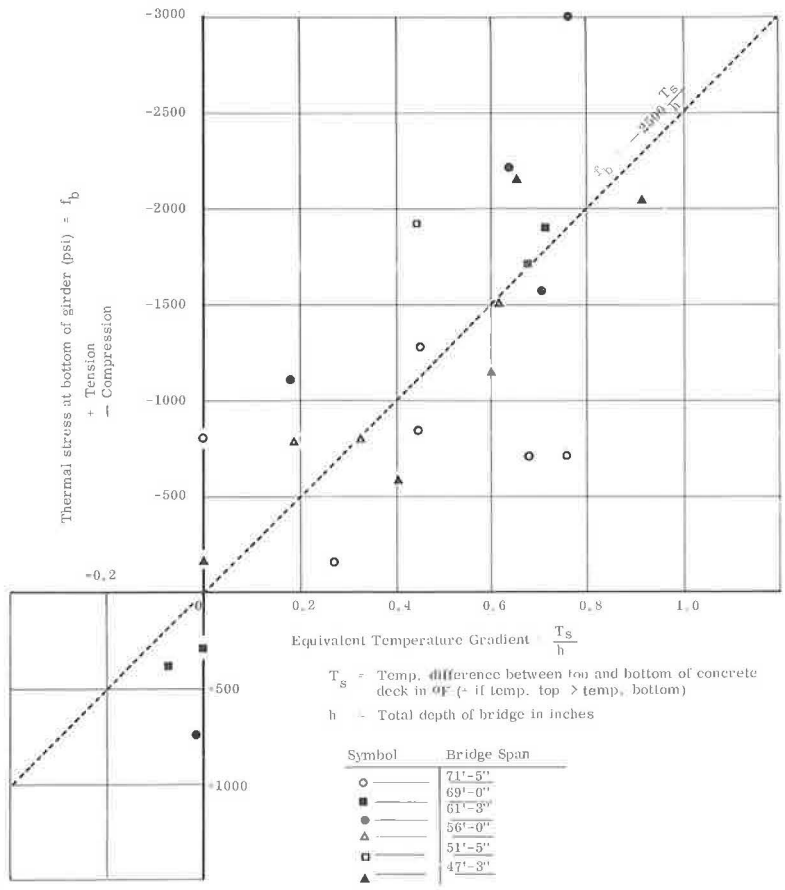


Figure 1. Plot of measured stress vs temperature gradient.

The initial simplifying approach taken was to reduce the more complex theoretical equations cited at the beginning of this paper to a few basic parameters by the process of eliminating small order terms. This process lead to two dimensionally correct equations in terms of the interface shear, F, and the interface moment, Q, as in Eqs. 2 and 3:

$$F = k E_c A_c T \tag{2}$$

and

$$Q = k_1 h F \tag{3}$$

where

$E_c$ = modulus of elasticity of concrete;
$A_c$ = area of concrete slab;
T = temperature changes from top of slab to bottom of girder;
h = total depth of bridge; and
$k_1$ = experimental nondimensional constants.

It was hoped that if a consistent set of k and $k_1$ values could be found, all thermal stresses in the bridge could thereby be computed from the known F and Q. However, the scatter of these constants proved too great for meaningful analysis. Therefore, as a next best course, thermal stresses in the lower flange (those generally controlling design) were plotted against the equivalent temperature gradient $T_S/h$, where $T_S$ is the temperature difference between the top and bottom of the concrete slab and h is the

total depth of the bridge. The results are shown in Figure 1. Although there is more scatter about the median line than is generally desirable, a trend does seem evident.

Three possible causes of the scatter are (a) neglect of secondary parameters such as material property variations and span length; (b) experimental error in measuring both the strain and the temperature (which could account for as much as ± 500 psi); and (c) the nonlinear nature of the friction at the movable bearing. Depending on the tendency of the girder to move thermally one way or the other, the friction restraint could cause the stresses to be raised or lowered as much as several hundred psi. The limiting sliding value of the coefficient of friction of 0.1 of Lubrite plates cannot always be assumed because full sliding may not actually be occurring at the time of measurement. To substantiate the friction hypothesis, a random selection of experimental data was compared with the author's more complex theories (previously cited), and it was found that much better agreement between theory and experiment could be obtained if bearing restraint was introduced into the force system.

Although the use of more sensitive and expensive instrumentation would probably reduce the scatter, it is believed that because of the action of statistical balancing, the position of the final median line would not be significantly affected.

## CONCLUSIONS

Until a better design method is found, it is suggested that thermal stresses in simply supported composite highway bridges can be approximately checked by data obtained from this study.

Since thermal stresses are generally of secondary magnitude, the following formula is believed reasonable:

$$f_b = 2,500 \frac{T_s}{h} \tag{4}$$

where

$f_b$ = thermal stress in bottom flange of girder (+ if tension, - if compression), psi;
$T_s$ = temperature difference between top and bottom of slab (+ if temperature at top is greater than temperature at bottom, and - if temperature at top is less than temperature at bottom), °F; and
$h$ = total depth of bridge (slab + girder), in.

The value of $T_s$ must be obtained on a regional basis, since the climate of the United States is too varied to permit specification of a fixed value. For guidance, however, it may be said that from tests conducted on bridges in the region of Charlottesville, Va., the maximum $+T_s$ is about 40 F, occurring in the summer, and the maximum $-T_s$ is about 10 F, occurring in the winter. For interior girders, the entire girder is at approximately a constant temperature equal to that at the bottom of the slab, so $T_s$ may also be interpreted as the temperature difference between the top and bottom of the bridge.

## ACKNOWLEDGMENTS

Grateful acknowledgment is made to the Virginia Council of Highway Investigation and Research and to the U. S. Bureau of Public Roads for their joint sponsorship of this study. Special mention is also made of the assistance of James Martin.

## REFERENCES

1. Zuk, William. Thermal and Shrinkage Stresses in Composite Beams. Jour. ACI, Sept. 1961.
2. Zuk, William. Thermal Behavior of Composite Bridges—Insulated and Uninsulated. Highway Research Record 76, pp. 231-253, 1965.

# Fatigue Tests of Two Prestressed Concrete I-Beams with Inclined Cracks

JOHN M. HANSON and C. L. HULSBOS
Respectively, Research Assistant Professor of Civil Engineering, and Research Professor of Civil Engineering, Lehigh University

• AN IMPORTANT question in the design of prestressed bridge structures concerns the magnitude of overload to which the structure can be subjected without subsequently limiting the life of the bridge under design loads. The first step in the consideration of this question requires that the effect of the overload on the bridge structure, which manifests itself by the appearance of cracks in the main load-carrying members, be evaluated. The second step requires investigation of the fatigue properties of the cracked section under repeated loads.

Cracks in prestressed beams caused by applied loads may be of three types: flexural, flexure shear, or diagonal tension. Flexural cracks occur in regions of high moment and low shear, and propagate perpendicular to the longitudinal axis of the beam. Flexure shear and diagonal tension cracks are both inclined to the longitudinal axis of the beam. However, a flexure shear crack begins as a flexural crack and, because of the presence of shear, turns and becomes inclined in the direction of increasing moment. Diagonal tension cracks initiate from an interior point in the beam.

If a pretensioned prestressed beam subjected to an overload of sufficient magnitude to cause flexural cracking, without causing yielding of any of the prestressing elements, is subsequently subjected to similar repeated loads of equal or lesser magnitude, the number of repetitions of this load that the beam can endure before failure may be controlled by the fatigue strength of the concrete in compression or that of the prestressing strand in tension. Warner and Hulsbos (1) have shown that the fatigue life of underreinforced beams will be controlled by the fatigue strength of the prestressing strand, and that stress repetitions smaller than the fatigue limit do not contribute to fatigue failure in the strand. Therefore, the overload will not cause failure if the beam is subsequently subjected to repeated loads which produce a stress in the strand less than the fatigue limit. Furthermore, in typical pretensioned prestressed beams which have been subjected to overloads great enough to cause flexural cracking, the stress level in the strand will reach the fatigue limit of the strand only under a moment substantially greater than that required to reopen the flexural cracks.

Next, in a pretensioned prestressed beam subjected to an overload of sufficient magnitude to cause inclined cracking, the fatigue life under lesser loads may again be controlled by either the concrete or the prestressing strand and, in addition, by the fatigue strength of the web reinforcement. The strain distribution in the region of the inclined cracking is nonlinear, and at the present time an analysis to determine accurately the stresses in the concrete, strand, and stirrups cannot be made. However, since inclined cracking occurs in regions of lesser moment, the stresses in the strand in this region are probably less critical than those in the region of maximum moment. Consequently, the critical component may be either the concrete or the web reinforcement. Research has shown that when deformed web reinforcement is crossed by diagonal tension inclined cracking, the stirrups in the region of the inclined crack yield immediately. Therefore, a pretensioned prestressed beam subjected to a single overload of sufficient magnitude to cause diagonal tension cracking may subsequently be critical in fatigue of the web reinforcement under lesser loads.

---

Paper sponsored by Committee on Concrete Superstructures.

To explore the possibility of the type of failure discussed, two prestressed I-beams were subjected to a symmetrical two-point loading equal to 78 percent of the ultimate flexural capacity of the section. This loading was sufficient to cause diagonal tension cracking in both shear spans of both beams. Repeated loadings of lesser magnitude were then applied until failure occurred. Web reinforcement provided in the two test beams was 57 and 43 percent, respectively, of that required to develop the ultimate flexural capacity according to paragraph 1.13.13 of the AASHO specifications (2). The two tests whose results are presented in this paper were part of a larger investigation (3, 4) of the ultimate strength of prestressed beams under the combined action of bending and shear, conducted by the Department of Civil Engineering at Fritz Engineering Laboratory, and sponsored by the Pennsylvania Department of Highways, U. S. Bureau of Public Roads, and the Reinforced Concrete Research Council.

## NOTATION

$A$ = area of beam cross-section;
c.g. = center of gravity of beam cross-section;
c.g.s. = center of gravity of prestressing strand;
$E_c$ = modulus of elasticity of concrete;
$f'_c$ = ultimate compressive strength of concrete;
$f'_r$ = modulus of rupture of concrete;
$F$ = resultant force in prestressing strand;
$F_i$ = initial prestress force, before prestress release;
$I$ = moment of inertia of beam cross-section;
$N$ = number of cycles of repeated loading;
$Q$ = moment, about c.g., of area of cross-section on one side of horizontal section on which shearing stress is desired;
$r$ = percentage of web reinforcement, based on web width;
$R$ = stress interval;
$S$ = stress in strand, in percent of static ultimate tensile stress;
$S_{max}$ = maximum stress in repeated load cycle;
$S_{min}$ = minimum stress in repeated load cycle;
$V$ = applied load shear in test beams;
$V_c^f$ = applied load shear in test beams causing flexural cracking;
$V_c^{dt}$ = applied load shear in test beams causing diagonal tension cracking; and
$Z$ = section modulus.

## TEST SPECIMENS

### Description

The test beams, E.10 and E.11, were identical except for the web reinforcement. Details of the beams are shown in Figure 1.

### Fabrication

The two beams were fabricated at the same time in a prestressing bed set up on the laboratory floor. The sequence of operations was as follows: tensioning the strands, positioning the web reinforcement, erecting the form, placing the concrete, curing, removing the form, instrumenting, and releasing the prestress.

Two 50-ton mechanical jacks were used to tension the straight strands. A special jacking arrangement was then used to adjust the tension in individual strands. The total prestress force at the time the concrete was placed, as measured by load cells placed on each strand, was 113.7 kips. The minimum and maximum prestress force in any individual strand was 18.7 and 19.1 kips, respectively.

Wire ties were used to secure the web reinforcement to the strand. Wood forms were used to cast the test beams. Checks made on the beams indicated that, in general,

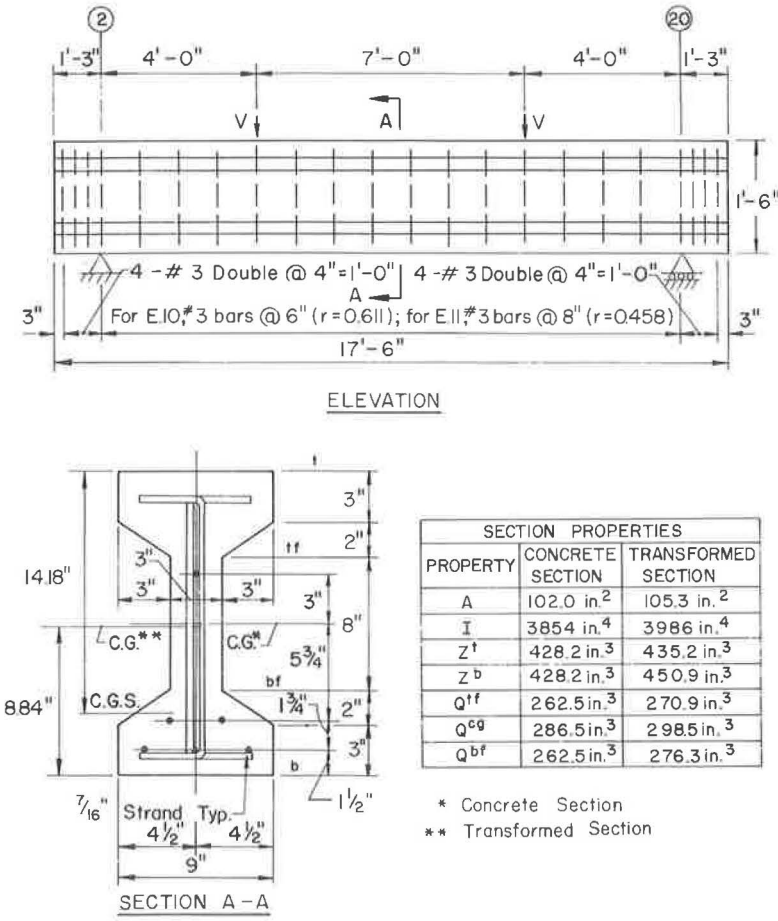


| SECTION PROPERTIES | | |
|---|---|---|
| PROPERTY | CONCRETE SECTION | TRANSFORMED SECTION |
| A | 102.0 $in.^2$ | 105.3 $in.^2$ |
| I | 3854 $in.^4$ | 3986 $in.^4$ |
| $Z^t$ | 428.2 $in.^3$ | 435.2 $in.^3$ |
| $Z^b$ | 428.2 $in.^3$ | 450.9 $in.^3$ |
| $Q^{tf}$ | 262.5 $in.^3$ | 270.9 $in.^3$ |
| $Q^{cg}$ | 286.5 $in.^3$ | 298.5 $in.^3$ |
| $Q^{bf}$ | 262.5 $in.^3$ | 276.3 $in.^3$ |

* Concrete Section

** Transformed Section

Figure 1. Details of test beams.

dimensions were maintained to within $\frac{1}{8}$ in., and consequently the nominal dimensions of the cross-section given in Figure 1 were used in all calculations. Cast simultaneously with each test beam were six 6- by 12-in. concrete cylinders and three 6- by 6- by 36- in. modulus of rupture specimens. Vibrators were used to place the concrete in both the test beams and the modulus of rupture specimens; the cylinders were rodded.

All specimens were covered with wet burlap and plastic sheeting for 5 days, after which the forms were removed. Instrumentation was positioned on the test beams on the sixth day. On the seventh day after casting, the prestress force was slowly released into the beams. The specimens were subsequently stored in the laboratory until tested.

## Materials

Ready-mixed concrete, with a cement-to-sand-to-coarse aggregate ratio of approximately 1 to 1.8 to 2.3, was used to cast the test beams. The mix contained 7.5 sk/cu yd of Type III portland cement, and the maximum size of the coarse aggregate was $\frac{3}{4}$ in. The amount of water added to the mix produced a slump of 2.5 in.

A stress-strain curve for the $\frac{7}{16}$-in. diameter seven-wire prestressing strand, determined from a tension test conducted in the laboratory, is shown in Figure 2. Failure occurred in the grips at an ultimate load of 26.3 kips. The stress-strain curve in Figure 2 was virtually identical with that provided by the manufacturer. According to

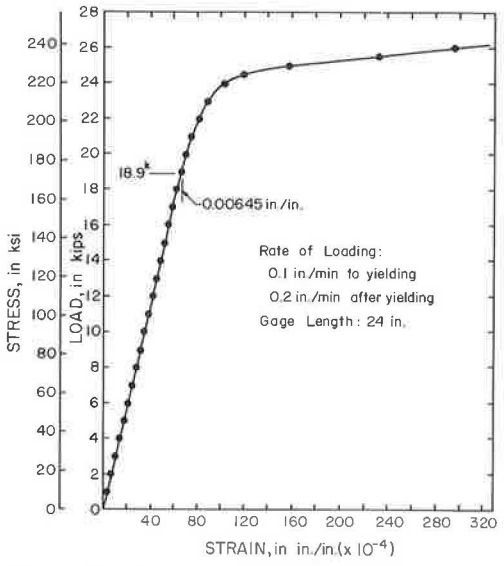


Figure 2. Stress-strain curve for prestressing strand.

the manufacturer, the ultimate load of the strand was 27.5 kips, corresponding to an ultimate stress of 252.2 ksi, and the elongation in 24 in. was 5.1 percent. The surface of the strand was free from rust, and care was taken to avoid getting any grease on the strand during fabrication.

The web reinforcement was fabricated from hot-rolled No. 3 deformed bars, with a yield point of 55.5 ksi and an ultimate stress of 82.7 ksi, based on an area of 0.11 sq in.

## Instrumentation and Loading Apparatus

The test setup and principal instrumentation employed on the test beams is indicated in Figure 3. Loads were applied symmetrically using two 55-kip Amsler hydraulic jacks bolted to a steel test frame. Vertical deflections were

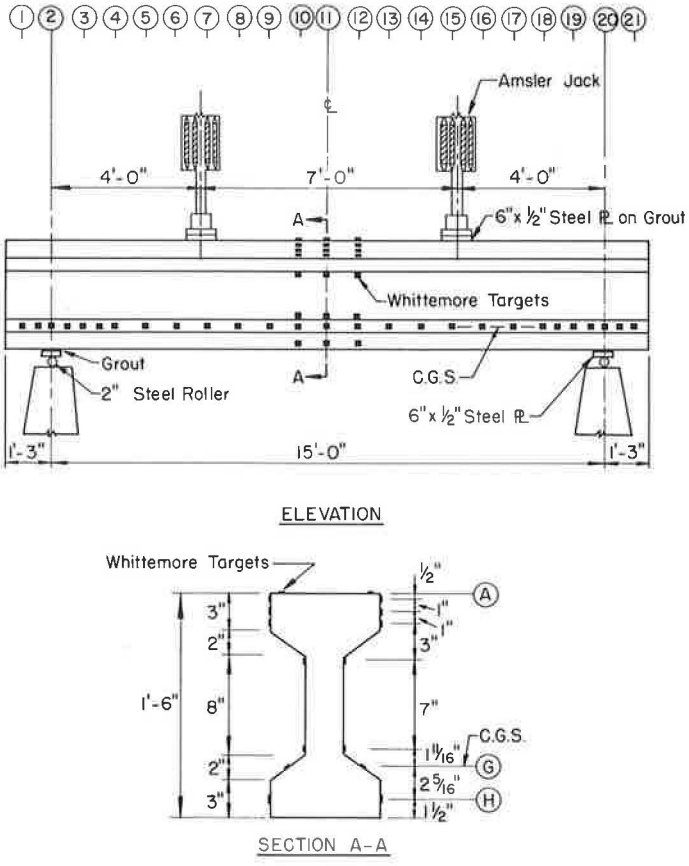


Figure 3. Test setup and principal instrumentation.

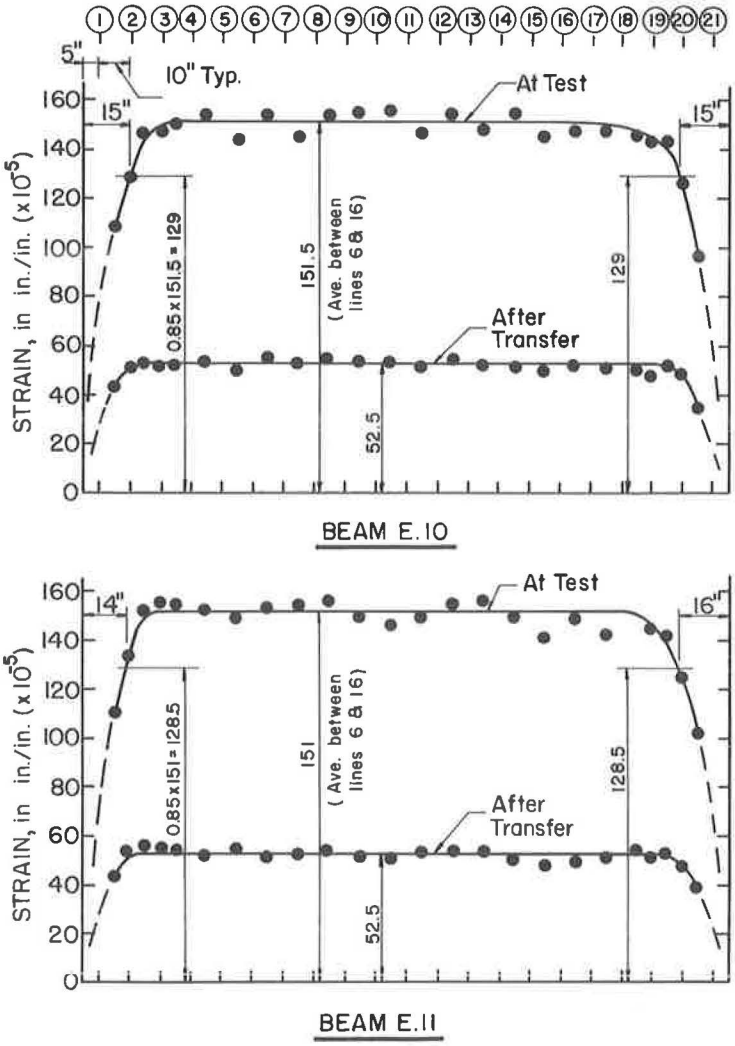


Figure 4. Concrete strain along c.g.s.

measured by Ames dial gages and level readings. Deformation data were taken using a 10-in. Whittemore strain gage. The Whittemore targets were cemented to the test beams with an epoxy resin. Crack widths were measured with a Gaertner 32 M/M EFL microscope with a built-in scale graduated to 0.001 in.

## PROCEDURE AND RESULTS

### Properties of Concrete

Compression tests were conducted on 6- by 12-in. cylinders to determine the ultimate compressive strength of the concrete, $f'_c$, associated with the test beams at prestress release and at test. Strains were measured on the cylinders with a compressometer to determine the modulus of elasticity of the concrete, $E_c$. Modulus of rupture tests were conducted on plain concrete beam specimens having a 6- by 6-in. cross-section and loaded at the third points of a 30-in. span. The results of these tests and the age of the concrete at the time the test was conducted are given in Table 1. Each value of $f'_c$, $f'_r$, and $E_c$ in Table 1 is an average of three tests.

TABLE 1

PROPERTIES OF CONCRETE

| Beam | At Transfer | | | At Test | | | |
|---|---|---|---|---|---|---|---|
| | Age (days) | $f'_c$ (psi) | $E_c$ (ksi) | Age (days) | $f'_c$ (psi) | $f'_r$ (psi) | $E_c$ (ksi) |
| E.10 | 7 | 6,160 | 3,600 | 228 | 7,360 | 950 | 4,400 |
| E.11 | 7 | 6,410 | 3,600 | 245 | 7,790 | 960 | 4,200 |

TABLE 2

PRESTRESS DATA

| Beam | Initial Prestress Force, $F_i$ (kips) | Losses (%) | | Prestress Force at Test, F (kips) | Transfer Distance (in.) | |
|---|---|---|---|---|---|---|
| | | At Transfer | At Test | | End 20 | End 20 |
| E.10 | 113.7 | 8.4 | 23.7 | 86.7 | 15 | 15 |
| E.11 | 113.7 | 8.3 | 23.7 | 86.7 | 14 | 16 |

Prestress Data

Strain data were taken along line G shown in Figure 3 to determine the losses in the prestress force and the distance from the ends of the test beam at which 85 percent of the prestress force was effective, hereafter called the transfer distance. Readings were taken immediately before releasing the prestress force, immediately after release, and again just before testing. The differences between the first and second and between the first and third set of readings, converted to concrete strain, were plotted along the length of the test beam, as shown in Figure 4. The loss in the prestress force was determined, assuming that the concrete strain measured on the surface of the test beams at the c.g.s. was equal to the average strain loss in the prestressing strand. The transfer distance was determined from the plot of total concrete strain along the length of the test beam at the time of test, as shown in Figure 4. These results are presented in Table 2.

Loading History

The loading history for the two test beams is summarized in Table 3. Both test beams were first loaded statically, in increments of 1 or 2 kips shear, to a maximum applied load shear of 32 kips. The shears causing flexural cracking, $V_c^f$, and diagonal tension cracking, $V_c^{dt}$, during the first load cycle are given in Table 3.

Particular attention was given to the state of cracking in the shear spans at the time of formation of the diagonal tension cracks. Sketches of the crack patterns just after the formation of the diagonal tension cracks are shown in Figure 5. In these elevation views of E.10 and E.11, the solid heavy lines indicate all cracking before the formation of the diagonal tension cracks. The suddenly appearing diagonal tension cracks are indicated by dashed heavy lines. The location of the vertical stirrups are also shown by

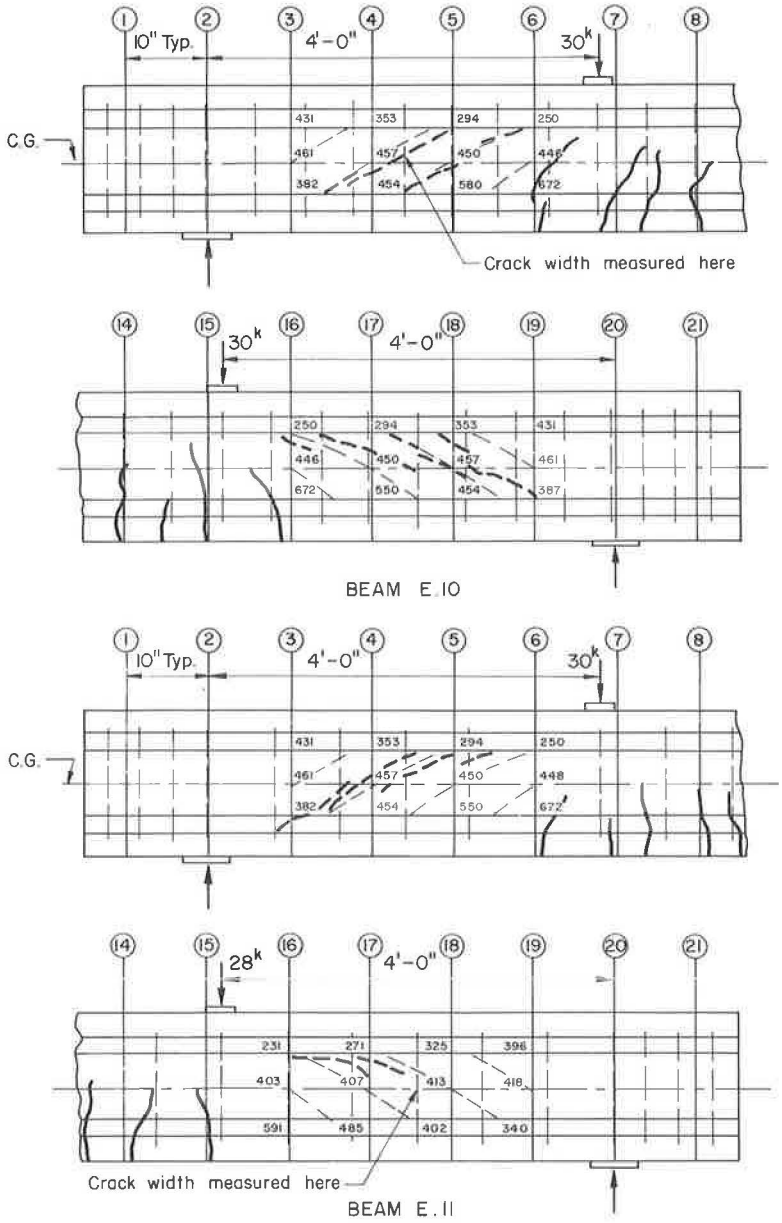


Figure 5. State of stress at diagonal tension cracking.

dashed light lines. Principal tensile stresses and the slopes of the compressive stress trajectories were calculated, using the properties of the transformed section, at the intersection of the grid lines within the shear span and the junction of the web and top flange, the mid-depth of the beam, and the junction of the web and bottom flange. It was assumed that the state of stress in the web was defined by a horizontal normal stress and a shearing stress and that the vertical normal stress was zero.

After being subjected to a maximum shear of 32 kips, the test beams were unloaded and subjected to several additional static tests to determine the load-deflection response of the cracked beam. In addition, Whittemore readings were taken during some of the static tests using primarily the group of targets on lines 10, 11, and 12. The width of

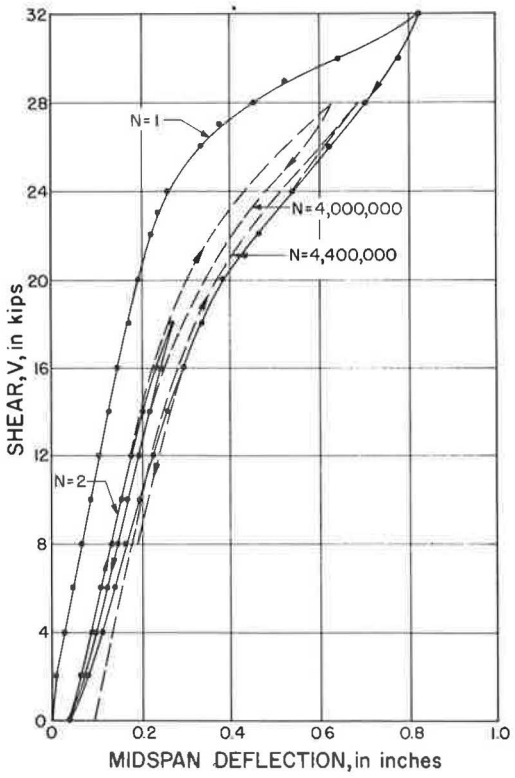


Figure 6. Load-deflection curve for E.10.

the diagonal tension cracks at the locations shown in Figure 5 was also measured.

The 0,8 kip notation for $V_{min}$ in Table 3 indicates that either of these values of shear correspond to the minimum load in the static load cycle. For example, in the case of E.10 beginning with the second load cycle, the load was varied from zero to a maximum of 18 kips and then back to zero. At this point, E.10 was permitted to rest overnight. Beginning with the third load cycle on the second day of the test, the load was taken from zero to 18 kips shear, and then back to 8 kips shear. The subsequent fourth through sixth static tests continued in the 8- to 18-kip range.

Similar static tests were conducted at selected intervals during the repeated loadings to take experimental readings. Rest periods, in general overnight, were permitted between static tests.

The repeated loading for both beams was applied at the rate of 250 cycles/min, except for the load cycles between 3,200,001 and 4,000,000 applied to E.10, when the loading rate was increased to 500 cycles/min. The magnitude of the maximum load applied in the repeated load cycle was controlled by the known load-deflection response of the member determined from the preceding static tests; i.e., the magnitude of the repeated loading was adjusted so that the maximum deflection of the test beam while subjected to the repeated loadings was the same as the deflection in the static test at the corresponding load. The tests on E.10 and E.11 extend over 16 and 9 days, respectively.

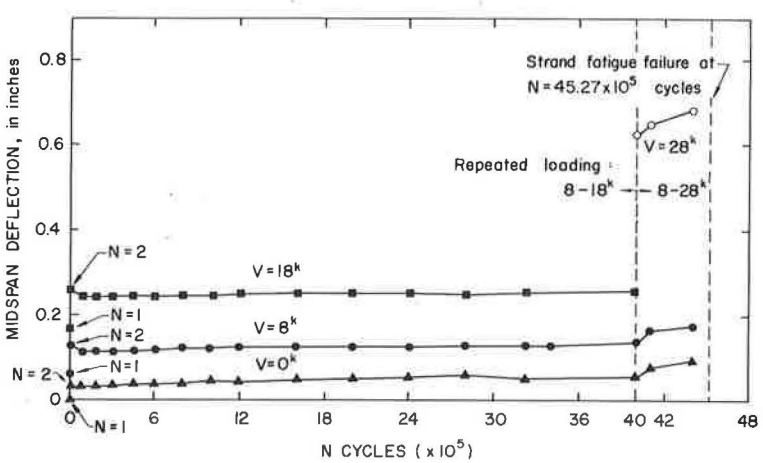


Figure 7. Deflection-N curves for E.10.

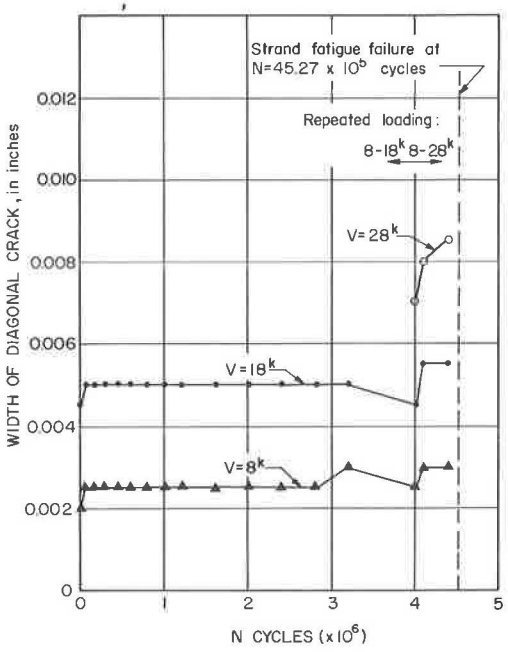


Figure 8. Variation in width of diagonal crack with N for E.10.

## Behavior of E.10

As indicated in Table 3, the repeated loading applied to E.10 for the first 4,000,000 load cycles ranged from 8 to 18 kips shear. At N equal to 4,000,000 there was no indication of structural damage in the member; this prompted the decision to change the loading range to between 8 and 28 kips shear. Failure in E.10 occurred at N equal to 4,526,900 load cycles as a fatigue fracture in one wire of one of the bottom strands.

The load-deflection curve for E.10 at N equal to 1, 2, 4,000,000, and 4,400,000 is shown in Figure 6. Between N equal to 2 and N equal to 4,000,000 the load-deflection diagrams obtained from the static tests remained essentially unchanged. Between N equal to 4,000,000 and N equal to 4,400,000, the load-deflection diagram continually moved to the right. The load-deflection data obtained are summarized by the deflection-N diagram shown for E.10 in Figure 7, where corresponding to 0, 8, 18, and 28 kips

TABLE 3

LOADING HISTORY

| Beam | Loading Cycle, N | $V_{min}$ (kips) | $V_{max}$ (kips) | Remarks |
|---|---|---|---|---|
| E.10 | 1 | 0 | 32 | Initial static test: $V_c^f$ = 24 kips; $V_c^{dt}$ = 30 kips, both ends. |
| | 2-6 | 0, 8 | 18 | Static tests. |
| | 7-3,200,000 | 8 | 18 | Repeated load test at 250 cycles/min. |
| | 3,200,001-4,000,000 | 8 | 18 | Repeated load test at 500 cycles/min. |
| | 4,000,001-4,526,900 | 8 | 28 | Repeated load test at 250 cycles/min; fatigue failure in one wire of bottom strand at N = 4,526,900. |
| E.11 | 1 | 0 | 32 | Initial static test: $V_c^f$ = 24 kips; $V_c^{dt}$ = 30 kips, end 2, 28 kips, end 20. |
| | 2-5 | 0, 8 | 24 | Static tests. |
| | 6-2,007,500 | 8 | 24 | Repeated load test at 250 cycles/min; fatigue failure in stirrup, end 2, at N = 2,007,500. |

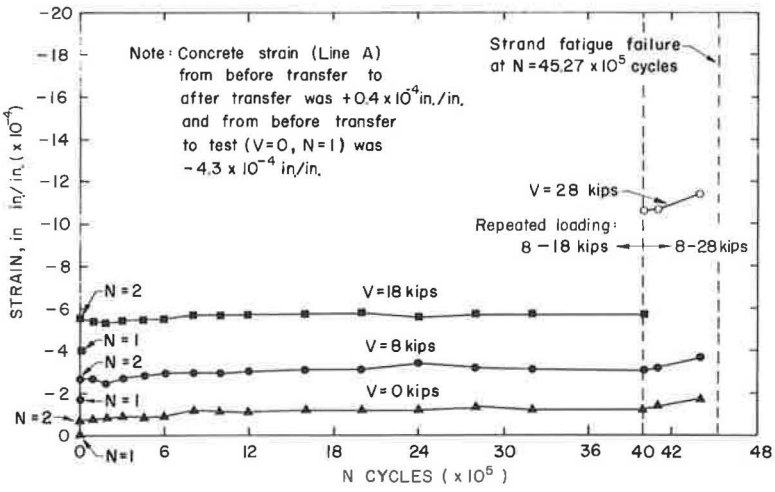


Figure 9. Variation in concrete strain of top fibers during test of E.10.

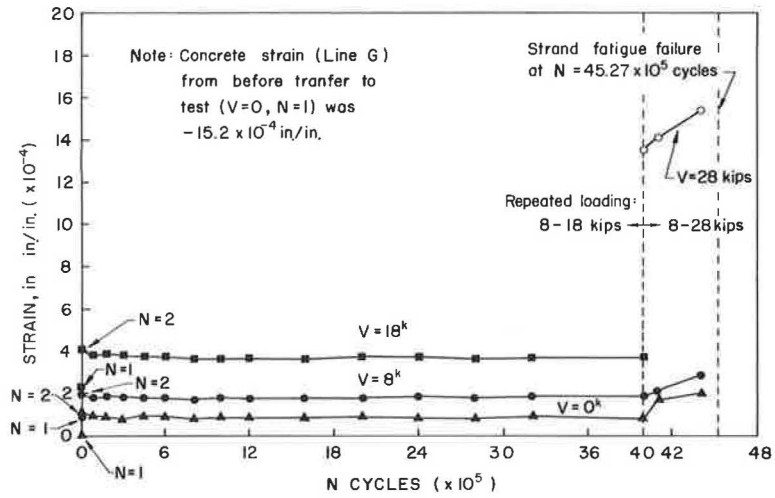


Figure 10. Variation in concrete strain at level of c.g.s. during test of E.10.

shear, midspan deflection is plotted against the N at which the static test was conducted.

After diagonal cracking in E.10, transverse crack width was measured at the location shown in Figure 5. At V equal to 30 kips, the crack width was 0.006 in. Increasing V to 32 kips opened the crack to 0.008 in. The width of the crack after the beam was unloaded was 0.002 in. Subsequent variation in the width of the crack at the minimum and maximum shear in the repeated load cycle with N is shown in Figure 8. In the static tests at any N, there was no observable opening of the crack up to a shear of 10 kips. From 10 kips to the maximum shear, the increase in crack width was approximately proportional to the increase in shear above 10 kips.

The Whittemore readings were used to determine the variation with N of the concrete strain in the top fibers (line A), at the c.g.s. (line G), and at the level of the lowest strand (line H) for the indicated values of shear, as shown in Figures 9, 10, and 11, respectively. Each point plotted in these figures is an average of four readings, i.e., an average of the readings between lines 10-11 and 11-12 on both sides of the member.

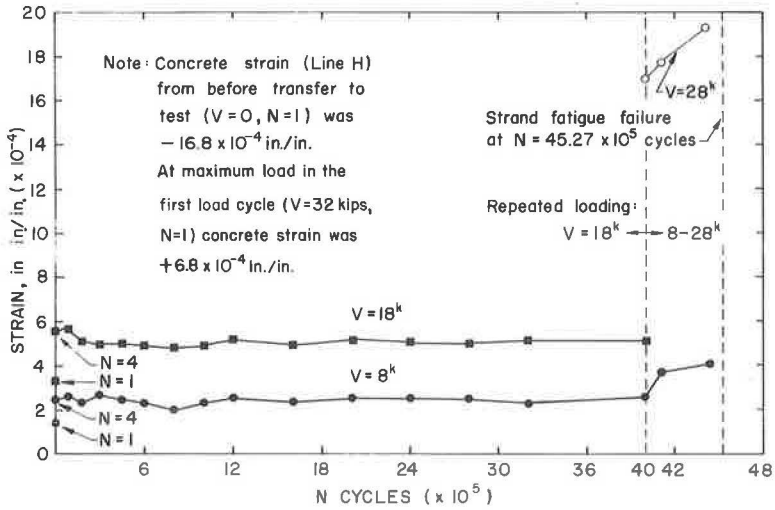


Figure 11. Variation in concrete strain at level of lower strand during test of E.10.

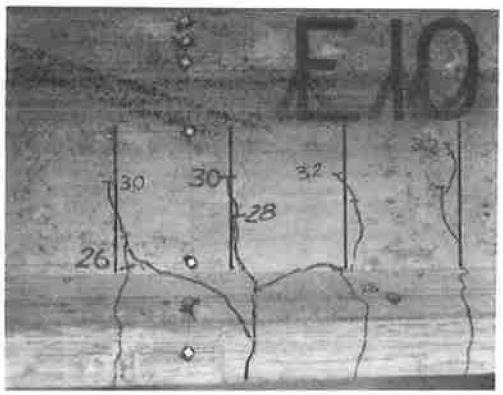


Figure 12. Strand fatigue failure region in E.10.

A closeup view of the failure region in E.10 is shown in Figure 12. The verticle line of Whittemore targets is line 12. The failure was characterized by a sudden increase in the deflection of the test beam and a noticeable opening of the flexural crack in the region where the fatigue fracture of the strand occurred.

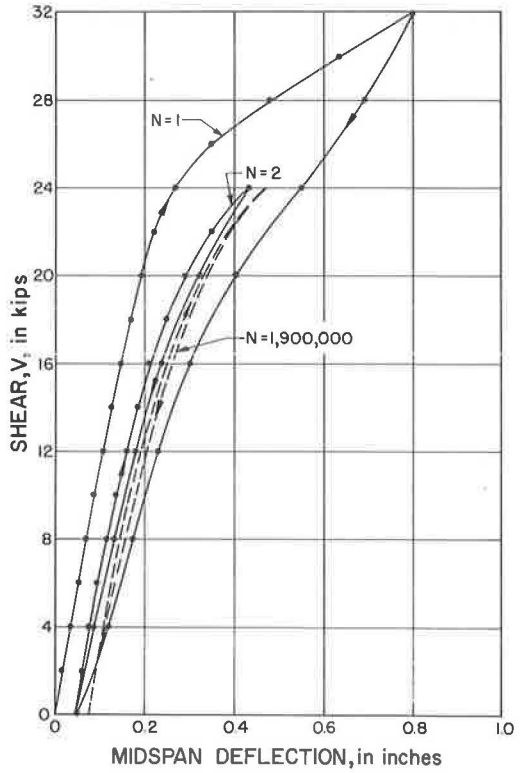


Figure 13. Load-deflection curve for E.11.

## Behavior of E.11

The repeated loading applied to E.11 varied between 8 and 24 kips shear. Failure in E.11 occurred at N equal to 2,007,500 load cycles as a fracture of the third stirrup from the support. An inspection of the failure region showed that the stirrup was not necked down at the fracture, and, therefore, the failure was considered to be a fatigue fracture.

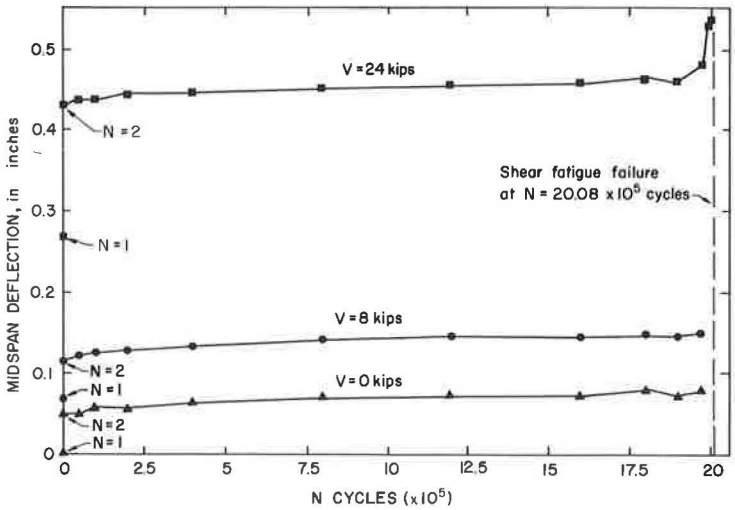


Figure 14. Deflection-N curves for E.11.

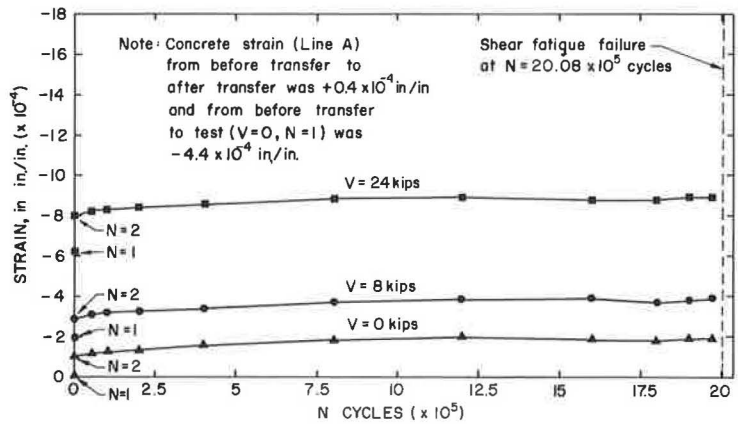


Figure 15. Variation in concrete strain of top fibers during test of E.11.

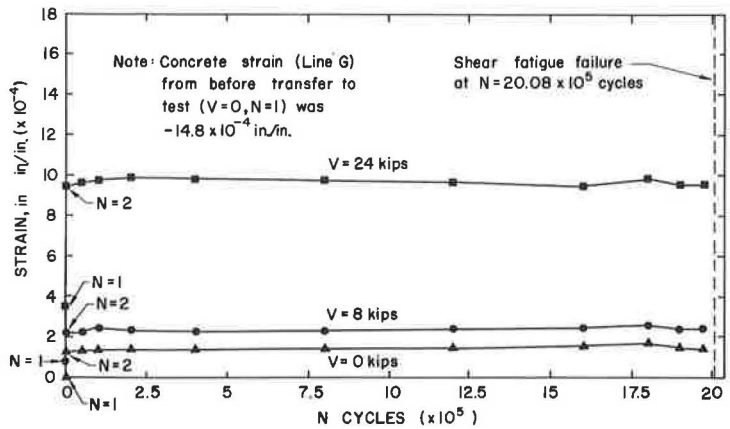


Figure 16. Variation in concrete strain at level of c.g.s. during test of E.11.

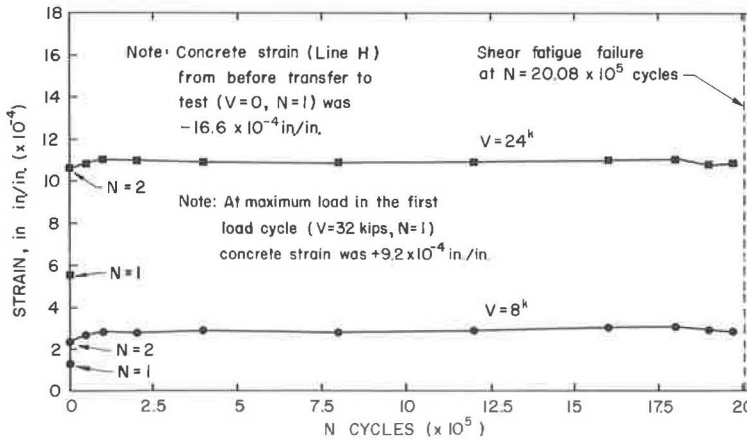


Figure 17. Variation in concrete strain at level of lower strand during test of E.11.

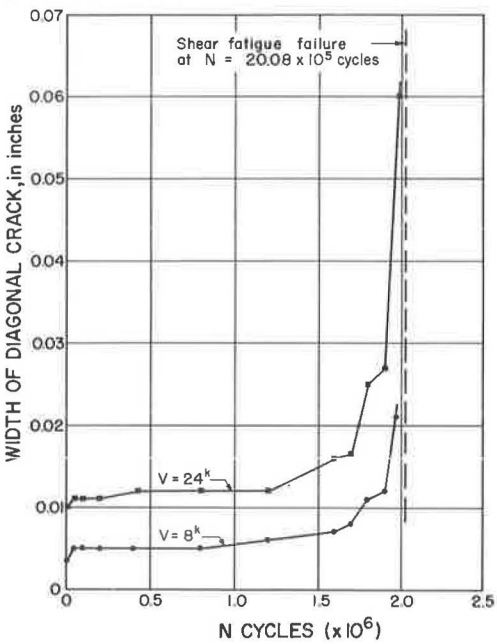


Figure 18. Variation in width of diagonal crack with N for E.11.

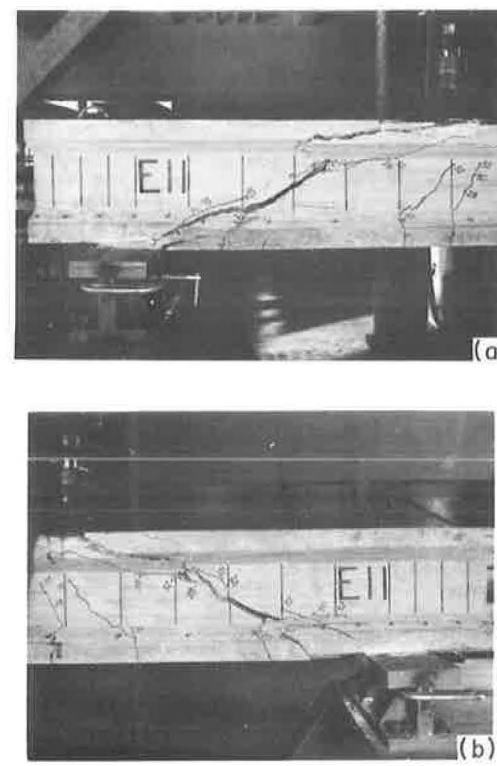


Figure 19. Shear fatigue failure region in E.11: (a) view of end 20; and (b) opposite side view of end 20.

Load-deflection curves for E. 11 at N equal to 1, 2, and 1,900,000 are shown in Figure 13. The deflection-N diagram shown in Figure 14 gives the variation in midspan deflection between N equal to 1 and 1,900,000 for values of shear equal to 0, 8, and 24 kips. Variation in concrete strain in the top fibers, at the c. g. s., and at the level of the lowest strand with N for the indicated values of shear is shown in Figures 15, 16 and 17, respectively.

The location shown in Figure 5 was selected to measure the transverse crack width after the crack had extended completely across the web at a shear of 30 kips. The width at V equal to 30 kips was 0.010 in., and the crack opened an additional 0.001 in.

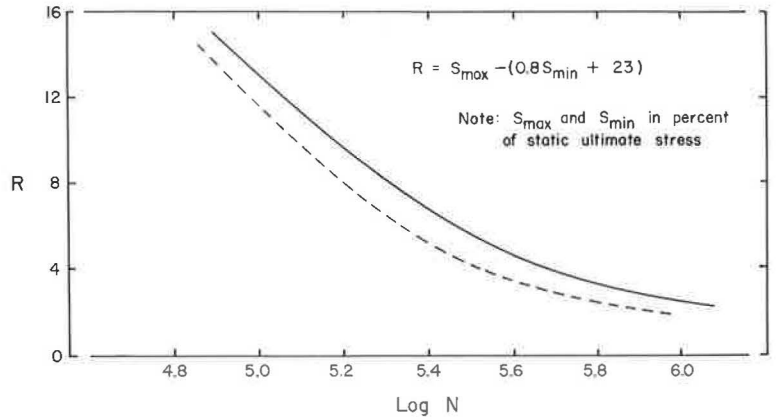


Figure 20. Fatigue properties of $^{7}/_{16}$-in. diameter air furnace stress-relieved prestressing strand.

when the shear was increased to 32 kips. After the beam was unloaded, the crack had a residual width of 0.003 in. Subsequent variation in the width of the crack with N is shown in Figure 18. Again, there was no noticeable opening of the crack up to a shear of 10 kips, after which the increase in width was proportional to the increase in shear.

Closeup views of both sides of the failure region for E.11 are shown in Figure 19. The first visual evidence of structural damage was the noticeable increase in width of the diagonal crack, at approximately N equal to 1,500,000 cycles. Subsequently, noticeable extension of the diagonal cracking occurred, particularly in the region of the tension flange. The last static test was conducted at N equal to 1,970,000 cycles, at which time failure appeared imminent. However, the test beam was able to sustain an additional 77,500 load cycles. During this period, the diagonal crack continued to grow in width, until at failure the width was estimated as greater than $^{3}/_{16}$ in., wide enough to see completely through the web of the beam. The width of the crack appeared to increase at a nonuniform rate to be associated with extensions of the diagonal cracking. Final failure occurred suddenly when the diagonal tension crack extended through the compression flange. After the failure, it was observed that the third stirrup from the support was fractured.

## DISCUSSION

The purpose of the tests on E.10 and E.11 was to determine if a prestressed beam subjected to an overload of sufficient magnitude to cause inclined diagonal tension cracking could subsequently be critical in fatigue of the web reinforcement under repeated loadings of linear magnitude. Identical counterparts of E.10 and E.11 (E.8 and E.9, respectively) have been statically tested by the authors (3, 4). These static tests were conducted on the same shear span to an effective depth ratio of 3.39 that was used for the repeated load tests on E.10 and E.11. Both E.8 and E.9 failed in flexure after the strand had yielded at the same ultimate moment of 167.7 kip-ft, including 2.9 kip-ft for dead-load moment. Therefore, the initial shear of 32 kips applied to E.10 and E.11 may be considered as an overload equal to 78 percent of their ultimate flexural capacity.

As indicated in Figure 11, the concrete strain in E.10 at the level of the lower strand was 0.168 percent compression from before transfer to test. The concrete strain at the same level caused by the application of the initial shear of 32 kips was 0.068 percent tension. Similarly for E.11, as indicated in Figure 17, the concrete strain from before transfer to test was 0.166 percent compression, and 0.092 percent tension due to the initial shear of 32 kips. Assuming that the concrete strain on the surface of the test beams at the level of the lower strand is equal to the change in strain in the strand, the strain in the lower strand at the 78 percent overload was still less than the initial prestressing strain of 0.645 percent. Therefore, no yielding of the strand occurred when the initial shear of 32 kips was applied to either E.10 or E.11.

After the initial overload, E.10 was subjected to 4,000,000 cycles of loading in which V ranged between 8 and 18 kips, corresponding to 21 and 45 percent of the ultimate flexural capacity of the beam. At V equal to 18 kips, the computed stress in the bottom fibers, assuming an uncracked section, was 210 psi tension. This loading range was regarded as representative of a typical bridge girder being repeatedly subjected to its design live load. However, after 4,000,000 cycles of this loading had been applied, there was no indication of structural damage in the member. Figures 7, 9, 10 and 11 show that there was no significant increase in deflection or change in strain in the constant moment region of the beam. Figure 8 shows that the width of the critical diagonal tension crack in the shear span had not increased and, furthermore, there had been no crack growth beyond that caused by the initial overload.

It was concluded that the 8- to 18-kip loading range was below the fatigue limit of the member and, therefore, the maximum shear in the loading range was increased to 28 kips. At V equal to 28 kips, E.10 was being subjected to a maximum moment equal to 69 percent of the ultimate flexural capacity, and the computed stress in the bottom fibers was 1,270 psi tension. Failure occurred after 526,900 cycles of this increased loading due to a fatigue fracture of one outer wire in one of the lower level strands. Figures 7 through 11 show that the deflection, crack width, and concrete strains had not stabilized during the period that this increased loading was applied. There is an indication, however, that this was due to creep, since these quantities were increasing at a decreasing rate and, therefore, were not an indication of the impending failure.

The fatigue fracture in E.10 was accompanied by a sudden increase in the deflection of the beam and a noticeable opening of the flexural crack in the region where the strand fracture occurred. The failure, however, was not catastrophic, and the beam could have carried, statically, a shear at least equal to the maximum shear of 28 kips applied in the repeated load cycle.

Following the initial overload to V equal to 32 kips, E.11 was subjected to a repeated loading which varied between 8 and 24 kips shear. At V equal to 24 kips, the maximum moment in the beam was equal to 59 percent of the ultimate flexural capacity, and the computed stress in the bottom fibers, assuming an uncracked section, was 810 psi tension. E.11 sustained 2,007,500 cycles of this loading before failure occurred.

Figures 14 through 17 show that the midspan deflection and the concrete strain in the constant moment region of E.11 remained nearly constant throughout the test, except for some slight effect of creep during the first part of the test. However, the increase in width of the critical diagonal crack, shown in Figure 18, after approximately 1,500,000 cycles is a definite indication of the impending failure in this region. The crack width was measured at the location where the fatigue fracture occurred. The increase in crack width was also associated with growth of the inclined cracking in the shear span, particularly in the later stages of the test.

The failure in E.11 occurred suddenly and would have been catastrophic under a gravity loading. The apparent cause of failure was the sudden extension of the inclined crack completely through the compression flange. It was subsequently determined that the third stirrup from the support had been fractured. However, it is quite possible that the fatigue fracture of the stirrup occurred before final failure, perhaps as early as N equal to 1,500,000 cycles.

The probable fatigue life of E.10 and E.11 may be determined, assuming that failure occurs at a fatigue fracture in the prestressing strand. The essential information required is the variation in stress with load in the most critically stressed strand, which for E.10 and E.11 is any one of the three lower strands. Since the Whittemore strain readings taken on line H are at the same level as the three lower strands, the assumption that the strain in the concrete is equal to the change in the strain in the strand from the initial prestressing strain permits the determination of the steel strain for any value of N directly from Figures 11 through 17.

Representative values of strain were selected at the minimum and maximum shear in the repeated load tests from Figures 11 and 17. These values were added algebraically to the initial strain of 0.645 percent and the strain from before transfer to test to give the strains in Table 4. The steel strains were converted to stress using the stress-strain curve for the strand in Figure 2.

TABLE 4

STRESS VARIATION IN LOWER LEVEL STRAND

| Beam | Shear, V (kips) | Lower Level Strand | | |
|---|---|---|---|---|
| | | Strain (%) | Stress (ksi) | S (%)[a] |
| E.10 | 8 | 0.500 | 133.0 | 52.6 |
| | 18 | 0.525 | 140.5 | 55.6 |
| | 28 | 0.645 | 173.5 | 68.6 |
| E.11 | 8 | 0.505 | 135.0 | 53.4 |
| | 24 | 0.585 | 157.5 | 62.3 |

[a]Of static ultimate tensile stress of strand.

Warner and Hulsbos (1) have conducted an investigation of the fatigue properties of $\frac{7}{16}$-in. diameter air furnace stress-relieved prestressing strand. The results of their tests are shown in Figure 20, where the solid line shows the relationship between the stress interval, R, and the mean fatigue life, N, of a single strand under constant cycle loading. The expected fatigue life of E.10 or E.11, however, would be less than the solid line because of the greater probability of failure in any one of the three lower level strands. This correction is indicated by the dashed line in Figure 20, which, therefore, represents the mean fatigue life of E.10 or E.11 assuming that a fatigue failure occurs in any of the lower level strand. For the 8- to 18-kip loading range on E.10 and the 8- to 24-kip loading range on E.11, R is negative, which indicates that the stress interval in the strand is below the fatigue limit. For the 8- to 28-kip loading range on E.10, however, R is equal to 3.5 and, therefore, a strand fatigue failure would be expected after 4,000,000 cycles. E.10 actually took 526,900 cycles of this loading range before failure occurred, which is good correlation.

The load-deflection curves for E.10 and E.11 in Figure 6 and 13, respectively, suggest a criterion for judging if fatigue may be critical in a prestressed beam with a diagonal tension crack. After cracking, the load-deflection response for E.10 was essentially linear for V from 0 to 18 kips, but definitely nonlinear as the shear was increased to 28 kips. The load-deflection response for E.11 was also nonlinear as V approached 24 kips. Therefore, in these tests the loadings which caused fatigue failures carried the beam into the nonlinear load-deflection range.

Finally, and perhaps most important, the results of the tests indicate that there are loadings for a prestressed beam which are more critical in fatigue of the web reinforcement than of the prestressing strand. Further testing is needed, particularly on different shear spans and with different amounts of web reinforcement, before the problem can be fully evaluated.

## CONCLUSIONS

A prestressed beam subjected to an overload of sufficient magnitude to develop diagonal tension inclined cracking may be more critical in fatigue of the web reinforcement than in fatigue of the longitudinal prestressing strand. However, the two tests on a shear span-to-effective depth ratio of 3.39 reported here indicate that, in beams with approximately one-half of the web reinforcement required by paragraph 1.13.13 of the AASHO specifications (2), an overload causing diagonal tension cracking will not cause a fatigue failure in the web reinforcement under design loads. A criterion for determining if the member is critical in fatigue after inclined cracking is the linearity of the load-deflection curve. That is, if the repeated loadings are within the range which permits the deflection of the member to remain essentially linear, the probability of a fatigue failure within the normal life of the member is small.

## REFERENCES

1. Warner, R. F., and Hulsbos, C. L. Probable Fatigue Life of Prestressed Concrete Flexural Members. Lehigh Univ., Fritz Eng. Lab. Rept. No. 223.24A, July 1962.
2. Standard Specifications for Highway Bridges. 8th Ed. AASHO, Washington, D. C., 1961.
3. Hanson, J. M., and Hulsbos, C. L. Overload Behavior of Prestressed Concrete Beams with Web Reinforcement. Lehigh Univ., Fritz. Eng. Lab. Rept. No. 223.25, Feb. 1963.
4. Hanson, J. M., and Hulsbos, C. L. Overload Behavior of Pretensioned Prestressed Concrete I-Beams with Web Reinforcement. Highway Research Record No. 76, pp. 1-31, 1965.

# Substructure Influence on Dynamic Stress Response of Superstructures in Composite Bridges

## An Experimental Study

K. H. KINNIER, Professor of Civil Engineering, University of Virginia, and Consultant to the Virginia Council of Highway Investigation and Research; and
WALLACE T. McKEEL, Jr., Bridge Design Engineer, Virginia Council of Highway Investigation and Research

The Virginia Council of Highway Investigation and Research has conducted a study of the dynamic stress response and vibration characteristics of two highway bridges with simply supported composite spans. A test vehicle, simulating an H20-S16-44 standard loading, made runs on the bridges. Both bridges had identical 66-ft 5-in. spans, but one had higher and less stiff piers than the other. Comparison of the data indicates that the stiffness of the substructure has an influence on the response of the superstructure to dynamic loading.

•THE NUMBER of simply supported composite highway bridge spans constructed has substantially increased in the past 10 years, and it appears that this type of bridge is continuing, if not increasing, in popularity. Its wide use can be attributed to ease of construction, economy of materials and aesthetic value. Utilization of the concrete slab to act structurally in conjunction with the steel beam, in addition to its normal function of spanning between the beams, has enabled the engineer to select a lighter steel section, resulting in an appreciable saving in costs. However, the lighter steel section, although satisfactory from a stress consideration, is more susceptible to the dynamic loads of highway traffic. One of the concerns of structural engineers in this type of construction is its frequently objectionable vibration characteristics. In many instances, certain combinations of amplitudes and frequencies of the oscillations of the bridge cause the public apprehension over the safety of the structure. Further, these oscillations have contributed to cracking in the bridge deck and may cause fatigue distress in some instances.

In an attempt to determine if any particular design features of a bridge were related to excessive dynamic response, a general survey of vibration characteristics of composite highway bridges in Virginia was conducted in the summer of 1960 (1). In this survey, amplitudes and frequencies of 67 composite spans excited by the crossing of a truck loaded to simulate an H15 standard loading were measured with an accelerometer pickup, a vibration meter, and a Brush recorder. In examining the resulting data, it was observed that in several instances bridges with very similar superstructures exhibited markedly different vibration responses. This led to a careful study of other bridge features that might influence the superstructure response, and the observation that the tops of relatively high piers oscillated with small, although measurable, amplitudes.

To examine in some detail the influence of the substructure on superstructure response to dynamic loads, a testing program was planned by the Virginia Council of

Paper sponsored by Committee on Field Testing of Bridges.

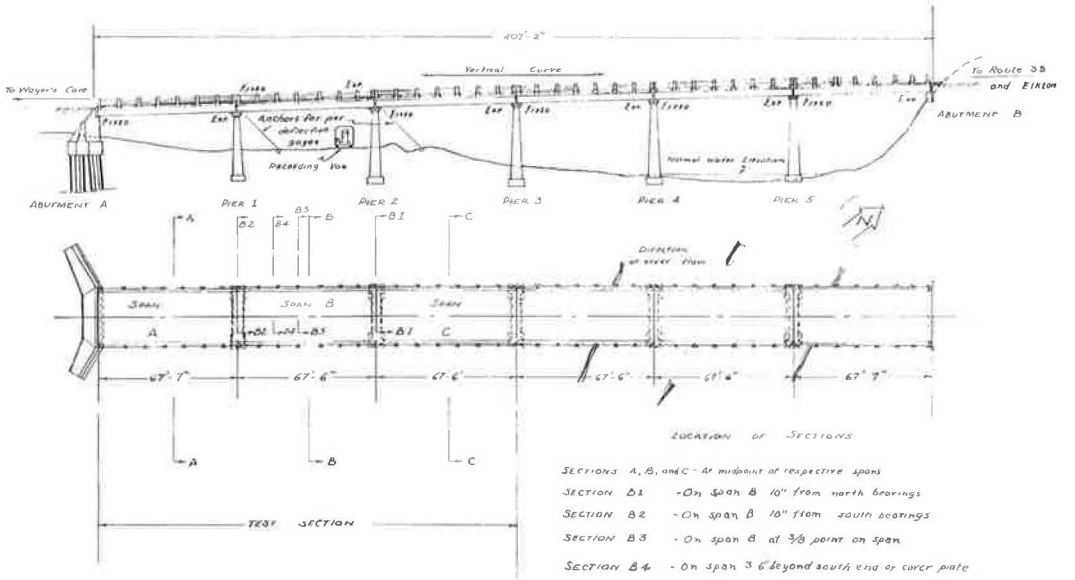


Figure 1. Profile and plan of Weyer's Cave Bridge, indicating test sections.

Highway Investigation and Research, with the cooperation of the Structures and Applied Mechanics Division of the U. S. Bureau of Public Roads. Two bridges were selected as test structures. Each included in its superstructure a Virginia Department of Highways Standard 66-ft 5-in. span, virtually identical, with a 24-ft clear roadway width, a 7 $\frac{1}{2}$-in. composite concrete slab and four 36-in. wide flange steel stringers. All comparative data listed in this paper are for the two like spans, one in each structure. These two spans are indicated as span B in Figures 1 and 2. The difference in the two structures was in the height of the similarly designed piers. The first structure, which was tested in the summer of 1961 is located on Rt. 276 near Weyer's Cave, Va., and is composed of six 66-ft 5-in. spans supported on one gravity abutment, one shelf-type abutment and five solid piers, on spread footings, of unsupported heights ranging from 18 to 22 ft measured from ground level to top of pier cap. The second structure, which was tested in the summer of 1962, is located on Rt. 729 across the Hazel River near Culpeper, Va., and is composed of three spans, a 66-ft 5-in. center span and two end spans of 61 ft 5 in. each. The substructure here consists of two shelf-type abutments and two solid piers of unsupported heights ranging from 14 to 15 ft, all of which are supported on timber piles. Pertinent details of both structures, including plan and elevation views, cross-sections of the 66-ft 5-in. spans, and details of the piers supporting the 66-ft 5-in. spans are shown in Figures 1, 2, 3 and 4.

The instrumentation and recording equipment, provided, installed and operated by personnel of the Structures and Applied Mechanics Division of the U. S. Bureau of Public Roads, were essentially the same as that used in the Illinois AASHO Road Test and in a number of similar bridge testing programs in other states. The equipment included an instrument trailer outfitted with oscillographs and amplifiers capable of permanently recording on sensitized paper through light-beam galvanometers the output of up to 48 strain or deflection gages. In effect, for the time of passing of the test vehicle on each of its runs, a complete recording was made for live-load strain at 34 bridge positions and live-load deflection at 12 positions. Pneumatic traffic tubes were installed at each end of the two bridges and several intermediate positions to operate air switches which recorded a signal on the sensitized paper each time a wheel crossed them. From these recordings the position of the test vehicle could be related to the resulting stresses and deflections. The oscillogram traces were easily converted to unit stresses or deflections by multiplying the ordinates measured from

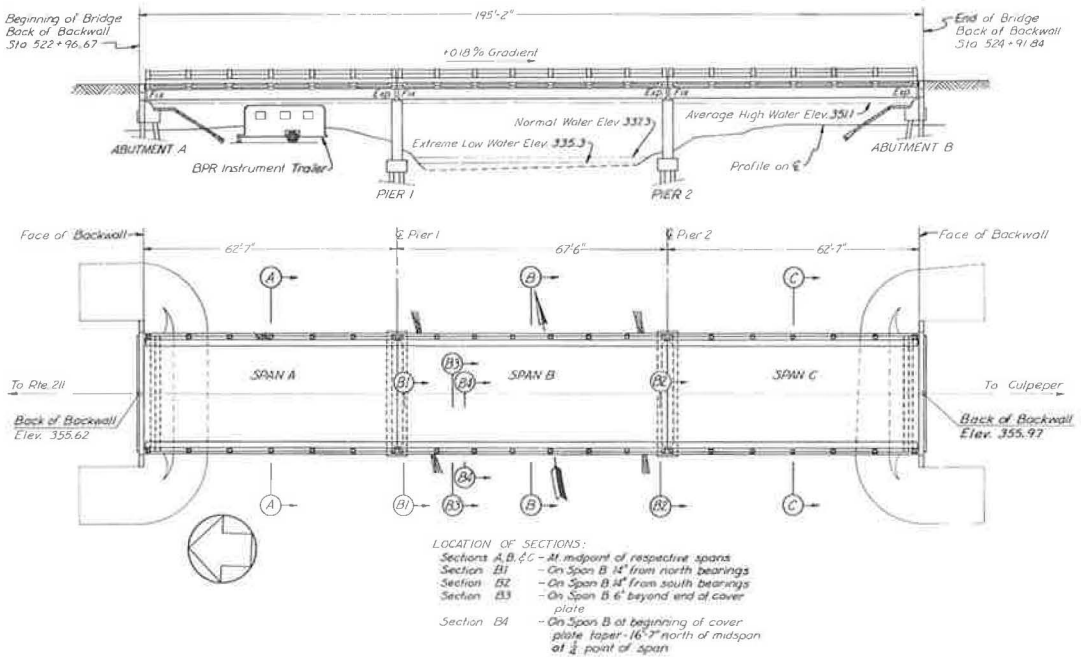


Figure 2. Profile and plan of Hazel River Bridge, indicating test sections.

the traces by constants computed from the equipment sensitivity and the individual gage characteristics. In addition to the oscillographs for recording the traces representing stresses and deflections, the instrument trailer also housed complete facilities to develop the sensitized record paper.

The testing procedure for both the Weyer's Cave Bridge and the Hazel River Bridge was essentially the same, although a greater number of runs were made on the Hazel River Bridge. The test results provided a very complete account of the stresses and deflections developed in both structures from the heavy H20-S16 loading passing over the bridges at a complete range of normal speeds and a full range of transverse positions.

The test procedure consisted of a 3-axle tractor-trailer, loaded to simulate an H20-S16-44 standard loading, passing across the test spans at speeds from creep (approximately 5 mph) to 45 mph in 5-mph increments and in three lateral positions for the Weyer's Cave Bridge and in five lateral positions for the Hazel River Bridge. Ninety-six crossings of the test vehicle were made in the Weyer's Cave tests and 189 crossings at Hazel River. The bridge responses measured and analyzed were midspan live-load deflections, live-load strains at 34 selected positions (32 on the Hazel River Bridge), and longitudinal displacement at pier tops.

From these measurements, the following characteristics of the test structures were determined and compared:

1. Transverse live-load distribution to the four stringers,
2. Position of the neutral axis in the stringers,
3. Fundamental frequency of vibration,
4. Logarithmic decrement of the bridge oscillation,
5. Amplitudes of vibration, and
6. Impact factors based on strains and deflections.

Only a portion of the results of this investigation is presented in this paper. However, detailed reports of these two tests, entitled A Dynamic Stress Study of the Weyer's Cave Bridge, 1963, and A Dynamic Stress Study of the Hazel River Bridge, 1964, are available from either the U. S. Bureau of Public Roads, Structures and

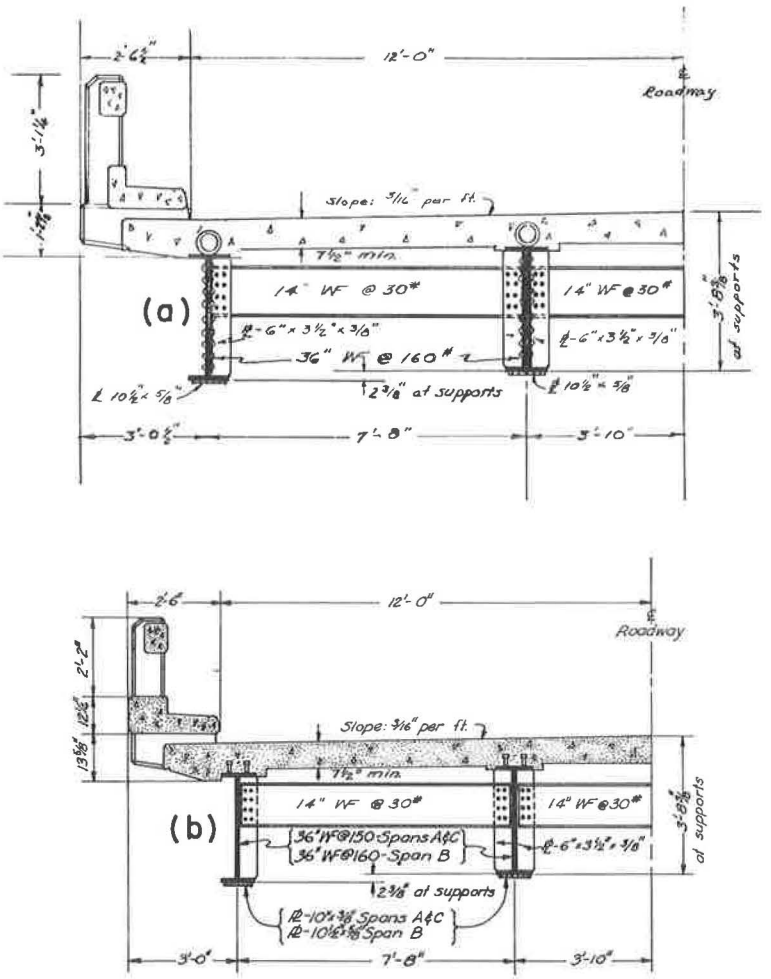


Figure 3. Half-transverse section of virtually identical 66-ft 5-in. spans B: (a) Weyer's Cave Bridge; and (b) Hazel River Bridge.

Applied Mechanics Division, or the Virginia Council of Highway Investigation and Research. Included in the second report are comparisons of the various measured responses of the superstructures and pier tops of the two bridges with the supporting test data.

Four of the most important conclusions are presented and discussed with the supporting experimental data in the following sections of this paper.

1. The lower flange midspan stresses and deflections of the Hazel River Bridge were appreciably smaller for each speed than the corresponding values for the Weyer's Cave Bridge. These comparisons can be observed in Table 1 which indicates that for the interior beams, 2 and 3, the Weyer's Cave Bridge stresses range from 8.2 percent (at 40 mph) to 23.4 percent (at 10 mph) above the corresponding Hazel River Bridge stresses. Also, the Weyer's Cave Bridge lower flange midspan deflections were larger than the corresponding values for the Hazel River Bridge. The percentage differences ranged from a low of 5.7 percent (20 mph) to 31.0 percent (10 mph).

2. The amplitudes of oscillation of the stringers increased with increased speeds for both bridges. The amplitudes for the Hazel River Bridge stringers were appreciably

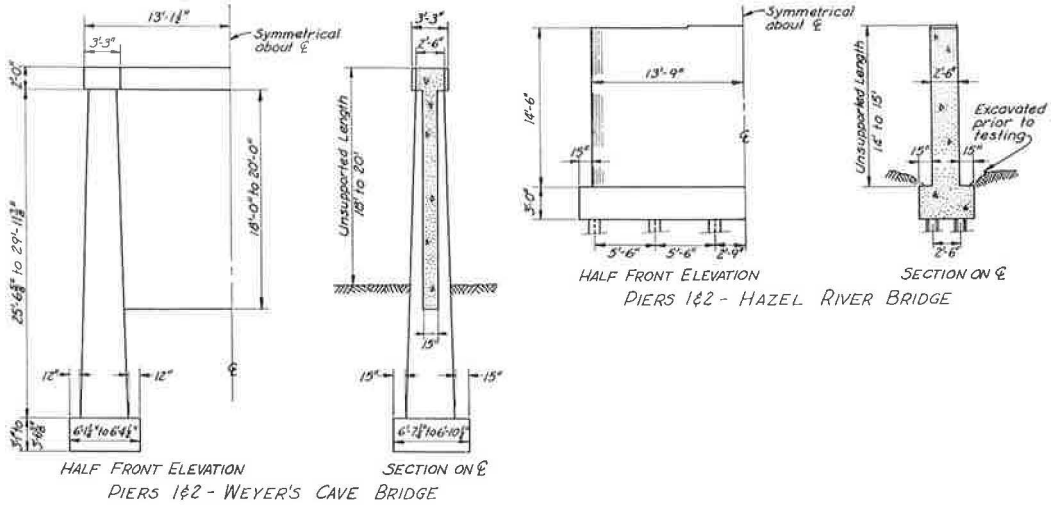


Figure 4. Details of pier supporting two 66-ft 5-in. spans B of Weyer's Cave Bridge and Hazel River Bridges.

TABLE 1

COMPARISON OF MIDSPAN STRESSES, DEFLECTIONS, DOUBLE AMPLITUDES AND PIER TOP MOVEMENTS

| Nominal (mph) | Speed: Average (mph) | | Peak Longitudinal Displacements of Pier Tops from Equilibrium Position: Pier 1 (in.) | | Pier 2 (in.) | | Pier 1 + Pier 2 (in.) | | Midspan Peak Stresses[a] (psi) | | Midspan Peak Deflections[a] (in.) | | Midspan Double Amplitude[a] (in.) | |
|---|---|---|---|---|---|---|---|---|---|---|---|---|---|---|
| | Weyer's Cave | Hazel River | Weyer's Cave | Hazel River | Weyer's Cave | Hazel River | Weyer's Cave | Hazel River | Weyer's Cave | Hazel River | Weyer's Cave | Hazel River | Weyer's Cave | Hazel River |
| Creep | - | 3.6 | 0.017 | 0.013 | 0.014 | 0.011 | 0.031 | 0.024 | 2710 | 2250 | 0.185 | 0.145 | 0.015 | 0.010 |
| 10 | 9.6 | 9.2 | 0.017 | 0.014 | 0.018 | 0.011 | 0.035 | 0.025 | 2885 | 2340 | 0.190 | 0.145 | 0.035 | 0.010 |
| 15 | 15.7 | 15.0 | 0.017 | 0.014 | 0.020 | 0.012 | 0.037 | 0.026 | 2630 | 2320 | 0.175 | 0.160 | 0.037 | 0.030 |
| 20 | 21.0 | 19.8 | 0.020 | 0.016 | 0.021 | 0.012 | 0.041 | 0.028 | 2930 | 2530 | 0.185 | 0.175 | 0.060 | 0.010 |
| 25 | 26.4 | 24.6 | 0.018 | 0.016 | 0.015 | 0.012 | 0.033 | 0.028 | 2580 | 2330 | 0.180 | 0.150 | 0.047 | 0.020 |
| 30 | 31.2 | 29.2 | 0.020 | 0.013 | 0.021 | 0.012 | 0.041 | 0.025 | 2900 | 2600 | 0.185 | 0.155 | 0.055 | 0.015 |
| 40 | 40.3 | 37.6 | 0.025 | 0.016 | 0.018 | 0.012 | 0.043 | 0.028 | 2910 | 2690 | 0.200 | 0.175 | 0.092 | 0.040 |
| Flank | 41.7 | 45.7 | 0.020 | 0.015 | 0.027 | 0.014 | 0.047 | 0.029 | 2925 | 2460 | 0.190 | 0.175 | 0.083 | 0.055 |

[a]Average of beams 2 and 3.

less than the corresponding amplitudes of the Weyer's Cave Bridge, as can be observed in Table 1 for the two interior beams, 2 and 3, for centerline runs. Figures 5, 6 and 7 show the double amplitudes plotted against speed for each of the four stringers, for the three instrumented spans of each structure and for test vehicle runs on the centerline as well as the two curb positions. As previously mentioned, span B of each structure is the one for which comparisons can be made as they are virtually identical Virginia Department of Highways 66-ft 5-in. span standard designs. Whereas spans A and C of the Weyer's Cave Bridge are identical to the spans B, spans A and C of the Hazel River Bridge are 61 ft 5 in. in length.

It can be observed from Figures 5, 6 and 7 that the double amplitudes of the midspan positions of the four beams are sensitive to the path of the test vehicle. The double amplitudes of beam 1 are the greatest when the test vehicle is in the east curb lane and the double amplitudes of beam 4 are the greatest when the test vehicle is in the west curb lane.

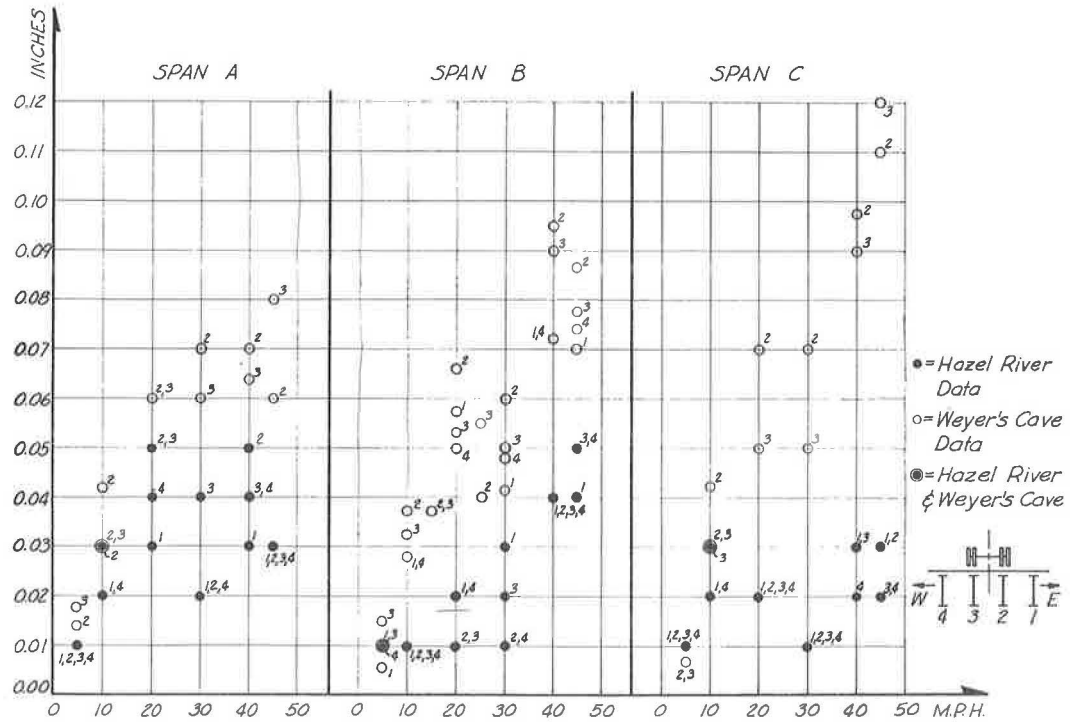


Figure 5. Average midspan double amplitudes vs nominal speeds (centerline).

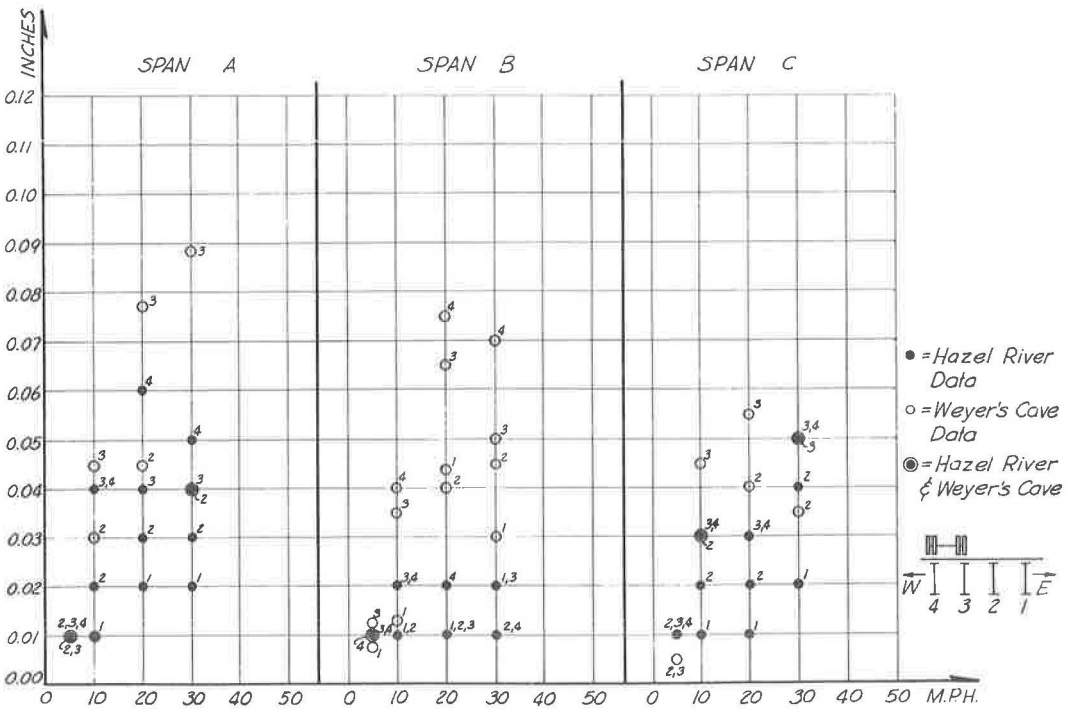


Figure 6. Average midspan double amplitudes vs nominal speeds (west curb).

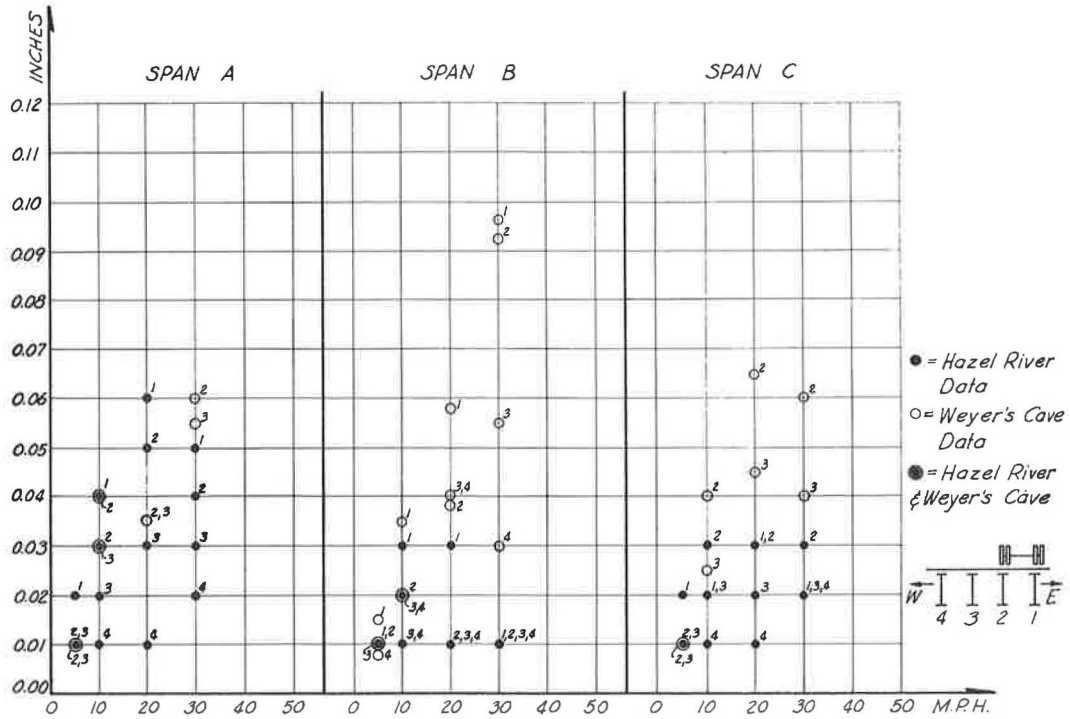


Figure 7. Average midspan double amplitudes vs nominal speeds (east curb).

3. The pier top longitudinal displacements were of comparable magnitude to the vertical oscillations of the deflected stringers at the midspan positions and were sensitive to the lateral position of the test vehicle on its runs. The magnitudes of the pier top movements of the Hazel River Bridge were considerably less than those of pier top movements of the Weyer's Cave Bridge.

The pier top displacement data are summarized for centerline runs in Table 1 and are given in more detail, including east and west curb runs, in Table 2.

For the centerline runs, the two gages on each pier moved in unison, but for the curb runs, there were noticeable differentials in the movements of the two gage positions. Larger pier movements occurred on the side of the test vehicle location, indicating slight twisting of the pier about a vertical center axis. The peak movements ranged from 0.007 to 0.018 in., with a great majority of the values falling in the 0.011- to 0.016-in. range.

It is interesting to compare the size of the pier movements with the double amplitudes (Table 1) of the midspan position of the span B stringers for each bridge. The pier movements for the Hazel River Bridge are consistently smaller than the corresponding values for the Weyer's Cave Bridge; however, they are larger in proportion to the double amplitudes of the midspan position of the 66-ft 5-in. span B. This, of course, follows from the fact that the midspan double amplitudes of span B of the Hazel River Bridge are substantially smaller than the corresponding values for the Weyer's Cave structure.

In the analysis of the strain gage and deflection gage data taken from the oscillogram tapes, the direction of the displacements and signs of the strains, as well as the magnitudes of the displacements and stresses, can be readily determined. Also on the oscillogram tapes were signals recorded when the test vehicle crossed air hoses laid across the bridge decks. From this information, it was observed that the pier tops were displaced toward the span on which the vehicle was located. It was also observed that the frequency of vibration of the piers with the vehicle off the structure was

TABLE 2

PEAK LONGITUDINAL DISPLACEMENTS OF PIER TOPS FROM EQUILIBRIUM POSITION

| Nominal Speed (mph) | Pier[a] | Hazel River | | | Weyer's Cave | | |
|---|---|---|---|---|---|---|---|
| | | Under Beam 2 (in.) | Under Beam 3 (in.) | Avg. (in.) | Under Beam 2 (in.) | Under Beam 3 (in.) | Avg. (in.) |
| (a) East Curb Runs | | | | | | | |
| Creep | 1 | 0.015 | 0.010 | 0.012 | 0.018 | 0.012 | 0.015 |
| | 2 | 0.010 | 0.007 | 0.008 | 0.016 | 0.010 | 0.013 |
| 10 | 1 | 0.014 | 0.009 | 0.012 | 0.019 | 0.020 | 0.020 |
| | 2 | 0.012 | 0.007 | 0.010 | 0.016 | 0.007 | 0.012 |
| 20 | 1 | 0.017 | 0.011 | 0.014 | 0.021 | 0.017 | 0.019 |
| | 2 | 0.011 | 0.010 | 0.010 | 0.017 | 0.010 | 0.014 |
| 30 | 1 | 0.013 | 0.012 | 0.012 | 0.018 | 0.015 | 0.017 |
| | 2 | 0.013 | 0.009 | 0.011 | 0.020 | 0.018 | 0.019 |
| (b) Centerline Runs | | | | | | | |
| Creep | 1 | 0.013 | 0.013 | 0.013 | 0.017 | 0.017 | 0.017 |
| | 2 | 0.010 | 0.012 | 0.011 | 0.015 | 0.013 | 0.014 |
| 10 | 1 | 0.015 | 0.014 | 0.014 | 0.017 | 0.016 | 0.017 |
| | 2 | 0.011 | 0.011 | 0.011 | 0.017 | 0.018 | 0.018 |
| 20 | 1 | 0.016 | 0.017 | 0.016 | 0.019 | 0.020 | 0.020 |
| | 2 | 0.011 | 0.014 | 0.012 | 0.020 | 0.022 | 0.021 |
| 30 | 1 | 0.012 | 0.014 | 0.013 | 0.020 | 0.020 | 0.020 |
| | 2 | 0.012 | 0.013 | 0.012 | 0.022 | 0.020 | 0.021 |
| 40 | 1 | 0.017 | 0.016 | 0.016 | 0.026 | 0.023 | 0.025 |
| | 2 | 0.011 | 0.013 | 0.012 | 0.016 | 0.019 | 0.018 |
| Flank | 1 | 0.016 | 0.014 | 0.015 | 0.019 | 0.020 | 0.020 |
| | 2 | 0.014 | 0.015 | 0.014 | 0.033 | 0.020 | 0.027 |
| (c) West Curb Runs | | | | | | | |
| Creep | 1 | 0.010 | 0.014 | 0.012 | 0.014 | 0.018 | 0.016 |
| | 2 | 0.010 | 0.013 | 0.012 | 0.012 | 0.015 | 0.014 |
| 10 | 1 | 0.010 | 0.016 | 0.013 | 0.017 | 0.016 | 0.017 |
| | 2 | 0.008 | 0.013 | 0.010 | 0.010 | 0.015 | 0.013 |
| 20 | 1 | 0.010 | 0.018 | 0.014 | 0.018 | 0.021 | 0.020 |
| | 2 | 0.007 | 0.016 | 0.012 | 0.014 | 0.019 | 0.017 |
| 30 | 1 | 0.009 | 0.015 | 0.012 | 0.017 | 0.018 | 0.018 |
| | 2 | 0.010 | 0.015 | 0.012 | 0.014 | 0.019 | 0.017 |

[a]Piers 1 and 2 support virtually identical spans B of the two bridges.

in close agreement with the frequency of the superstructure. This would indicate that the movements of the piers resulted from a forced vibration, contributed by the superstructure.

4. Logarithmic decrements as determined from the recorded traces of selected representative strain and deflection gages indicated that the oscillations of the Hazel

TABLE 3

AVERAGE LOGARITHMIC DECREMENTS

| Position | Lower Flange Strains | | Deflection Gages | |
|---|---|---|---|---|
| | Weyer's Cave | Hazel River | Weyer's Cave | Hazel River |
| Midspan A | 0.137 | 0.117 | 0.074 | 0.134 |
| Midspan B | 0.064 | 0.143 | 0.063 | 0.131 |
| Midspan C | 0.085 | —[a] | 0.067 | 0.170 |
| Pier 1 | - | - | 0.113 | -[a] |
| Pier 2 | - | - | 0.108 | -[a] |

[a]Strains and deflections at these positions not adaptable to determinations of logarithmic decrements.

River Bridge damped out more quickly than did the oscillations of the Weyer's Cave Bridge. Logarithmic decrements of the oscillations recorded on the oscillograms were determined for as many traces as could be used for this purpose. However, only the oscillograms showing a regular decay pattern representative of viscous damping were used to compute the decrements and most of the strain and displacement recordings for the two short (61-ft 5-in.) end spans of the Hazel River Bridge were eliminated from consideration. Further, logarithmic decrements could not be determined from any of the traces of the Hazel River Bridge pier top movements because of the rapid dying out of the oscillations.

It is noted for comparison in Table 3 that the logarithmic decrements for the 66-ft 5-in. span B of the Weyer's Cave Bridge averaged 0.064 for the strain traces of the four stringers and 0.063 for the deflection traces. For span B of the Hazel River Bridge, the logarithmic decrements were 0.143 for the strain traces and 0.131 for the deflection traces. It is evident that the vibrations of the Hazel River Bridge center span died out consistently quicker than did the vibrations of the Weyer's Cave Bridge.

Also for comparison, it is noted that logarithmic decrements of 0.113 and 0.108 were determined for the two instrumented pier tops of the Weyer's Cave Bridge, whereas the pier top oscillations of the Hazel River Bridge were of such short time duration and of such an irregular nature that logarithmic decrements could not be determined. These relative results are consistent with what one would predict, inasmuch as the Weyer's Cave Bridge piers are 18 to 22 ft high and the Hazel River Bridge piers are 14 to 15 ft high, in each instance measured from the ground level to the top of pier cap.

## SUMMARY AND CONCLUSIONS

The results of this study indicate that when a vehicle crosses a simply supported span, the tops of the supporting piers are displaced toward the center of the span. The amount of this displacement varies substantially with the stiffness of the piers.

Span B of the Weyer's Cave Bridge, virtually identical to span B of the Hazel River Bridge but supported on higher more flexible piers, showed the following noticeably different responses from the dynamic loading:

1. Midspan peak stresses and deflections were generally higher for the Weyer's Cave Bridge than for the corresponding measurements for the Hazel River Bridge;
2. Midspan amplitudes of vibration were greater for the Weyer's Cave Bridge than the corresponding values for the Hazel River Bridge; and
3. Vibrations were damped out less rapidly in the Weyer's Cave Bridge than in the Hazel River Bridge.

It may be concluded from this investigation that the stiffness of the substructure elements can, in some cases, affect the characteristics of the superstructure under dynamic loading.

Although it is obvious that excessive vibration in bridge structures of this type can be controlled by stiffening the bridge stringers themselves, it appears from the results of these tests that the superstructure vibration can be meliorated, to some extent, by selecting a more rigid substructure. Frequently, in the selection of types of piers to be used for a bridge structure, a choice is made between slender more flexible piers with a saving in material and more costly formwork, or heavier more bulky piers which utilize more material but require less expensive formwork. It is suggested that the second alternative would be the better choice for longer spans where objectionable vibrations are most likely to develop. It can also be pointed out, for example, that an increase from 20- to 24-in. diameter pier columns would result in more than doubling the moment of inertia of the columns and probably in a more tolerable vibration condition in the bridge deck.

## REFERENCE

1. Progress Report No. 1, Vibration Survey of Composite Bridges. Virginia Council of Highway Investigation and Research.

# Tests Evaluating Punching Shear Resistance of Prefabricated Composite Bridge Units Made with Inverted Steel T-Beams

J. F. McDERMOTT, Senior Research Engineer, U. S. Steel Applied Research Laboratory, Monroeville, Pennsylvania

Design information is developed for a special type of prefabricated composite superstructure unit for bridge spans in the 30- to 70-ft range. These steel and concrete units consist of span-length, 7-in. thick reinforced concrete slabs 6 to 10 ft wide. The webs of a pair of inverted T-shaped steel beams are embedded in each slab. Horizontal steel studs welded at intervals to the beam webs act as shear connectors. Since no steel top flanges are present over the beam webs, the spacing of the studs might be critical in preventing the web from punching through the slab under wheel loads of heavy trucks. To evaluate the resistance of two particular prefabricated units to punching shear and to develop general design information for determining safe stud spacings, tests were conducted on two 10-ft wide by 5½-ft long specimens representing a section of a typical bridge. The studs were spaced at 4-in. intervals in one specimen and at 10-in. intervals in the other. Both specimens were supported and loaded so that they would be subjected to punching shear.

Both specimens failed in a similar manner at loads that were about 5 times greater than the maximum wheel load (including 30 percent for impact) specified by AASHO for H20 or H20-S16 type trucks. The mode of failure appeared to be a combination of tension and bond failure in the concrete rather than a punching-type failure. Therefore, under actual highway loadings, failure of the slab by punching of the web through the concrete would not be expected even with large stud spacings in the portions of a bridge span where punching shear is the major force transferred between the concrete and the steel. The vertical shears created by wheel loads seem to be transferred from the slab to the beam web by both shear in the studs and bearing on top of the web. However, the amount of shear transferred by each mechanism could not be determined.

A method of determining the safe spacing of studs for resisting combined punching and horizontal shear was developed and was based on the conservative assumption that the studs carry all the punching shear. It was also assumed that the intensity of the punching shear was proportional to the deflection of the slab near the web, and that a conservative approximation of this relationship is that the shear intensity varies parabolically—from zero to maximum shearing stress to zero—over an 8-ft length. This procedure permits calculation of the maximum vertical shear per stud, thereby enabling possible use of conventional procedures in designing these prefabricated superstructure units.

---

Paper sponsored by Committee on Steel Superstructures.

•IN COOPERATION with the Indiana Steel Fabricators Association, the U. S. Steel Applied Research Laboratory is developing design information for a special type of prefabricated composite steel and concrete superstructure unit for highway bridges that is intended to be competitive mainly with prestressed concrete box beams for spans ranging from about 30 to 70 ft. These prefabricated bridge units are designed to be 6 to 10 ft wide and of span length. Typical details of their construction are given in the nondimensional sketch shown in Figure 1. Each unit consists of a 7-in. thick reinforced concrete slab supported by a pair of span-long steel beams that have the shape of an inverted T instead of the usual I-shape. The two beams are so placed that the top $3\frac{1}{2}$ in. of each web are embedded in the concrete. Horizontally positioned steel studs are welded to each side of each steel web along a line $1\frac{3}{4}$ in. from the top of the web. These studs transfer shear between the concrete and the steel shapes, and thereby make composite action possible. At the bridge site, adjacent slabs are connected through longitudinal grouted keyways and by transverse tie rods (Fig. 1).

Most of the problems involved in the design of bridges in which these prefabricated units are to be used can be solved by standard bridge design procedures. However, the elimination of the conventional steel top flanges suggests that wheel loads might cause the steel webs to punch through the concrete locally because no top flange is present to support heavy wheel loads, such as the 20,800-lb total wheel load (16,000-lb live load plus 30 percent for impact) specified by the American Association of State Highway Officials (AASHO) (1) for the H20 and H20-S16 loadings for which most major highways are designed.

The behavior of the slab in resisting this tendency of the web to punch through is very complex. When a wheel load is placed on a deck, vertical shears are created in the slab around the wheel and must be transferred into the beams by a combination of (a) bearing on the top surfaces of the studs, (b) bearing on the top surface of the beam webs, and (c) bond between the concrete and the adjacent vertical faces of the steel webs, although the contribution of this bond is probably small. Furthermore, near the ends of a bridge, the horizontal shear developed in the studs by composite action interacts significantly with the vertical shear transferred by the studs. The basic design problem, therefore, is to determine safe stud spacings that will resist mainly punching shear in the center of the span, where not much horizontal shear is present, and also resist combined punching and horizontal shear near the ends of the span, where horizontal shear is usually most significant. However, because the manner in which the vertical shears from the wheel loads are transferred from the slab to the studs and webs is very

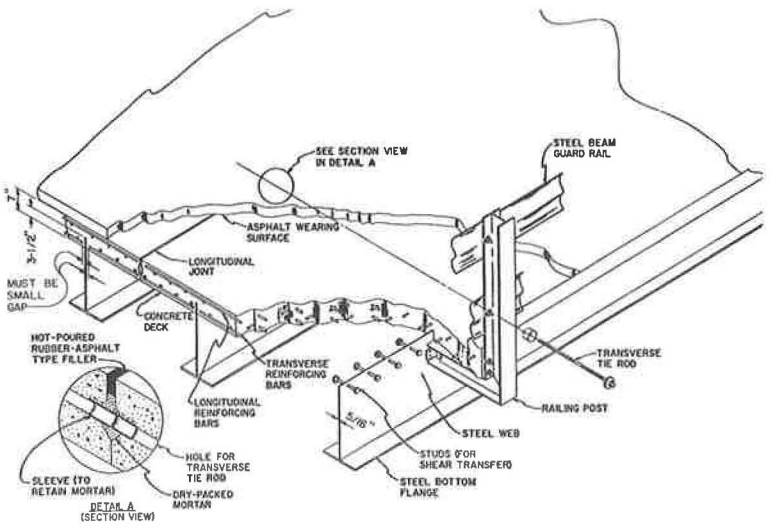


Figure 1. Prefabricated composite highway bridge unit with inverted steel T-Beams.

complex, accurate calculations for determining the stud spacing required to resist punching shear alone or punching shear in combination with horizontal shear due to composite action could not be made on a theoretical basis.

Consequently, the simple tests described herein were performed to determine experimentally whether a 4- and a 10-in. stud spacing would be adequate for resisting punching shear due to an H20 or H20-S16 loading, and if possible, to establish rules for calculating safe stud spacings to resist combined punching and horizontal shear. The results of the tests and the development of design information for determining these safe stud spacings are described.

## MATERIALS AND EXPERIMENTAL WORK

For the testing program, two double-web units, differing only in the number of steel studs welded to the webs, were constructed at the U. S. Steel Applied Research Laboratory. The steel T's with studs attached were furnished by the Indiana Steel Fabricators Association. As shown in Figure 2, each test specimen was 10 ft wide by $5\frac{1}{2}$ ft long. This specimen size represented a portion of a 10-ft wide prefabricated unit between two transverse cross-sections $5\frac{1}{2}$ ft apart. The 10-ft width was selected for the tests because, theoretically, localized shears are greater in a 10-ft wide unit than in a narrower unit. The $5\frac{1}{2}$-ft length was selected because before the tests were performed it was believed that the punching shears from a wheel load would be most critical within such a length, and because of the size limitations in the laboratory test setup. The beams were fabricated T's consisting of $7\frac{1}{2}$- by $\frac{5}{16}$-in. webs and $7\frac{1}{2}$- by $\frac{5}{16}$-in. flanges of ASTM A441 steel, the thickness of the web being the least that would be used in an actual bridge. These particular flange and web dimensions were used for convenience in testing and are different from those that would be used in an actual bridge; however, these dimensional differences would not affect the type of test performed. The transverse distance between centers of the webs (interior span) was 6 ft, and each cantilever

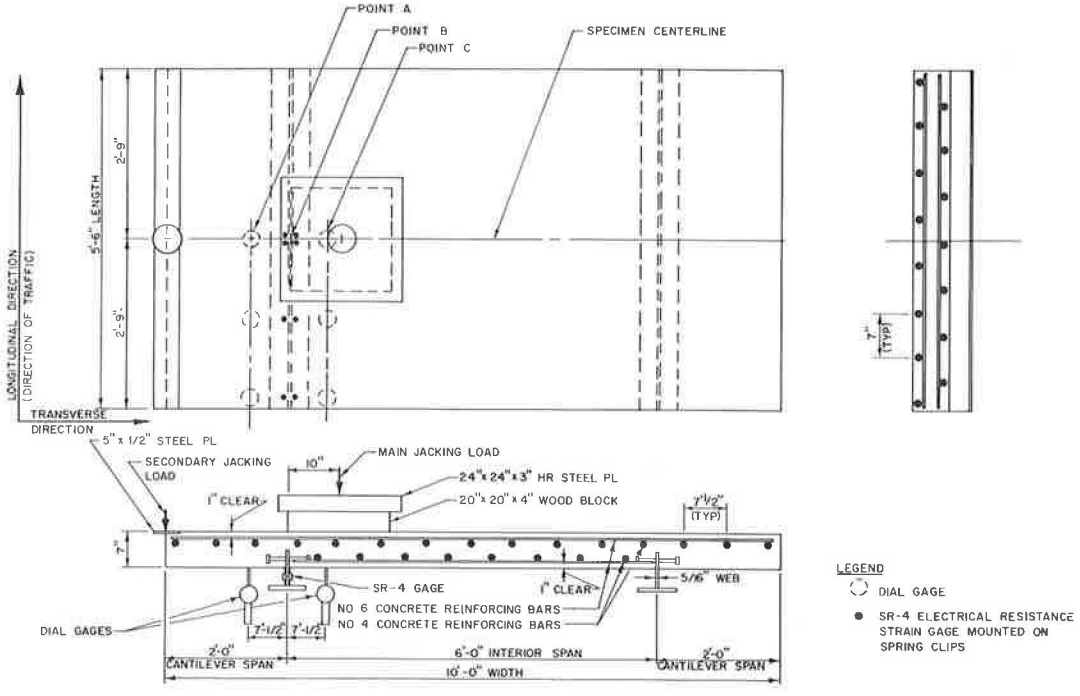


Figure 2. Testing arrangement for experimental T-cast units and details of their construction.

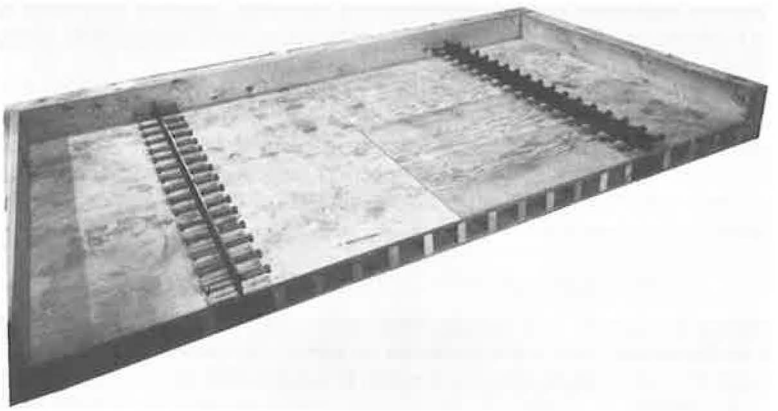

Figure 3. Casting form (one side removed) showing arrangement of studs (spaced at 4-in. intervals) on webs in experimental unit made for test 1.

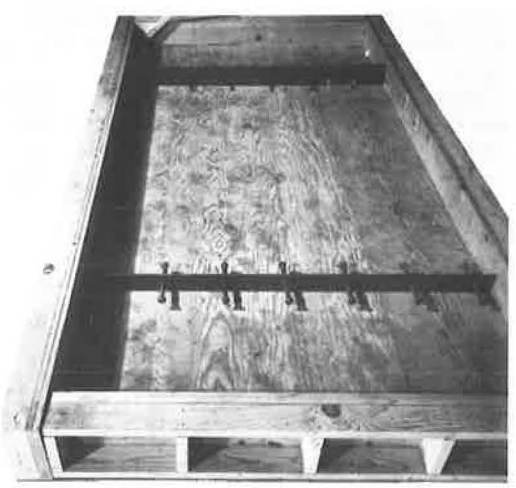

Figure 4. Casting form showing arrangement of studs (spaced at 10-in. intervals) on webs in experimental unit made for test 2.

span projected 2 ft beyond the web. The stud spacing on each side of each web was 4 in. for the specimen used in test 1 and 10 in. for the specimen used in test 2, as shown in Figures 3 and 4, respectively. These standard welded studs (1) were 4 in. long, with a $\frac{3}{4}$-in. diameter shank and a $1\frac{1}{4}$-in. head diameter. In accordance with the formulas in the highway bridge specifications (1), both slabs were reinforced transversely and longitudinally with intermediate grade steel reinforcing bars of sizes No. 6 and No. 4, respectively. Their locations in the slab are shown in Figure 2. The average ultimate compression strength of the concrete at the time the bridge units were tested was 3,710 psi, as determined by compression tests on four 6-in. diameter by 12-in. high concrete cylinders.

In each test, the specimen was placed with the steel T-flanges resting on a firm support so that no horizontal shear would occur. As shown in Figures 5 and 6, vertical loads were then applied by hydraulic jacks, in a manner simulating tire loadings from heavy H20-S16-type trucks positioned to produce maximum punching shear in the specimen. That is, the main vertical load was applied on a 20- by 20-in. wood block that simulated the imprint area of dual H20-type tires and was centered on the specimen centerline so that the edge of the wood block lined up with the interior face of a web. Positioning of the main load at this point should produce maximum punching shear in the interior span. However, in bridges built with these prefabricated units, consideration must also be given to the effect of loads on adjacent units. For example, when two trucks are simultaneously in adjacent lanes, and wheel loads of each truck are located so that they are 4 ft apart across the longitudinal joint between units, a downward reaction from the adjacent unit may occur along the joint edge. This reaction, theoretically as much as about 30 percent of a wheel load, increases the maximum punching shear in the interior span of the unit re-

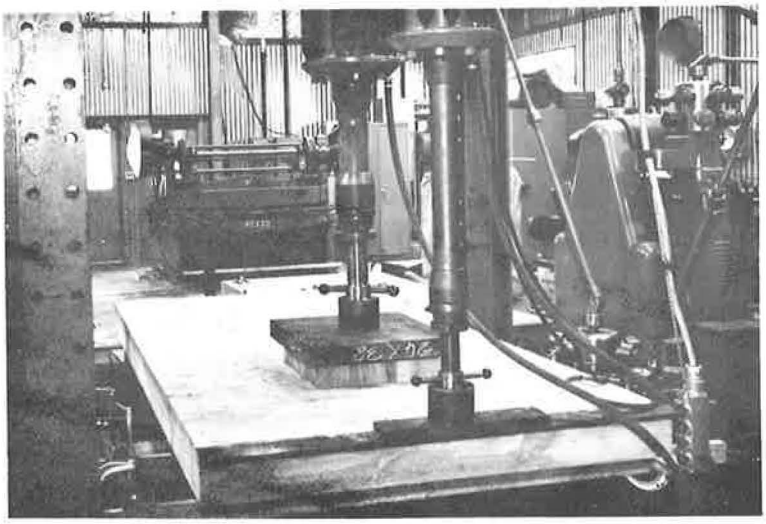

Figure 5. General view of loading arrangement for testing experimental units.

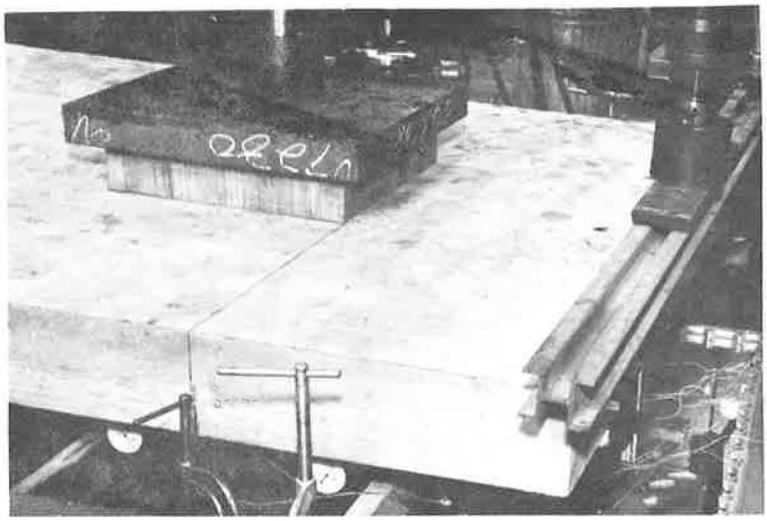

Figure 6. Close-up of experimental unit showing positions of main and secondary loads with respect to edge of beam web (pencil line on concrete); two of the dial gages for measuring deflections shown beneath slab.

ceiving the downward reaction. To simulate this situation in the test specimen, a secondary vertical load was applied at the edge of the specimen. Because it was not known how critical such a downward reaction at this point would be, the behavior of the specimen was studied under secondary vertical loads of up to 30 percent of the main load.

As shown in Figure 2, instrumentation for each test consisted of six dial gages, three in line with point A and three in line with point C, placed $7\frac{1}{2}$ in. from the web nearest the load, and eight electric resistance strain gages mounted on specially fabricated spring clips that were bolted to the web in line with point B. Since the top of each clip

was in contact with the concrete, the vertical movement of the clip, which was calibrated with respect to the strain measured in its bent portion, was equal to the vertical slip of the concrete relative to the steel web.

The main load was applied in increments ranging from 5,000 to 10,000 lb. After each increment was applied, the slab was inspected for cracks, and both dial- and strain-gage readings were recorded. Then, with the main load constant, the secondary load was increased from zero to 30 percent of the main load. After another set of gage readings was recorded, the secondary load was reduced to zero, and the main load was increased one increment. This procedure was repeated until failure of the specimen occurred.

## RESULTS AND DISCUSSION

The behavior of the two experimental superstructure units was almost identical. Because of this similarity of behavior, the test results for both units will be discussed together throughout the remainder of the paper.

As shown in the load-deflection curves in Figures 7 and 8, the vertical deflection of the slabs at point A on the specimen centerline (in cantilever span, $7\frac{1}{2}$ in. from web) increased as the main load increased up to about 50,000 lb and then decreased slightly for greater loads. At point C on the specimen centerline (in the interior span, $7\frac{1}{2}$ in. from web), increasing the main load continuously increased the deflection up to the maximum load applied, as would be expected. The deflections at point C were considerably greater than the deflections at point A and were, therefore, considered to be of much significance in analyzing the behavior of the slab. The increase of the deflection at point A and the decrease of the deflection at point C when the secondary load was applied are readily explained by the fact that the web between these points acts as a fulcrum. Also, as expected, the deflection of the slab was less at points away from the specimen centerline. For example, at a 90,000-lb main load and zero secondary load,

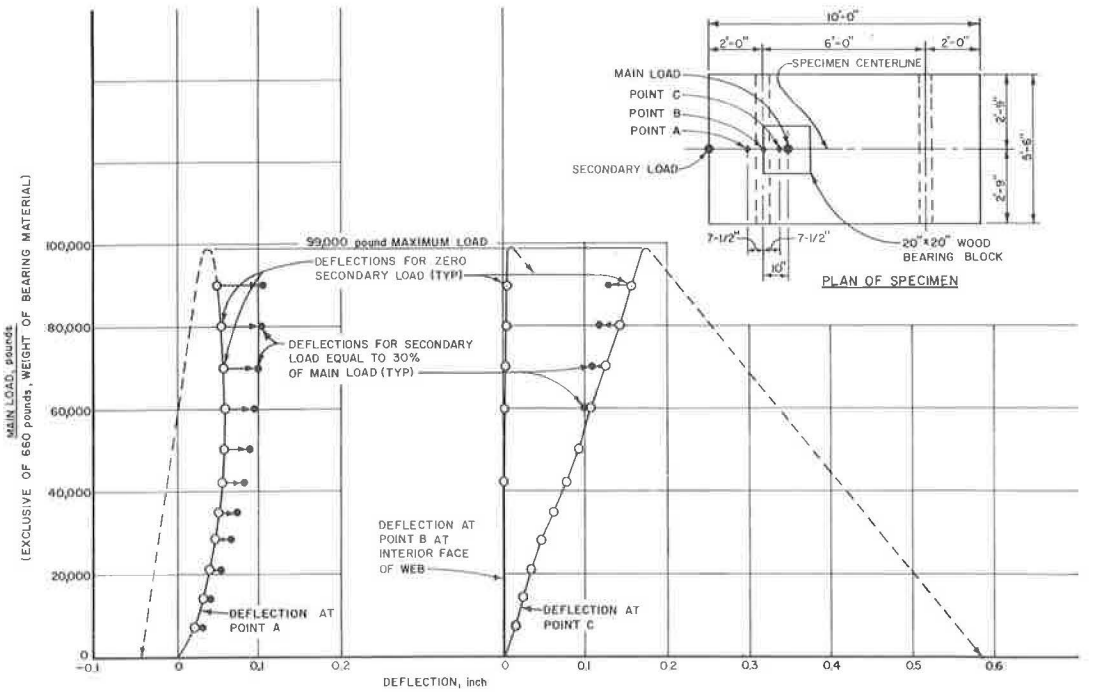


Figure 7. Specimen centerline deflections for test 1 ($4$-in. stud spacing on webs).

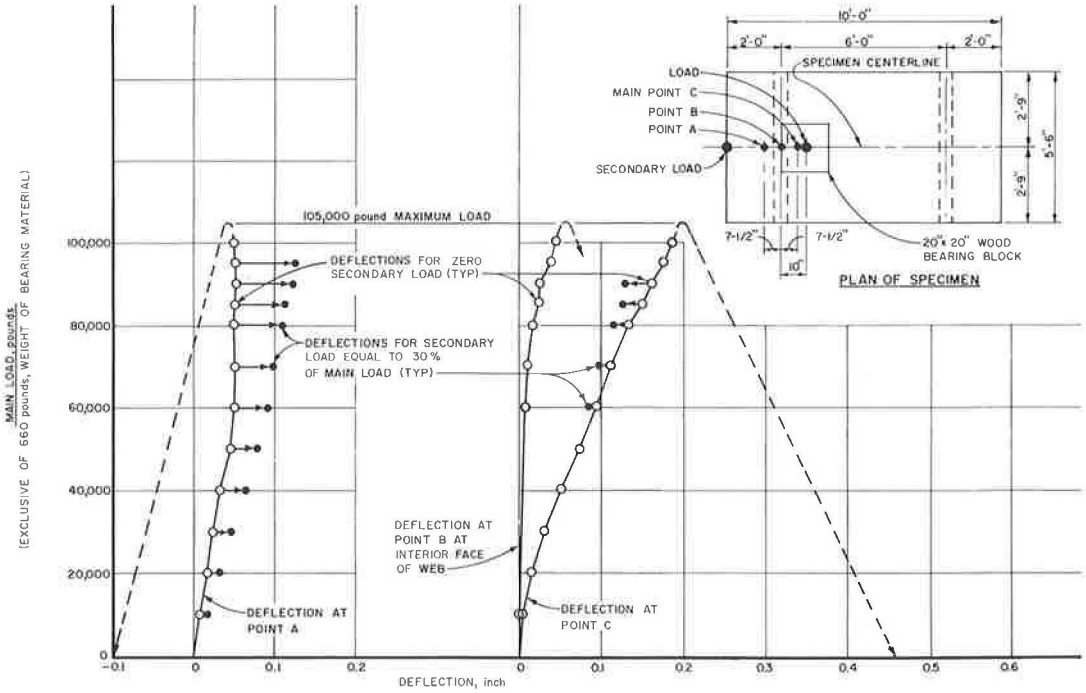


Figure 8. Specimen centerline deflections for test 2 (10-in. stud spacing on webs).

TABLE 1

VERTICAL DEFLECTIONS ALONG LONGITUDINAL LINE THROUGH POINT C[a]

| Test No. | Stud Spacing (in.) | Deflections (in.) | | |
|---|---|---|---|---|
| | | At Centerline | Halfway Between Centerline and Edge | At Edge |
| 1 | 4 | 0.160 | 0.147 | 0.094 |
| 2 | 10 | 0.163 | 0.139 | 0.085 |
| Avg. | | 0.162 | 0.143 | 0.090 |

[a]At 90,000-lb main load and zero secondary load.

the distribution of vertical deflection along the longitudinal line through point C was as given in Table 1. It is seen that the edge deflections were about 50 to 60 percent of the deflections at the specimen centerline. The magnitude and distribution of the deflections did not appear to depend on the stud spacing.

As Figures 7 and 8 also show, the vertical movement (slip) between the steel web and the adjacent concrete at point B (the web itself) on the specimen centerline also increased progressively, but at a slower rate than the deflections at points A and C, as the load increased. At a main load of 90,000 lb, the slip at the specimen centerline was about 0.005 in. for the specimen with a 4-in. stud spacing and about 0.03 in. for

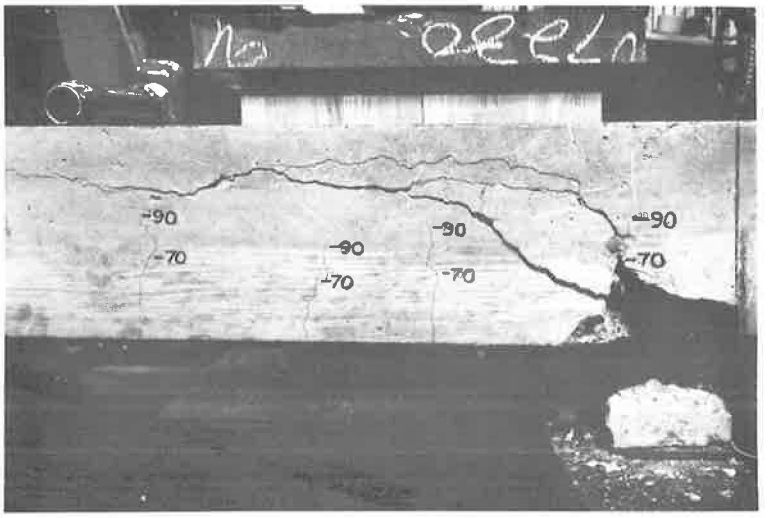


Figure 9. View of transverse face of failed test unit with 4-in. stud spacing; large failure cracks developed suddenly at main load of 99,000 lb.

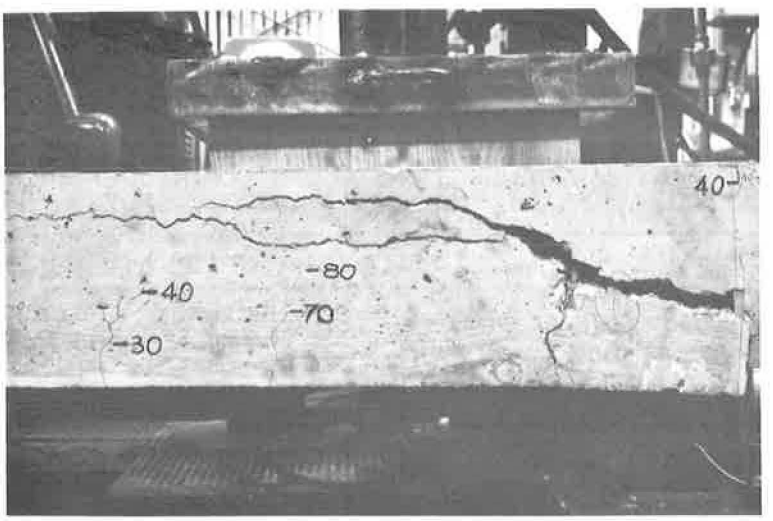


Figure 10. View of transverse face of failed test unit with 10-in. stud spacing; large failure cracks developed suddenly at main load of 105,000 lb.

the specimen with a 10-in. stud spacing. The edge slips were about 0.004 and 0.02 in., respectively, for the two specimens. It is, of course, logical that the specimen with the 10-in. stud spacing slipped more than the specimen with the 4-in. stud spacing. However, even at a 90,000-lb load, no cracking of the concrete in the vicinity of the steel web was observed in either test, and the slight slip at that load was apparently not detrimental to the specimens.

At about a 40,000-lb main load, vertical hairline cracks began to form at the bottom of the interior span and at the top of the cantilever span near the web. As the main load increased, these cracks progressed farther into the slab and extended beyond the mid-

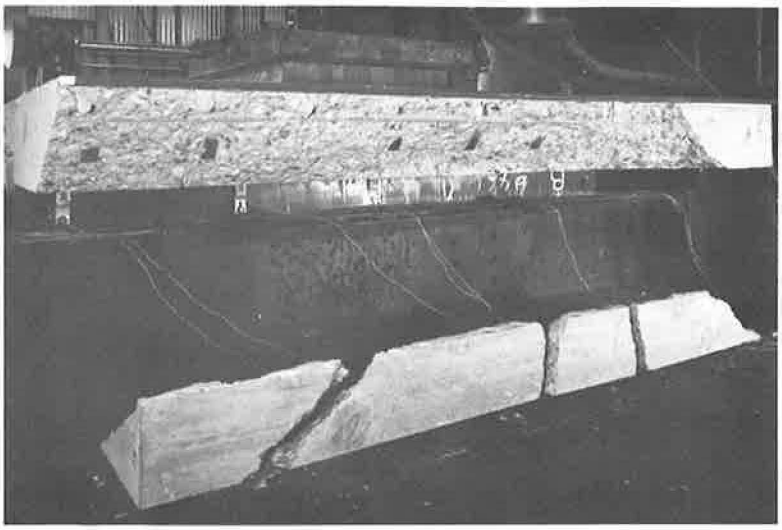

Figure 11. View of failed test unit with 10-in. stud spacing showing diagonal tension failure of the cantilever span under a secondary load of 28,500 lb; failure occurred when main load was 95,000 lb and did not affect main results of test.

thickness when the main load was 90,000 lb. The point to which a particular main load caused these cracks to progress was marked on the slab adjacent to the cracks. Failure of the specimen with the 4-in. stud spacing occurred suddenly at a main load of 99,000 lb. The specimen with the 10-in. stud spacing failed in a similar manner at a main load of 105,000 lb. As the views of the failed slabs in Figures 9 and 10 indicate, however, the main failure cracks, which formed suddenly just beyond the ends of studs under the main load and across part of the interior span, did not join the previously formed vertical hairline cracks. (The two-digit numbers adjacent to the hairline cracks shown in Figures 9 and 10 are the main-load values expressed in thousands of pounds that marked the progress of the cracks during the tests.) The 99,000-lb failure load for the specimen with the 4-in. stud spacing and the 105,000-lb failure load for the specimen with the 10-in. stud spacing were, respectively, 476 and 505 percent of the 20,800-lb AASHO design load that includes 30 percent of the live load for impact. The secondary loads were zero when the failures occurred. A diagonal tension failure, shown in Figure 11, occurred in the cantilever span of the specimen with a 10-in. stud spacing when the main load was 95,000 lb and the secondary load was 28,500 lb. This failure did not influence the strength of the interior span because the interior span did not fail until an additional main-load increment of 10,000 lb was applied. Before the formation of the main cracks, each specimen had successfully sustained a 90,000-lb main load simultaneously with a 27,000-lb secondary load. Thus, even for positions of truck wheels that would cause edge loading, the results indicated that a $5\frac{1}{2}$-ft long portion of a bridge with the test configuration could sustain at least about 430 percent of design load including impact.

As shown in Figures 9 and 10, the large failure cracks were vertical near the bottom (at the stud location), inclined at about 45 deg to the horizontal at mid-depth, and were almost horizontal near the top of the slab. Corresponding views on the opposite side of each specimen indicated the same positions of failure cracks. Because these cracks occurred approximately where the planes of maximum diagonal tension would theoretically occur, it can be concluded that failure was due to diagonal tension possibly in conjunction with some bond slippage, rather than to punching shear. This supposition appears logical because, at the failure loads, the theoretical bond stresses exceeded 800 psi, which is in the range of values of ultimate bond strengths obtained in many independently conducted flexural tests (2) on deformed bars with diameters less than or

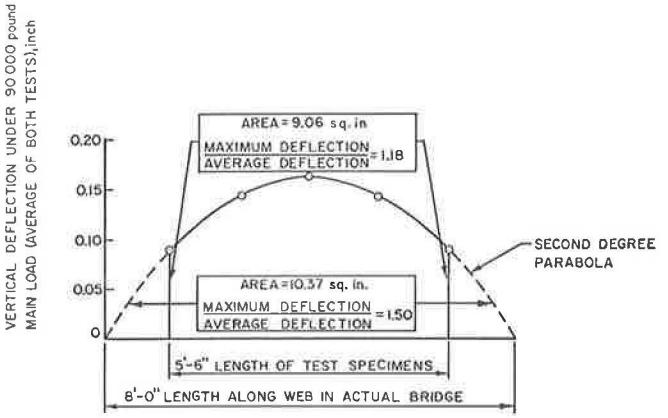


SLAB DEFLECTION IN INTERIOR SPAN 7½ INCHES FROM WEB NEAREST LOAD

| ASSUMPTIONS | | | MAXIMUM UNIT SHEARS FROM TOTAL SHEAR V | |
|---|---|---|---|---|
| CASE | LENGTH OF WEB RESISTING VERTICAL SHEAR | VARIATION OF SHEAR INTENSITY | SHEAR PER INCH OF WEB | SHEAR PER FOOT OF WEB |
| I | 5'-6" | DIRECTLY PROPORTIONAL TO SLAB DEFLECTIONS | $\frac{1.18\,V}{66} = \frac{V}{55.9}$ | $\frac{1.18\,V}{5.5} = \frac{V}{4.66}$ |
| II | 8'-0" | DIRECTLY PROPORTIONAL TO ORDINATES OF PARABOLA | $\frac{1.50\,V}{96} = \frac{V}{64.0}$ | $\frac{1.50\,V}{8.0} = \frac{V}{5.33}$ |

Figure 12. Distribution of vertical shear intensity assumed proportional to slab deflection.

slightly greater than the ¾-in. diameter bars used in the present specimens. The maximum diagonal tension stress that would develop from shear in a reinforced slab at the failure loads was calculated to be between about 260 and 280 psi, which, as an isolated stress, would probably not be enough to cause a diagonal tension break. However, under the loads that caused bond slippage and the main cracks, the theoretical maximum tension stress at the ends of the studs for an unreinforced slab would be over 600 psi, which is probably greater than the ultimate tensile strength of the concrete. (Calculations were made for an unreinforced slab because, if there is bond slippage, the reinforcing bars in the vicinity of the slippage are usually not very effective in helping to support a load.) Therefore, it appears that a progressive failure occurred, probably starting with bond slippage and terminating with tension failure initiated at the ends of the studs. Because bond is evidently critical, it is important that the bottom transverse reinforcing bars be sufficiently long so that the gaps between the bar ends and the beam web are small (Fig. 2).

Since the failures were apparently combined tension-bond failures rather than punching-shear failures, it can be concluded that the bearing area of the top of the web in combination with the studs spaced at up to 10 in. along the web are together capable of carrying punching shears exceeding those existing at the experimental failure load. Furthermore, the occurrence of deflections at the transverse edges of the specimens indicates that a wheel load on an actual bridge would be distributed over more than a 5½-ft length. Because of this longer distribution, the resistance to punching shear in the bridge would be larger than in the tested specimens. Therefore, it is obvious that the 10-in. spacing of studs is extremely conservative for studs carrying punching shear alone, and that the spacing of studs loaded in this manner could be increased considerably without resulting in a punching type of failure under standard highway loadings.

TABLE 2

MAXIMUM INTENSITIES OF SHEAR ALONG WEB AT SPECIMEN FAILURE[a]

| Test No. | Stud Spacing (in.) | Main Load (lb) | Total Shear (V) (lb)[b] | Maximum Unit Shear (V/55.9) (lb/in.) |
|---|---|---|---|---|
| 1 | 4 | 99,000 | 85,000 | 1,520 |
| 2 | 10 | 105,000 | 90,400 | 1,620 |

[a]Based on case I, Figure 12.
[b]Because center of main load located 10 in. from web, maximum shear is 86.1 percent of main load.

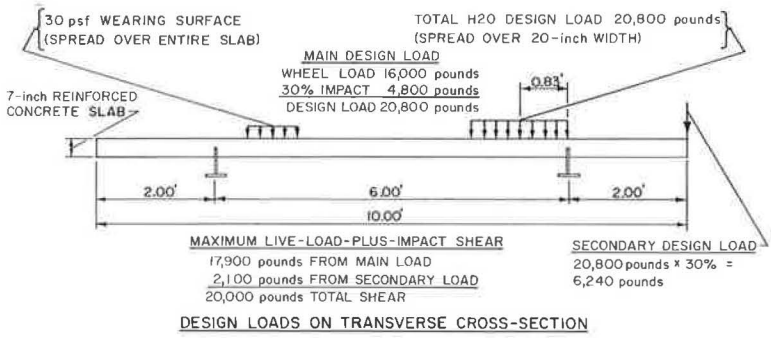


| VERTICAL SHEAR ALONG ONE SIDE OF STEEL WEB | |
|---|---|
| COMPONENT | SHEAR, pounds per inch |
| DEAD LOAD OF SLAB AND WEARING SURFACE | 29 |
| LIVE LOAD PLUS IMPACT (FORMULA ON FIGURE 12) | $\frac{20,000}{64.0} = 313$ |
| TOTAL | 342 |

| SUGGESTED EXPRESSION FOR VERTICAL SHEAR PER STUD |
|---|
| VERTICAL SHEAR PER STUD = 342 S pounds WHERE S IS THE SPACING (IN inches) OF THE STUDS ON ONE SIDE OF THE STEEL WEB. |

Figure 13. Vertical shears on studs from H20 truck loading.

To evaluate the results further and to develop design information for combined punching and horizontal shear, it was necessary to obtain an approximation of the variation of vertical shear along the web. To accomplish this, the distribution of vertical shear transferred from the slab to the beam web was assumed to be proportional to the vertical deflections of the slab near the web. Also, because stud designs are usually based on ultimate strength, it was assumed that the variation of vertical deflections under the 90,000-lb main load would be more pertinent than the variation under lesser loads. On the basis of these assumptions, the expressions for the intensity of shearing force along the web were derived (Fig. 12).

In the first group of expressions (case I) in Figure 12, it is assumed that the shear is resisted by only a $5\frac{1}{2}$-ft length of web, as in the tests. The maximum intensities of shear along the web at failure of each specimen were then computed to be as given in Table 2.

It was not possible to determine from the test results how much of the shear was transferred from the slab to the web by the studs and how much was transferred by bearing on top of the webs. Because the studs deflected downward with the concrete slab at the studs, the studs were strained in bending and, therefore, supported at least part of the punching shear. If the studs had transferred all the shear, the maximum shear per stud would have been 16,200 lb for the 10-in. stud spacing, which is about 43 percent more than the maximum useful capacity of 11,300 lb specified (1) for $^{3}/_{4}$-in. diameter studs used with concrete having a compression strength of 3,710 psi. If all the shear had been transferred in bearing on the $^{5}/_{16}$-in. wide top of the web, the maximum bearing stress would have been 5,180 psi, which is about 40 percent more than the ultimate compression strength of the concrete, but which might not exceed the capacity of the concrete for resisting compression under the triaxial stress condition existing in the concrete over the web. It thus appears likely that both the studs and the bearing surface on top of the web participated in the transfer of vertical shear from the slab to the web.

In designing an actual bridge, however, it would be conservative and convenient to neglect the contribution of bearing on the top of the webs and to assume that all vertical punching shear, as well as horizontal shear caused by longitudinal bending, is transferred from the slab to the web by the studs. To design the studs and determine their spacing, it is, of course, necessary to know the intensity of shearing force along the web to know how much vertical shear will be applied to a given stud. The formula for determining the maximum shear intensity used here for evaluating the test data would be overly conservative for an actual bridge. Therefore, as demonstrated in Figure 12, it appears reasonable to assume that the intensity of shear would vary parabolically over at least 8 ft. This assumption is based on fitting a parabolic curve to the observed deflections. It is a conservative assumption because, in an actual bridge, the vertical deflections would not terminate abruptly within an 8-ft length but would tend to taper off more gradually.

On the assumption that the intensity of vertical shear from the wheel load varies parabolically over an 8-ft length, the second group of expressions (case II) in Figure 12 would apply. Then, as determined in Figure 13, the design maximum vertical shear per stud for H20 loading would be 342 S lb, where S is the spacing of studs in inches. To determine the maximum shear on the stud for the given spacing, this vertical shear would be added vectorially to the horizontal shear per stud, if present, and the result would be compared with the allowable shear per stud, which would be the useful capacity given in the specification (1) divided by a factor of safety.

## ACKNOWLEDGMENT

Appreciation is extended to the Indiana Steel Fabricators Association for supplying the steel T's with attached studs used for the tests described herein.

## REFERENCES

1. Standard Specifications for Highway Bridges. AASHO, 1961.
2. Ferguson, P. M., and Thompson, J. N. Development Length of High Strength Reinforcing Bars in Bond. Jour. ACI, Fig. 16, July 1962.

# Fatigue Strength of ¾-Inch Stud Shear Connectors

A. A. TOPRAC, Professor, Department of Civil Engineering, University of Texas

Results of fatigue tests performed on seven steel-concrete composite beams are presented. The shear between the steel 24 WF 68 beams and the 6-in. thick slab is developed by means of ¾-in. diameter headed steel studs. The beams were all identical except for the number of studs. The beams were 36.0 ft long and were divided into two groups: (a) four commercially good and acceptable specimens, and (b) three inferior specimens not acceptable to the Texas Highway Department.

Test results indicate that: (a) there is a difference (as much as 3 ksi) in fatigue strength between ½- and ¾-in. studs; (b) the American Association of State Highway Officials (AASHO) specifications allowable stress for stud shear connectors prudently could be increased by reducing the factors of safety presently in use; (c) two of the three defective specimens tested exhibited fatigue strengths equal to those of commercially acceptable specimens; and (d) for 10 million cycles the fatigue strength of the studs tested, expressed in terms of stress range, is at least 13 ksi.

•COMPOSITE construction consisting of a concrete slab attached to a steel beam with mechanical shear connectors has become quite common in buildings and bridges. The shear connectors, welded to the steel section and embedded in the concrete, force the slab and the steel beam to act as an integral unit in resisting loads on the structure. When attached to the compression flange, the slab is very effective as a cover plate for the steel beam. As a result, the deflection of the structure is significantly reduced and savings in steel are possible (1). Channels, spirals, and welded studs have been used successfully as shear connectors. Due to ease in fabrication and flexibility in design, welded studs are currently the most popular.

Research on composite construction with shear connectors dates from 1933. However, studies of welded studs as shear connectors in composite construction began in 1954. These tests included static and fatigue tests of pushout specimens (direct shear), fatigue and static tests of one double T-beam (flexure), fatigue tests of bare studs, and static tests of plate-reinforced concrete beams (2). More recently a program of fatigue tests on flexural members with welded studs as shear connectors was instituted at Lehigh University (3, 4). A total of 12 beams, four with 10-ft spans and eight with 15-ft spans, were studied. For all of these beams ½-in. diameter welded studs were used as shear connectors.

Results from the Lehigh tests correlate well with other fatigue investigations (5) and it appears that a design criteria for ½-in. diameter studs can now be established which will give a realistic factor of safety against fatigue failure. One question which still remained unanswered was the validity of applying the results of tests on small-scale specimens to full-size composite beams, and the "size effect," if any, for studs larger than ½-in. diameter.

Paper sponsored by Committee on Steel Superstructures.

This paper is a report of fatigue tests performed on seven full-size composite beams. The purpose of the investigation was (a) to observe the overall effects of fatigue loading on composite beams, (b) to determine whether results of tests on small-scale specimens could be extrapolated and applied to full-size beams, (c) to obtain additional information concerning the minimum number of stud shear connectors required for beams under dynamic loading conditions, and (d) to investigate the effect of defective stud welds on the fatigue strength of such beams.

## TEST SPECIMENS

In this study, seven composite beams were tested. The specimens were divided into Group 1, consisting of four beams, and Group 2, consisting of three beams. Each specimen consisted of a 24 WF 68 steel beam connected with $\frac{3}{4}$-in. diameter welded stud shear connectors to a 6-ft wide by 6-in. thick concrete slab. The test specimens were tested as simple beams with a span of 36 ft. They were loaded with two equal concentrated loads 14 ft from each support. Figure 1 shows the overall dimensions of the test specimens.

### Specimen Details

Steel Sections. —The dimensions of the test specimens were identical except for the number and spacing of the welded stud shear connectors. The $\frac{3}{4}$-in. diameter shear connectors had a height of 4 in. and were welded to the steel beam by a stud welding process. As shown in Figure 2, the studs were placed in pairs throughout the 14-ft shear span on each end of the beam. In addition one pair of studs was placed at the center of the beam. Specimens A, B, and C in each group had 90, 66 and 54 studs, respectively, and specimen 1-D of Group 1 had 78 studs. Figure 2 shows the details and spacing of the studs.

Concrete Reinforcement. —Intermediate grade, deformed steel bars were used for the concrete reinforcement. The transverse bars were $\frac{1}{2}$ in. in diameter, placed at 6-in. intervals throughout the length of the beam. The longitudinal bars were $\frac{3}{8}$ in. in

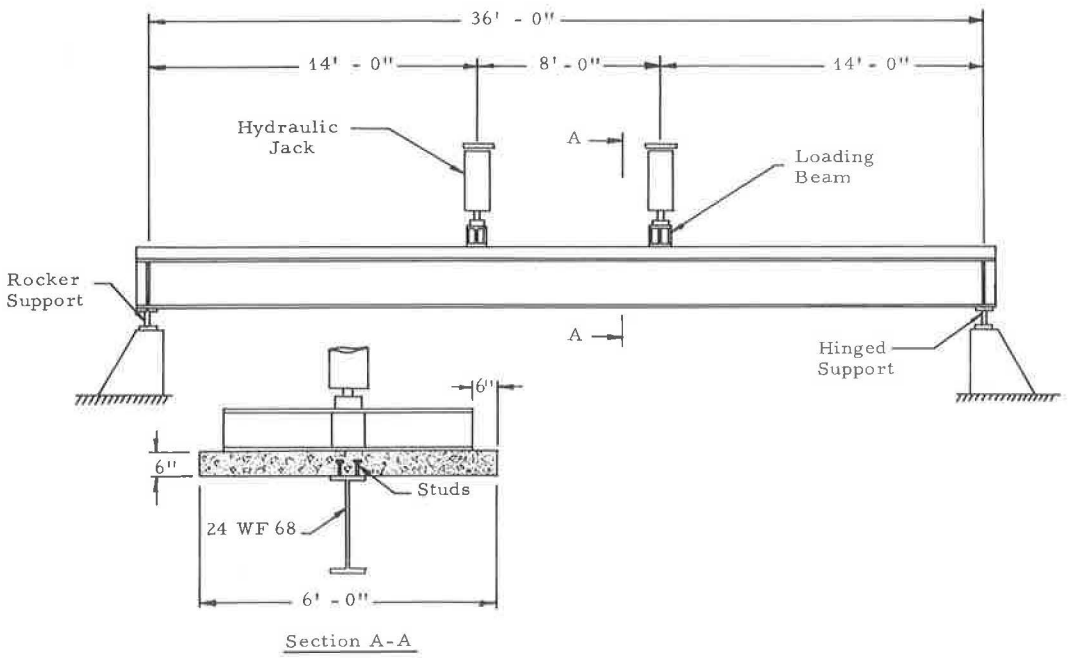


Figure 1. Loading arrangement.

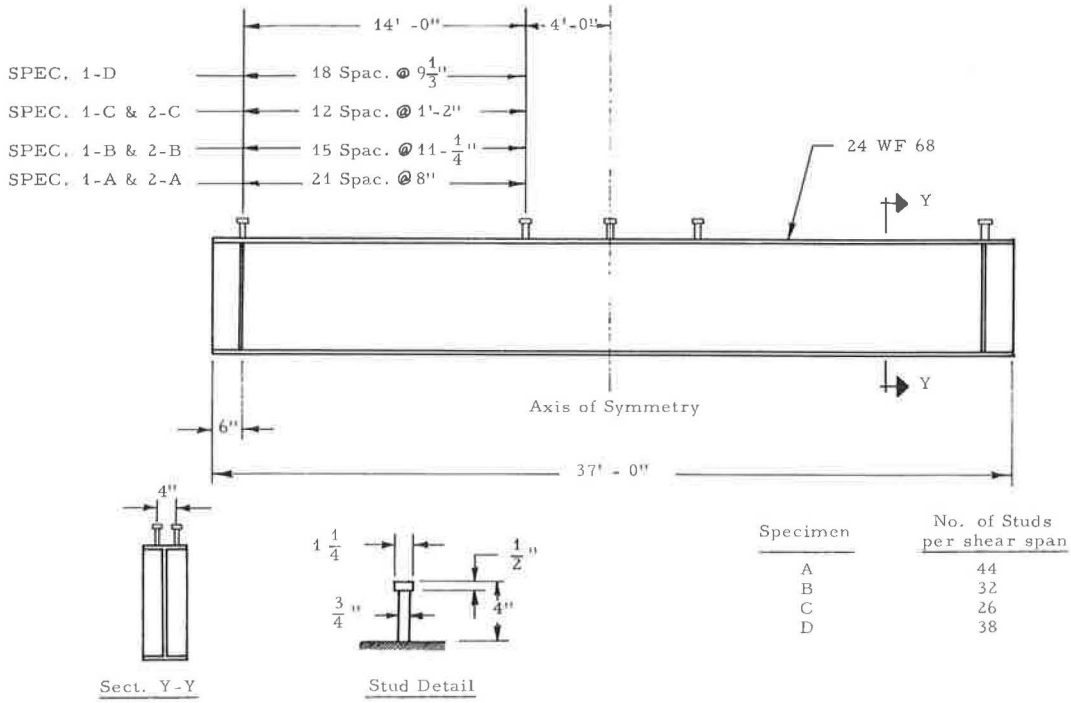


Figure 2. Details of steel beams.

diameter, placed at 12-in. intervals. There were two layers of identical steel in each of the slabs with 1-in. concrete cover on both top and bottom. Figure 3 shows the reinforcement in a typical section and also the details of the reinforcement at the end of the beam.

Concrete. —The concrete for these specimens was ready-mix concrete and was supplied by a local contractor. High early-strength cement was used, and the maximum aggregate size was 1 ½ in.

Since the composite beams were designed to simulate unshored construction, the entire weight of the forms and the concrete were supported by the steel beam. The steel beam itself was supported by concrete blocks only at the ends. The forms for the concrete slab were made of exterior-grade plywood and built in sections so that they were readily reusable. The weight of the concrete was transferred from the wooden forms to the bottom flange of the steel beam by a flange hanger arrangement.

To insure that no bond would exist between the slab and the steel beam, the top flange of the steel beam was given a light coat of oil which, before the concreting operation, was wiped off so that only a very thin film remained.

The casting operation always began at one end of the beam and proceeded toward the other end in a continuous manner. After the concrete was troweled to a smooth finish, the exposed surface was covered with a polyethylene sheet for curing. This covering and the forms were left in place from 4 to 6 days to allow the slab to cure under moist conditions. At the end of this period the forms were removed and the specimen was allowed to cure for a minimum of about 10 days under dry conditions before testing was begun.

End Supports. —To reduce vibrations caused by small, practically unavoidable eccentricities in the loading setup and the test specimens, braces were used at both ends of the beams. These braces consisted of four pairs of angles bolted to the supports and to the steel beam and the slab. Figure 4 shows the details of these braces. The braces were not only effective in reducing vibrations but also important as lateral supports for the specimens which, because of their top-heavy nature, were unstable.

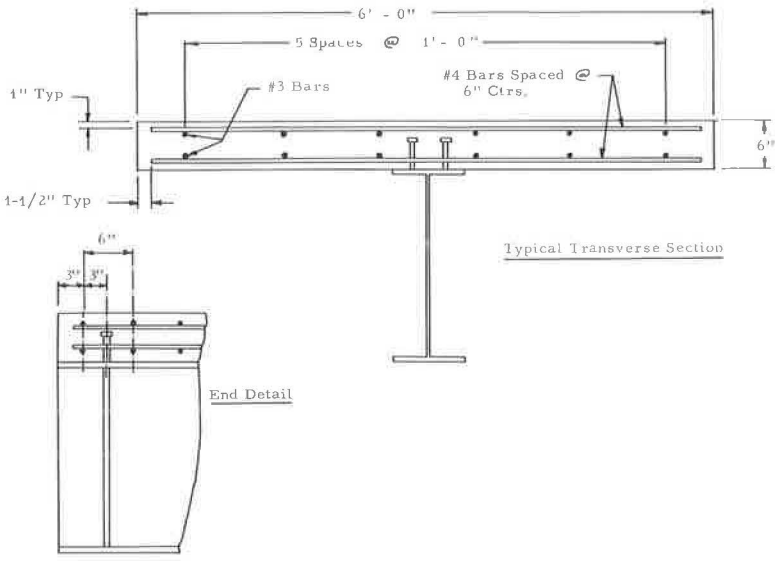


Figure 3. Concrete reinforcing steel.

TABLE 1

TENSILE TESTS OF BEAM STEEL

| Beam Group | Coupon No. | Coupon Location | Static Yield Point (psi) | Diagram |
|---|---|---|---|---|
| 1 | 3 | Web | 56,000 | 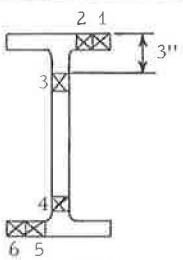 |
| | 4 | Web | 55,000 | |
| | Avg. | — | 55,500 | |
| | 1 | Flange | 35,000 | |
| | 2 | Flange | 35,800 | |
| | 5 | Flange | 39,300 | |
| | 6 | Flange | 35,300 | |
| | Avg. | — | 36,350 | |
| 2 | 4 | Web | 35,800 | 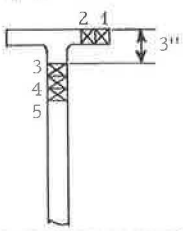 |
| | 3 | Web | 35,000 | |
| | 5 | Web | 36,200 | |
| | Avg. | — | 35,700 | |
| | 2 | Flange | 34,200 | |
| | 1 | Flange | 36,400 | |
| | Avg. | — | 35,300 | |





TABLE 2

MILL TEST REPORT FOR BEAM STEEL

| Beam Group | Yield Point (psi) | Tensile Strength (psi) | Elongation In. | Elongation % | Chemical Analysis C | Mn | P | S |
|---|---|---|---|---|---|---|---|---|
| 1 | 41,800 | 72,500 | 8 | 27 | 0.24 | 0.78 | 0.016 | 0.025 |
| 2 | 37,600 | 66,600 | 8 | 27 | 0.25 | 0.73 | 0.013 | 0.019 |

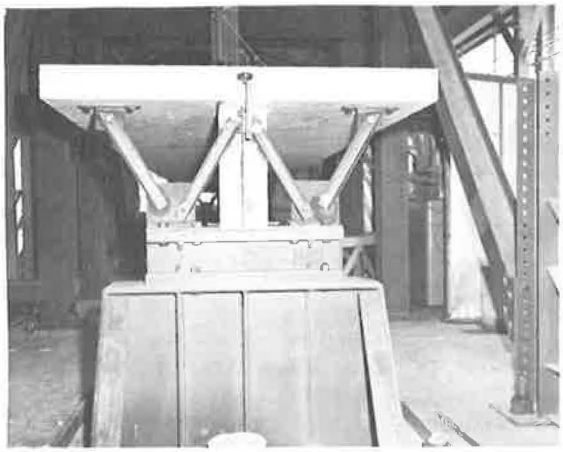

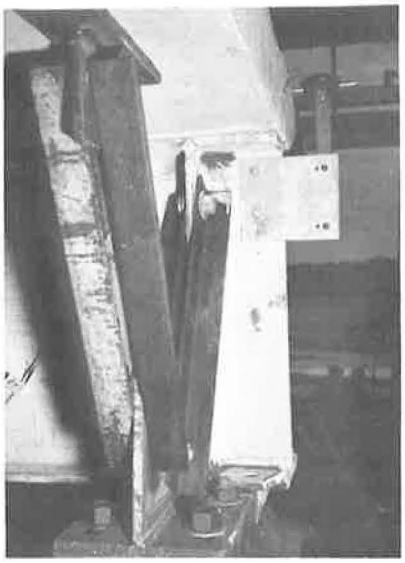

Figure 4. End braces and end slip measuring device.

Lifting Apparatus. —Moving test specimens to and from the testing area was accomplished by using a 25-ton overhead crane. To avoid tensile stresses in the concrete while moving the specimens, a 40-ft lifting beam was used. Near each end of the test specimens, pipe sleeves were cast into the concrete slab. This allowed $\frac{5}{8}$-in. diameter cables to be put completely around the bottom flange of the test specimens and then attached to the lifting beam.

## Material Properties

To obtain the mechanical properties of the materials used, concrete cylinders and tensile coupons from the steel in the beams and the studs were tested.

Steel Sections. —The seven steel sections were of ASTM A36 steel, each group of the same heat. Tensile coupons were made from a 12-in. stub of the same 24 WF 68 used in the specimens of each group. The coupons were 12 in. long, 1 in. wide, and machined to a constant width of $\frac{1}{2}$ in. in the center portion. An extensometer with a 2-in. gage length was used to measure the strain. After the tensile coupon had reached its yield point, further straining of the specimen was stopped for a period of about 6 to 8 min. The stress at the end of this waiting period was recorded as the static yield strength. This procedure was repeated several times in the plastic range. Table 1 gives the results of all tensile tests and the averages of the web and flange coupons.

Table 2 gives the chemical analysis of the steel as taken from the mill report. The yield point shown in the mill report was 41,800 psi for Group 1 beams and 37,600 psi for beams of Group 2. A faster rate of loading than described previously is the reason for the higher yield point values given in the mill reports.

Concrete. —Usually nine standard test cylinders were made with each beam. Three of the cylinders were made from concrete taken near one end of the beam, three from the opposite end, and three from the center. Approximately one-third of these cylinders were tested at the beginning, one-third at the end, and one-third during the dynamic test. The average concrete strength for the various beams tested varied from 4,150 psi for specimen 2-C to 5,730 psi for specimen 1-A. Table 3 gives a complete summary of the results from the cylinder tests.

Shear Connectors. —The stud shear connectors were made from a low carbon steel. Tensile coupons were machined from two extra studs furnished by the manufacturer

TABLE 3

RESULTS OF CONCRETE CYLINDER TESTS

| Beam | No. Cylinders Tested | Cylinder Stress (psi) | | | Age (days) |
|---|---|---|---|---|---|
| | | Avg. | Min.[a] | Max.[a] | |
| 1-A | 9 | 5,730 | 4,630 | 6,650 | 41 |
| 1-B | 5 | 5,425 | 4,780 | 5,940 | 34-39 |
| 1-C | 9 | 5,710 | 5,500 | 6,050 | 32-39 |
| 1-D | 6 | 4,570 | 4,210 | 4,880 | 16-53 |
| 2-A | 9 | 4,440 | 4,030 | 4,670 | 26-50 |
| 2-B | 10 | 4,724 | 4,620 | 4,920 | 16-34 |
| 2-C | 9 | 4,151 | 3,650 | 4,580 | 6-20 |

[a]Of particular group tested.

and tensile tests were made. Yield points of 54,000 and 57,100 psi were recorded with ultimate tensile strengths of 64,000 and 67,600 psi, respectively. The elongation in the 2-in. gage length was 22 percent.

## Stud Welding Inspection

All beam specimens for this project were inspected by Texas Highway Department inspectors. The welds in beams of Group 1 were found satisfactory and acceptable for highway construction. These specimens were regarded as beams of commercial quality.

The beams of Group 2 were also checked by the Texas Highway Department inspectors to ascertain the degree of deficiency of the faulty stud welds. Visual inspection indicated that all beams had corrective welds, deficient fillets, undercuts, etc. Of the three beams in this group, only specimen A was inspected thoroughly. The results of this inspection, reported in a letter from the Texas Highway Department (6), were as follows:

1. The criteria for inspection were as described in Texas Highway Department Construction Bulletin C-5 (7).
2. Visual inspection of stud welding was made. It was estimated that approximately 30 percent of the studs did not have a full fillet around the base of the stud, indicating that these studs did not have 100 percent weld. Some of the studs with deficient fillets had corrective manual fillet welds.
3. Of the studs with manual repair and insufficient fillet welds, ten were selected for bending to approximately 30 deg off vertical. Two studs failed (broke off). The failure was in the stud side heat-affected zone, which appeared crystallized. The stud appeared brittle at the point of fracture.
4. The inspector expressed the opinion that additional testing would merely produce additional failures and further testing was discontinued.
5. The studs welded on the girder inspected did not comply with Texas Highway Department Construction Bulletin C-5.

The deficiencies in beams 2-A, 2-B, and 2-C were enough to make them unacceptable for bridge construction. Since it was thought that useful data might be obtained, the specimens were tested after the studs that were broken off or bent as a result of the inspection were replaced.

## Specimen Design Philosophy and Objectives

Fatigue tests by other investigators (3, 4) have indicated that fewer shear connectors than presently required by the American Association of State Highway Officials (AASHO) specifications (8) may be satisfactory for bridges. The primary objective of this study was to determine whether or not the results obtained from small-scale fatigue tests can be extrapolated to full-size beams, and to obtain data with substandard beam specimens. All seven specimens were identical except for the number of shear connectors.

Specimen A.--The number of shear connectors for beams 1-A and 2-A was determined from the AASHO specifications (8), assuming a maximum permissible steel stress of 20,000 psi in the tension flange of the beam. The "factor of safety" as defined in the AASHO specifications was 3.70. Forty-four shear connections were required in each shear span. Thus, a total of 90 studs were required. (It should be noted, however, that the maximum test stress in the steel beams was in excess of yielding in beam 1-A and 31,000 psi in all other beams, so that the maximum load in connectors was at least 50 percent over that allowed by AASHO specifications.)

Specimen B. —These beams (1-B and 2-B) were designed according to Section 1.11.4 of the American Institute of Steel Construction (AISC) Specifications for the Design, Fabrication, and Erection of Structural Steel for Buildings (9). This design called for 32 studs in each shear span or a total of 66 studs for the beam. According to conventional design procedures, this beam had the minimum number of shear connectors for static loading conditions. AISC specifications for shear connectors are based on a factor of safety of 2.50 against their demonstrated ultimate strength (10).

Specimen C. —These beams (1-C and 2-C) were designed to have the theoretical minimum number of shear connectors required for development of the full flexural static strength of the beam (11). This required 26 studs per shear span or a total of 54 studs for the beam.

Specimen D. —This specimen had 38 shear connectors in each of the shear spans. Thus, the number of studs for this beam was between specimens B and A.

## INSTRUMENTATION AND TEST PROCEDURE

The instrumentation for these tests included measurements of vertical deflection of the beam, slip between the concrete slab and the steel beam, flexural stresses in the steel beam, and localized stresses in the upper flange of the steel beam caused by the presence of the studs. The steel beam was also whitewashed with a lime-water solution so that yield lines could be easily observed. Instrumentation was essentially the same for all specimens. Exceptions to this are noted in the following discussion.

### Vertical Deflection Gages

Vertical deflection was measured on the bottom flange of the beam at the center and 4 ft on either side of the center with dial indicators. On beams 1-D, 2-B and 2-C, only the differential deflection (the deflection observed as the load was increased from zero to the maximum) was recorded. No attempt was made to measure residual deflection as it accumulated during the dynamic test. On all other specimens, however, the residual deflection as well as the differential deflection was measured. As a result it was possible to record total deflection for specimens 1-A, 1-B, 1-C and 2-A.

### End Slip Gages

The slip of the concrete relative to the steel beam was measured at each end of the beam using dial indicators. The dial indicators were rigidly attached to the steel beam and held in the same position throughout the test. To avoid damage to the gage, the point was restrained from touching the concrete during dynamic tests. Figure 4 shows the apparatus used to measure end slip.

### Electric Strain Gages

Baldwin paper-backed wire strain gages were used throughout these tests to measure flexural strains in the steel beam and to determine an approximate index of the load on the studs.

Flexural Stresses. —Three strain gages were used on each specimen to determine flexural strains at the center of the beam. One gage was placed on the bottom of the

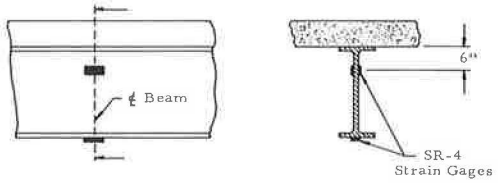


Figure 5. Strain gages for flexural strain measurement.

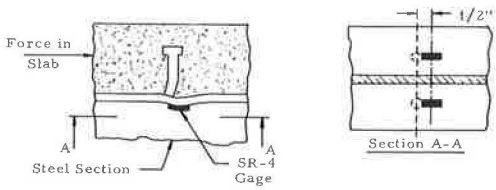


Figure 6. Strain gages for loads on studs.

tension flange. The other two gages were placed 6 in. below the top flange on either side of the web (Fig. 5).

Shear Connector Forces. —An attempt was made to measure, at least qualitatively, the load on individual studs. This was done by placing strain gages on the underside of the top flange of the steel beam in the immediate vicinity of the stud under consideration. The force on the stud created localized deformations in the top flange which were recorded by the strain gages. As shown in Figure 6, the strain gages were not directly under the studs but were located ½ in. from the center of the stud on the side of the connector nearest the end of the beam. In every case tensile strains were recorded from these gages. This procedure, developed in earlier investigations (4), made it possible to determine when an individual stud started to fail. At least three pairs of studs near each end of the beam were instrumented in this way. In beams A, B and C of Group 1, the second pair of studs beyond the load points was also instrumented in the same manner.

## Test Procedure

Initially each beam was loaded statically 3 times to the maximum load which was to be applied dynamically. During these cycles of static testing, strain, deflection, and end slip data were taken at load increments from zero to the maximum. This procedure was followed so that any small inelastic deformations caused by the initial loading could be determined before the start of the dynamic tests.

Following this initial static test, the beam was tested dynamically from the minimum to the maximum load at the rate of about 180 cycles/min. Periodically, the dynamic test was interrupted to make static tests in which the strain, deflection, and end slip measurements were again taken at incremental loads. This general procedure was followed throughout the tests with only slight variations in the number of cycles between static tests. No deflection, slip or strain measurements were made while the specimen was under dynamic loading.

The applied dynamic load for all beams, with the exception of 1-A, was identical and ranged from 4 to 33 kips. For beam 1-A, the imposed dynamic load range was 5.2 to 51 kips per hydraulic jack.

# TEST RESULTS

The results of the fatigue tests are presented in the following sections. Each beam was tested from a condition of complete composite action to one approaching no composite action. All of the test specimens failed by shear failure in the studs. Usually the studs in one shear span failed completely and the studs on the opposite end showed definite deterioration but were not completely sheared off. As should be expected, the

TABLE 4

SUMMARY OF FATIGUE TEST RESULTS

| Specimen | Load[a] (kips) | | Avg. Stud Stress (ksi) | | Stress Range (ksi) | No. Cycles to Failure | | |
|---|---|---|---|---|---|---|---|---|
| | $P_{max}$ | $P_{min}$ | Max. | Min. | | First Stud | First Pair of Studs | Beam |
| 1-A | 51 | 5.2 | 18.4 | 1.9 | 16.5 | 70,000 | 85,000 | 105,200 |
| 1-B | 33 | 4 | 16.5 | 2.0 | 14.5 | 1,620,000 | 4,330,000 | 4,490,000 |
| 1-C | 33 | 4 | 20.3 | 2.5 | 17.8 | 205,000 | 230,000 | 260,500 |
| 1-D | 33 | 4 | 13.9 | 1.7 | 12.2 | 1,400,000 | 2,380,000 | 2,870,000 |
| 2-A | 33 | 4 | 11.9 | 1.4 | 10.5 | 1,500,000 | 1,800,000 | 2,282,000 |
| 2-B | 33 | 4 | 16.5 | 2.0 | 14.5 | 600,000 | 900,000 | 1,333,000 |
| 2-C | 33 | 4 | 20.3 | 2.5 | 17.8 | 90,000 | 103,000 | 120,000 |

[a]Force (two on each specimen) applied by each hydraulic jack.

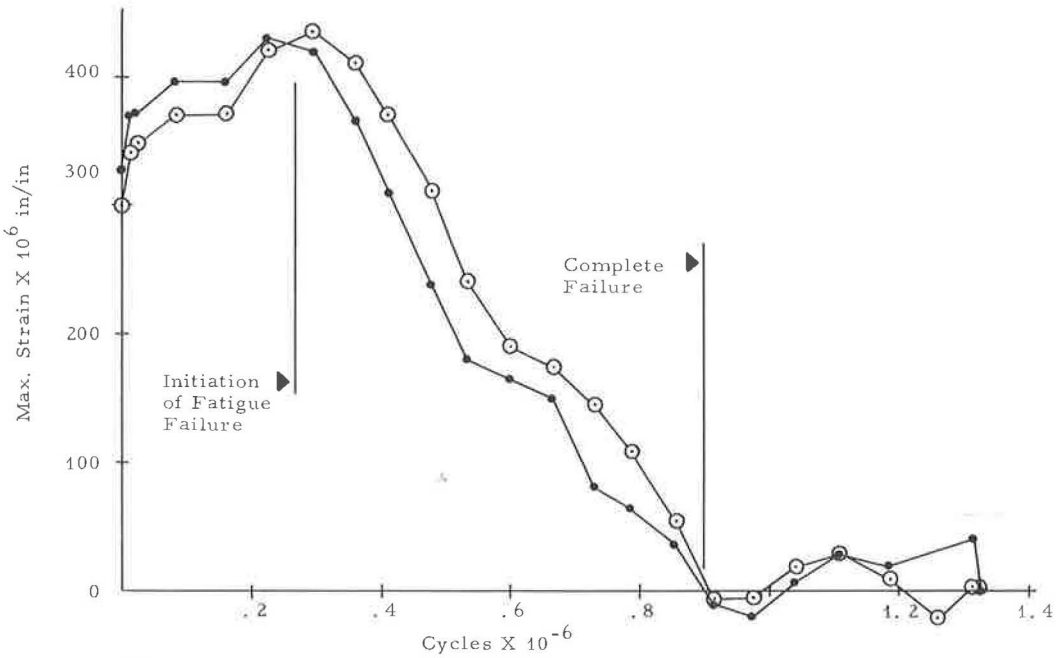


Figure 7. Local strain readings vs cycles for one pair of studs.

end slip in the shear span that failed was much greater than that on the opposite end. This is illustrated in the discussion of beam 1-B. The fatigue test results are summarized in Table 4.

## Loads on Individual Studs

As described earlier, an attempt was made to measure the effectiveness of individual shear connectors. In the initial static test, at maximum load, tensile strains of 150 to 400 $\mu$ in./in. were recorded from these gages. When the beam was unloaded, small residual strains were present. As the dynamic test progressed, the strains from these gages increased. Then, as the studs cracked and became less effective as shear connectors, the strains gradually went to zero and eventually went into compression when the stud was completely sheared off. Figure 7 shows strain readings from a pair of studs in specimen 2-B. The readings plotted in Figure 7 are qualitatively typical of all the studs instrumented.

It should be noted that the strains recorded from these gages serve only as an index to the magnitude of the load transferred from the slab to the steel section by a particular stud. The information derived from these measurements is relative and shows only the effectiveness of a stud as the number of cycles increases. These local strains cannot be compared from stud to stud.

In all beam tests, stud failure was observed by the foregoing technique before measurements of deflection and end slip indicated any significant deterioration of composite action.

## Steel Beam Stresses

The maximum stress under dynamic loading conditions in the tension flange of the steel beam varied from about 9,900 to 31,000 psi for all specimens except 1-A, whose bottom flange yielded extensively during the initial loading. These values were effectively constant throughout the fatigue tests. The only measurable increase in tension flange stress occurred near the end of the dynamic test when each beam rapidly lost composite action.

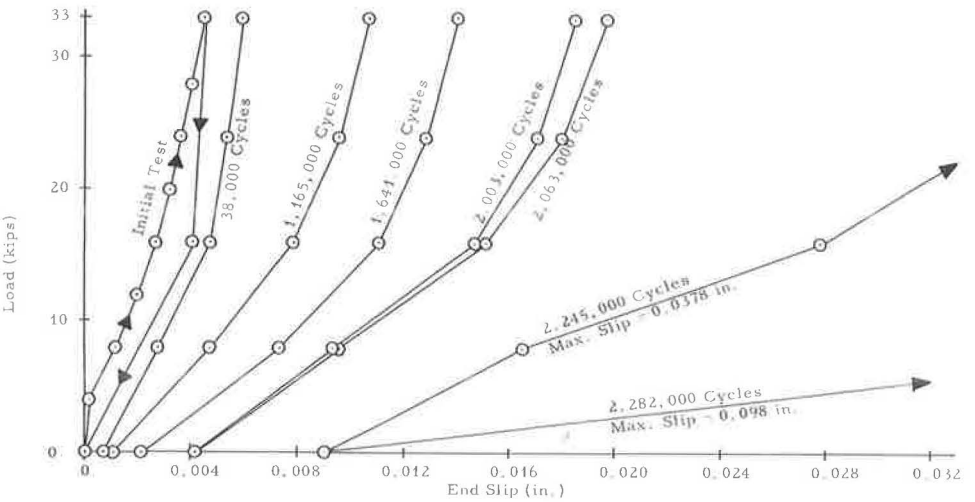


Figure 8. End slip vs load at hinged support on specimen 2-A.

## Effects of Bond

As discussed previously, an attempt was made to eliminate bond between the concrete and the top flange of the steel beam by applying a light film of oil to the beam before the concrete was cast. An evaluation of the success of this effort is necessary to determine accurately the loads applied on the shear connectors.

The initial static load test produced end slip which gradually increased as load increased. This condition was true for both ends in all beams. It seems unlikely that a significant amount of slippage would occur if bond was present. Furthermore, measured midspan deflections in the first static test were always slightly greater than those calculated.

Other data pertinent to the evaluation of the effects of bond come from the strain gages used to determine loads on specific studs. On the initial static test all of the studs instrumented produced tensile strains which progressively increased with the applied load, although the gages were on the compression side of the neutral axis. This indicated a significant load on the shear connectors which, in turn, showed that there was little, if any, bond between the steel beam and the concrete.

In addition, a quantitative appraisal of the strains recorded from the gages placed underneath the studs not only reinforced the hypothesis that bond was not present, but also indicated that the strains were simply proportional to the force on the stud.

This evidence seems to indicate that bond was not a significant factor in these tests. Therefore, in calculations of connector shear stresses, no bond was assumed between the slab and the steel beam.

## Group 2—Beams with Defective Stud Welds

Specimen A (44 Studs per Shear Span).—Under dynamic loading the average stud shear stress for beam 2-A, as computed from elastic theory and assuming complete composite action, fluctuated from 1,400 to 11,900 psi (range, 10,500 psi). The first stud failed at 1,500,000 cycles and the first pair failed at 1,800,000 cycles. (Failure was measured by local strains produced by the force on each stud. When this strain becomes zero the stud is considered to have cracked throughout.) Two additional pairs had failed before 1,900,000 cycles were recorded. As the fatigue test was continued, other studs failed. At 2,282,000 cycles, dynamic testing was discontinued because the beam exhibited very little composite action and tension cracks in the concrete were noted in the constant moment region. The stud shear failure occurred primarily on

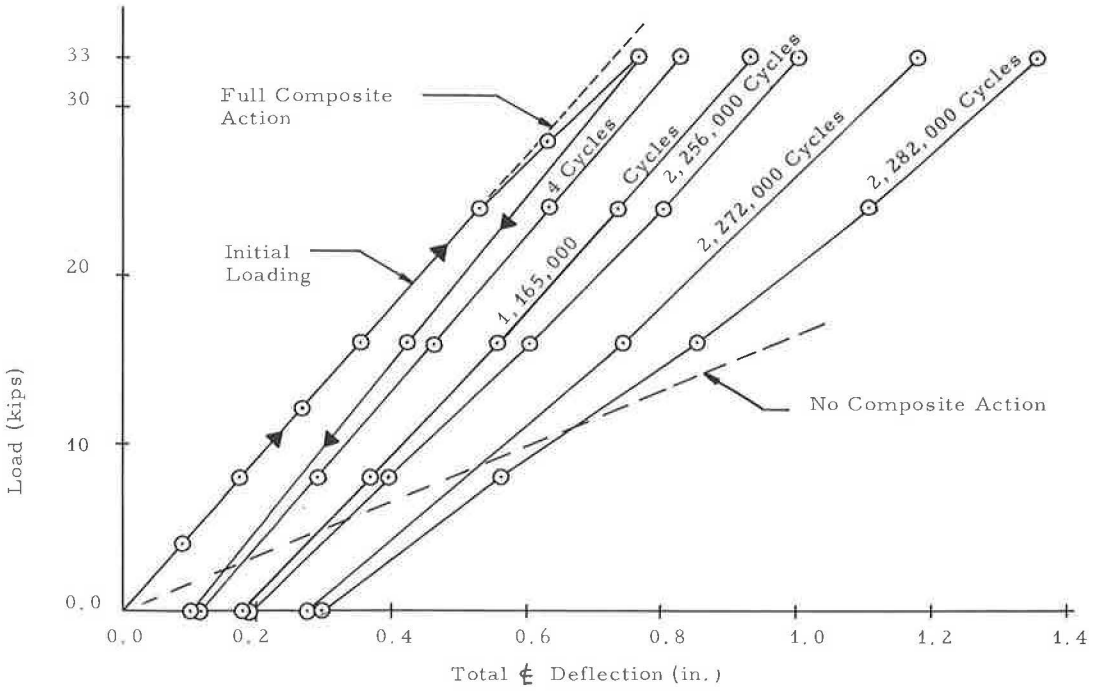


Figure 9. Total centerline deflection vs load for specimen 2-A.

the end with the hinged support. Figures 8 and 9 show the end slip on the hinged end and the midspan deflection of specimen 2-A. (The load in these and subsequent figures denotes the force applied by one of the hydraulic jacks; the total load on each beam is twice as much as shown.)

On specimen 2-A the concrete was carefully broken up and removed from both ends of the beam, allowing visual inspection of the studs. In the shear span which showed the principal failure, all of the studs were completely sheared off. Most of the fractures were in the heat-affected beam metal. Twelve of the studs were fractured in two places, in the beam metal forming a crater and about $\frac{3}{4}$ in. above the beam flange. It is of interest to note that eleven of the studs which fractured in two places were located in a longitudinal row on one side of the flange.

None of the studs in the shear span with the smaller end slip were sheared off completely. Most of these studs, however, were visibly cracked on the side nearest the center of the beam and were easily removed from the beam flange by striking them with a light hammer. Several of the studs were detached from the beam in this manner. The studs which were the most difficult to remove had a fatigue crack extending over about 40 percent of the stud area. Other studs which were more easily removed had fatigue fractures over about 90 percent of their area. It was quite evident from these observations that complete stud fracture in this shear span was imminent.

Specimen 2-B (32 Studs per Shear Span).—Stud shear stress on specimen 2-B ranged from 2,000 to 16,500 psi (range, 14,500 psi). The first stud failed at 600,000 cycles and the first pair of studs failed at 900,000 cycles. Additional stud failures were noted as cycling continued and the test was concluded at 1,333,000 cycles. In contrast to specimen 2-A, stud shear failure occurred primarily in the shear span nearest the rocker support.

The concrete was also removed from specimen 2-B. In the shear span that failed, all of the studs were completely sheared off. Most of the fractures were in the heat-affected beam metal. Seven of the studs were fractured in two places as in specimen 2-A. Figure 10 shows the bottom portion of one of these studs in place on the steel

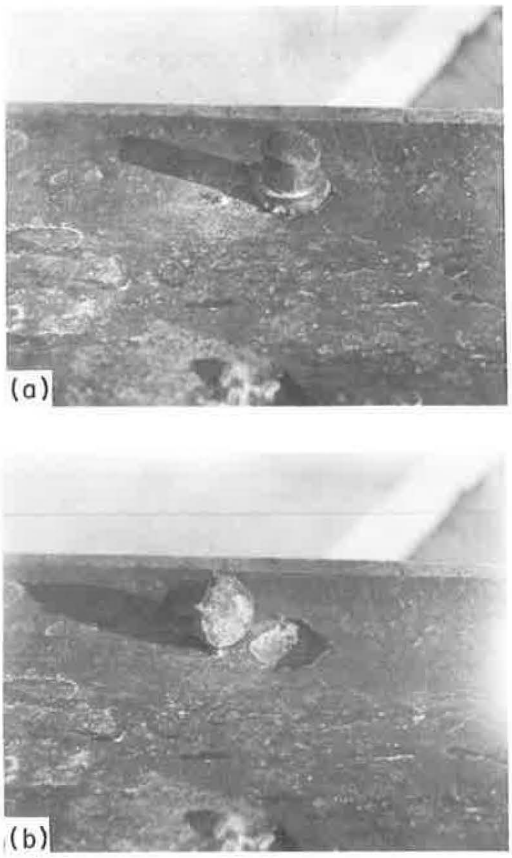


Figure 10. Stud failure on specimen 2-B.

beam flange. Figure 10b shows the same stud and the crater in the beam flange. The crater in the beam flange is typical of stud failures of specimens 2-A and 2-B.

Figure 11 presents load-slip curves after various cycles of dynamic loads were applied. Figure 12 shows the deflection at midspan measured after the indicated cycles of loading.

As in specimen A, tension cracks in the concrete were developed in the constant moment region under the loads and near the centerline. In the shear span showing the smaller slip, the studs were still attached to the beam flange. Serious fatigue cracking was present, however, and several of these studs could be pushed over and separated from the beam flange by hand. This indicates, as in specimen 2-A, that failure occurred in both shear spans at about the same number of cycles.

Specimen 2-C (26 Studs per Shear Span). —Stud shear stresses on specimen C fluctuated from 2,500 to 20,300 psi (range, 17,800 psi). Because this beam failed earlier than anticipated, sufficient data were not taken to determine precisely the first stud failure. Data from other studs on this test seem to indicate that the first stud failed at about 90,000 and the first pair of studs failed at 103,000 cycles. Fatigue testing was continued and at 120,000 cycles, all of the studs in the shear span nearest the hinged end had failed. As in specimens 2-A and 2-B, tension cracks in the concrete developed in the constant moment region.

Concrete was also removed from specimen C. Visual inspection of the stud fracture seemed to indicate defective welds. One of these failures is shown in Figure 13.

Figures 14 and 15 give the slips and deflections for this beam after the indicated cycles of loading were carried by the beam.

## Group 1—Beams with Acceptable Stud Welds

Specimens B, C and D. —These otherwise identical beams had 32, 26 and 38 studs per shear span, respectively. They were subjected to the same dynamic loads. Accumulated deflections were measured for 1-B and 1-C and are plotted in Figures 16 and 17. The load-deflection curve for beam 1-D is shown in Figure 18.

Load slips after various cycles are shown for these beams in Figures 19 through 22. It was stated that invariably one shear span indicated more slip than the other. Some specimens showed the larger slips at the rocker end, whereas others slipped more at the hinged end. There was no definite pattern. In Figures 19 and 20 the measured slips for both ends are plotted. It can be noted that at the end of the test while the north end slipped over 2 in., the south slipped less than ½ in. The load-slip curves presented for all the other six specimens show the data obtained only from the end that slipped most.

The beam, which sagged about 2 in. due to this failure, was jacked up and repaired by welding a T-section replacing two-thirds of the lower portion of the beam. Beam

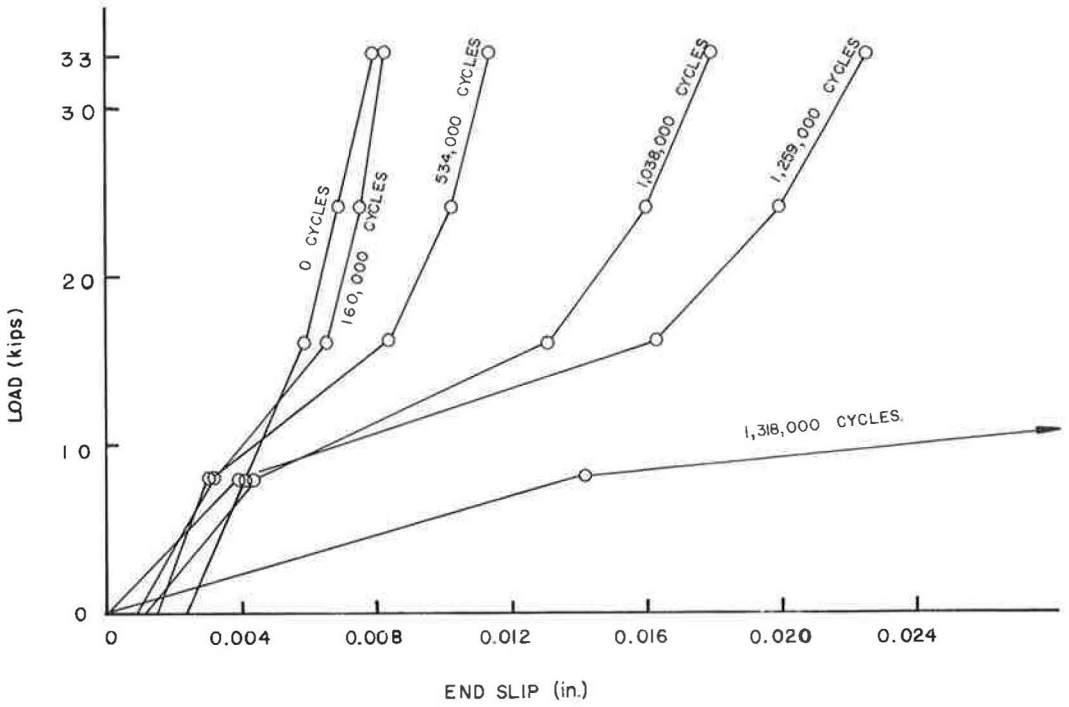


Figure 11. End slip vs load for specimen 2-B.

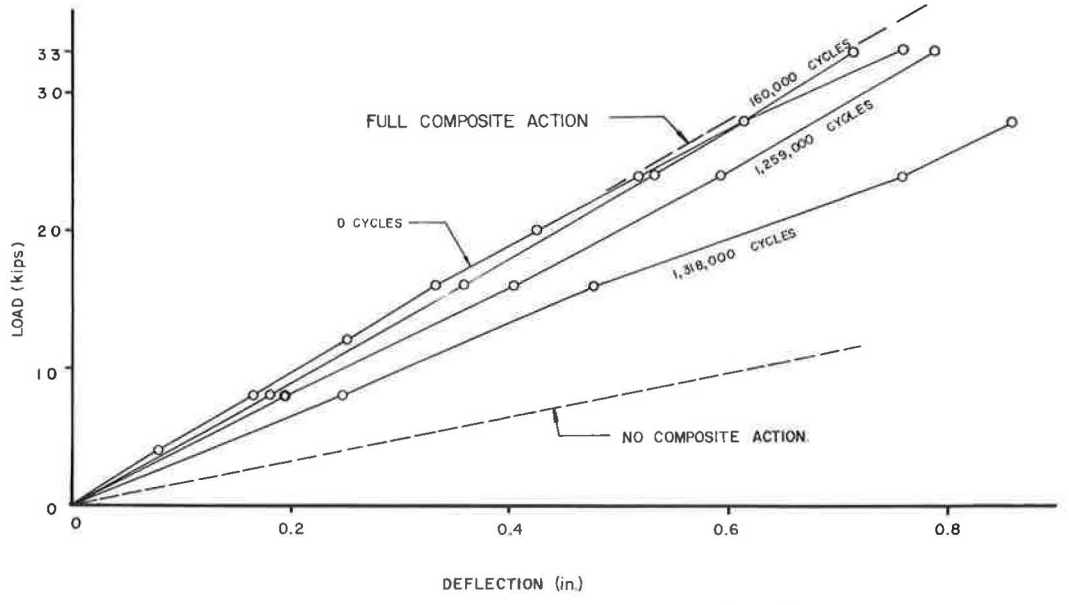


Figure 12. Deflection vs load for specimen 2-B.

Figure 13. Stud failure in specimen 2-C.

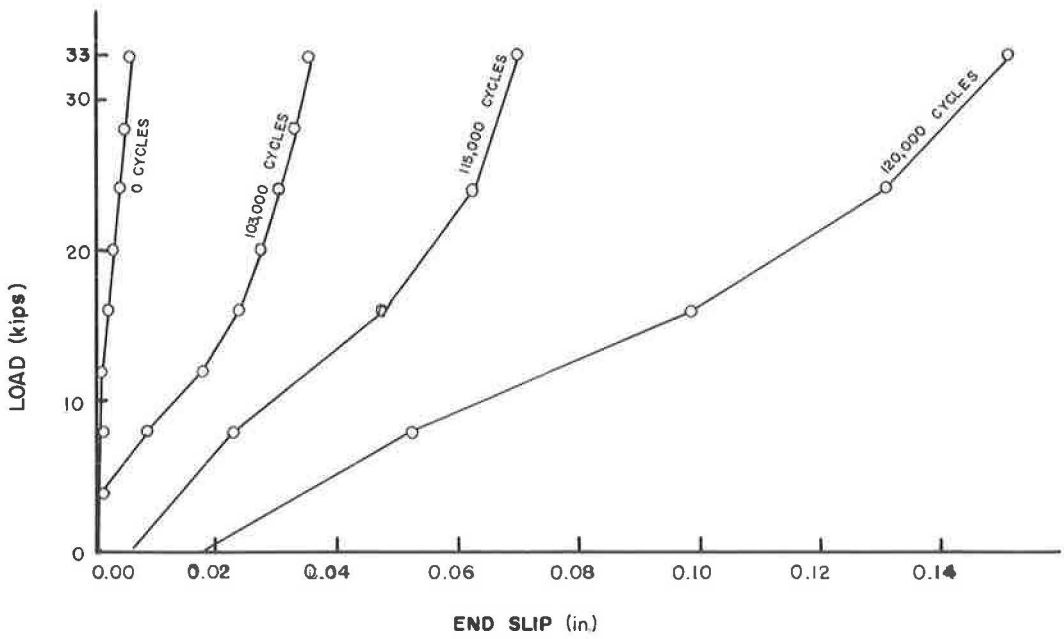


Figure 14. End slip vs load for specimen 2-C.

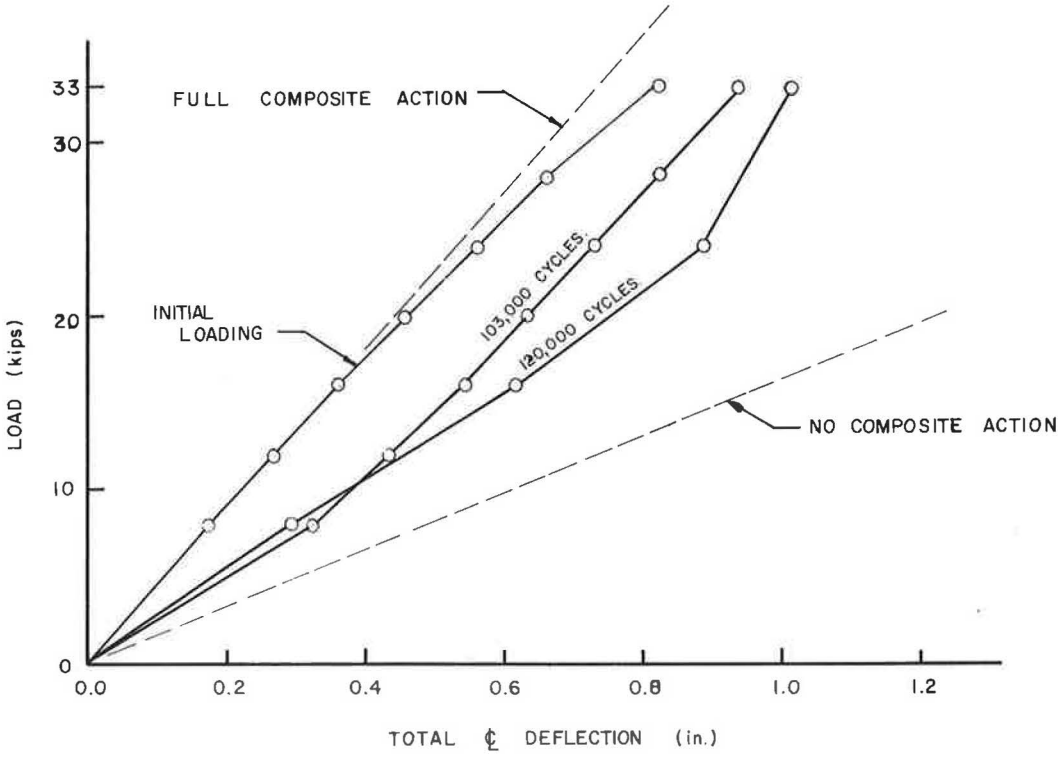


Figure 15. Total deflection vs load for specimen 2-C.

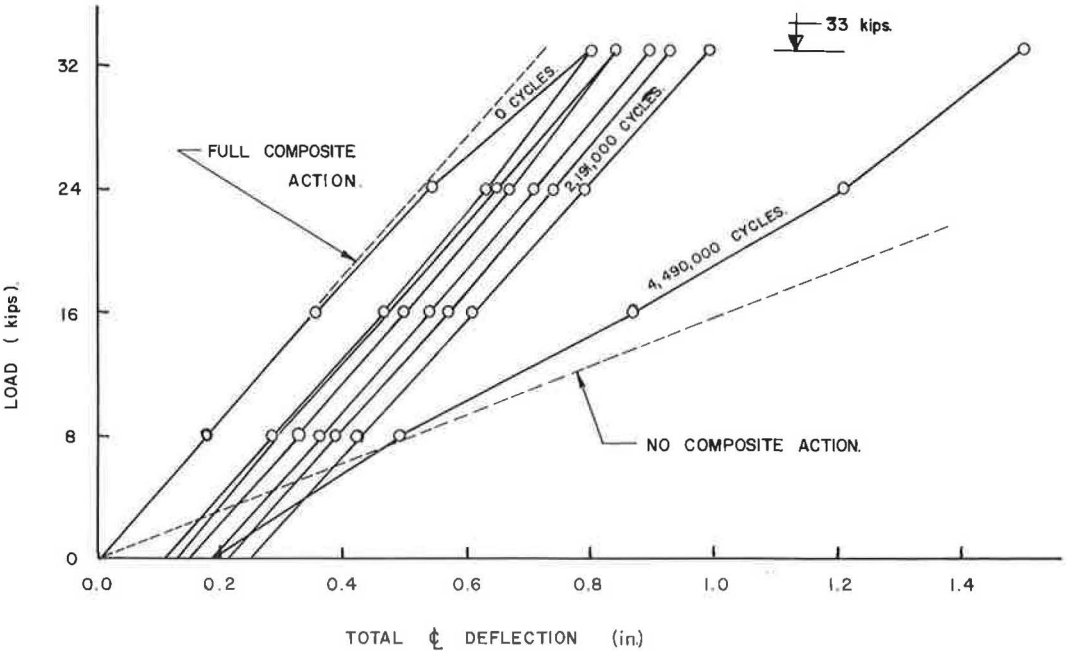


Figure 16. Total centerline deflection vs load for specimen 1-B.

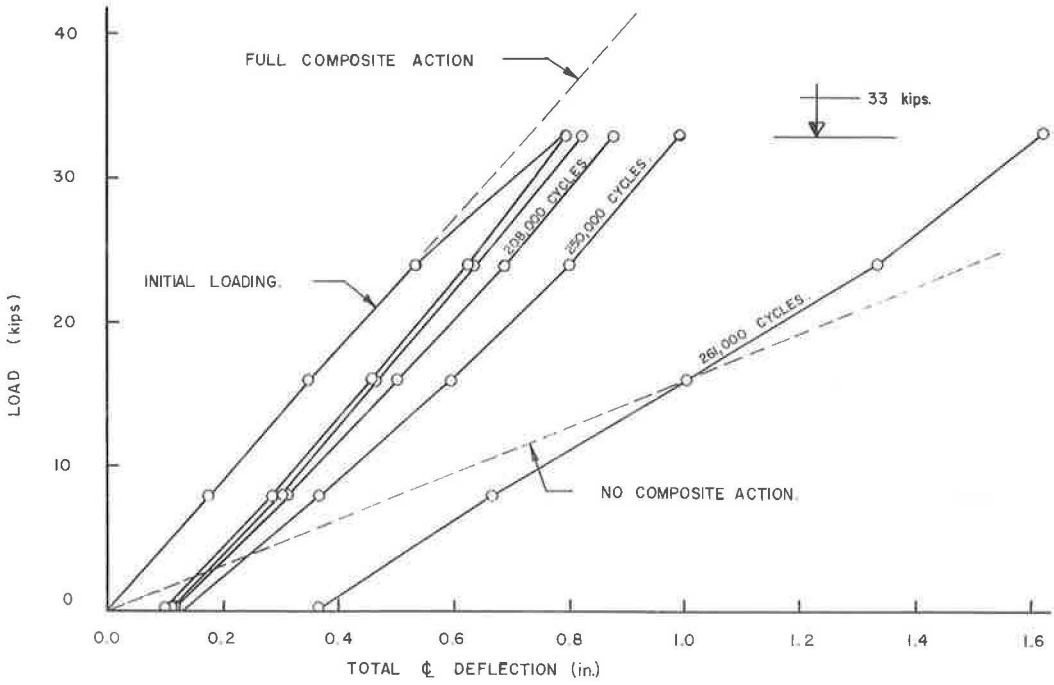


Figure 17. Total centerline deflection vs load for specimen 1-C.

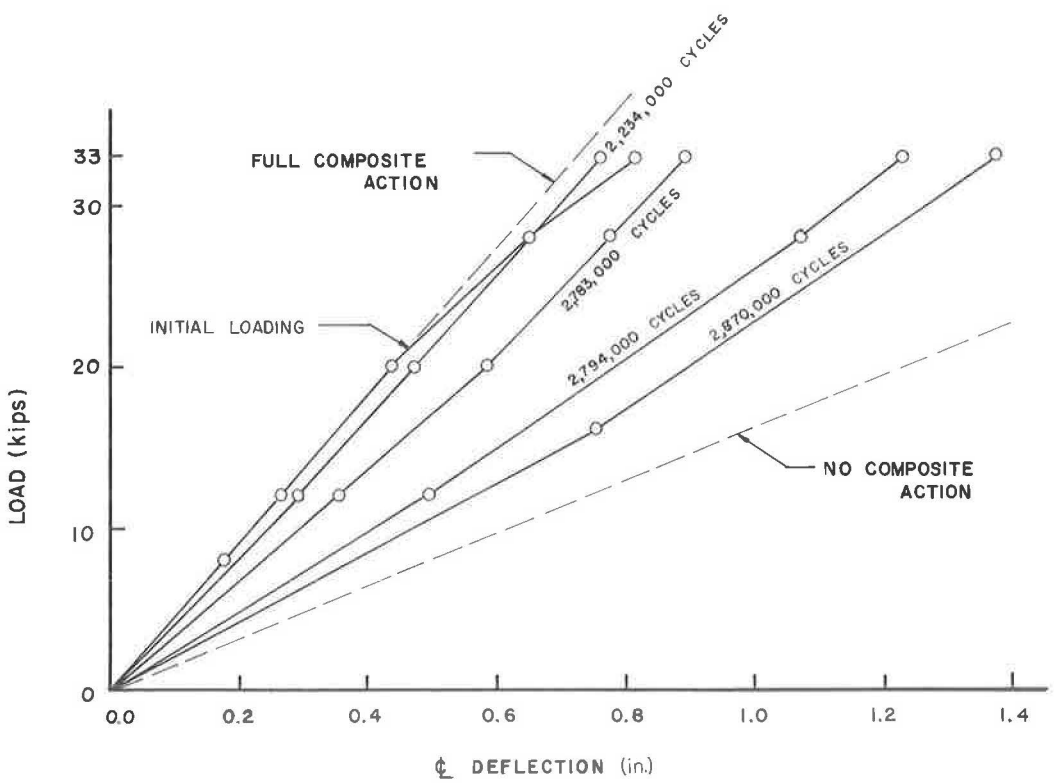


Figure 18. Centerline deflection vs load for specimen 1-D.

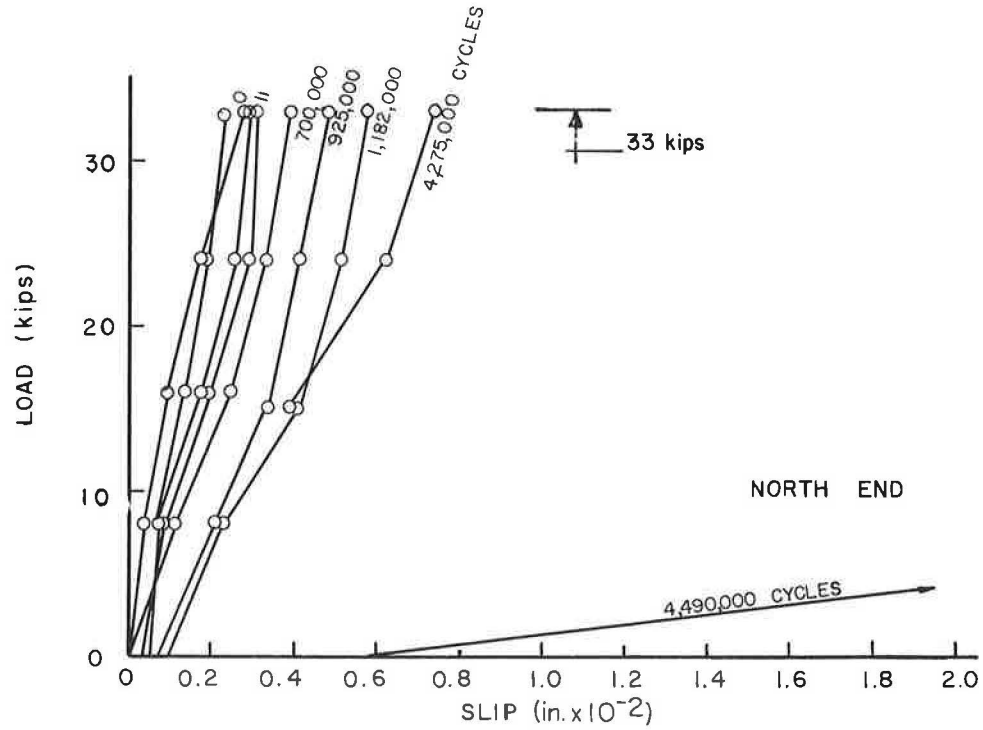


Figure 19. Slip vs load for specimen 1-B.

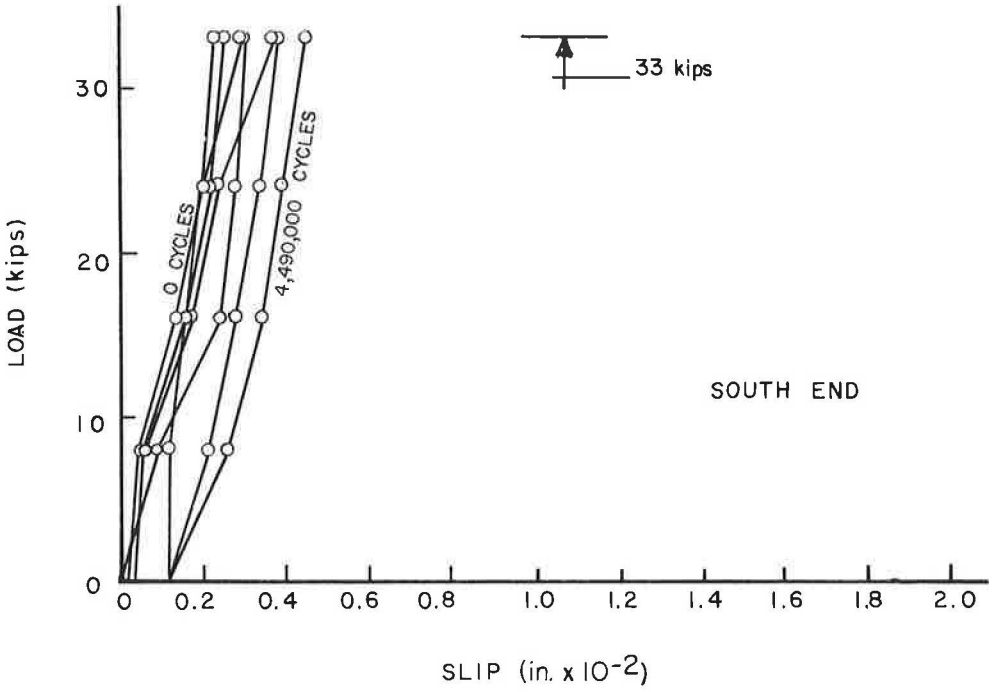


Figure 20. Slip vs load for specimen 1-B.

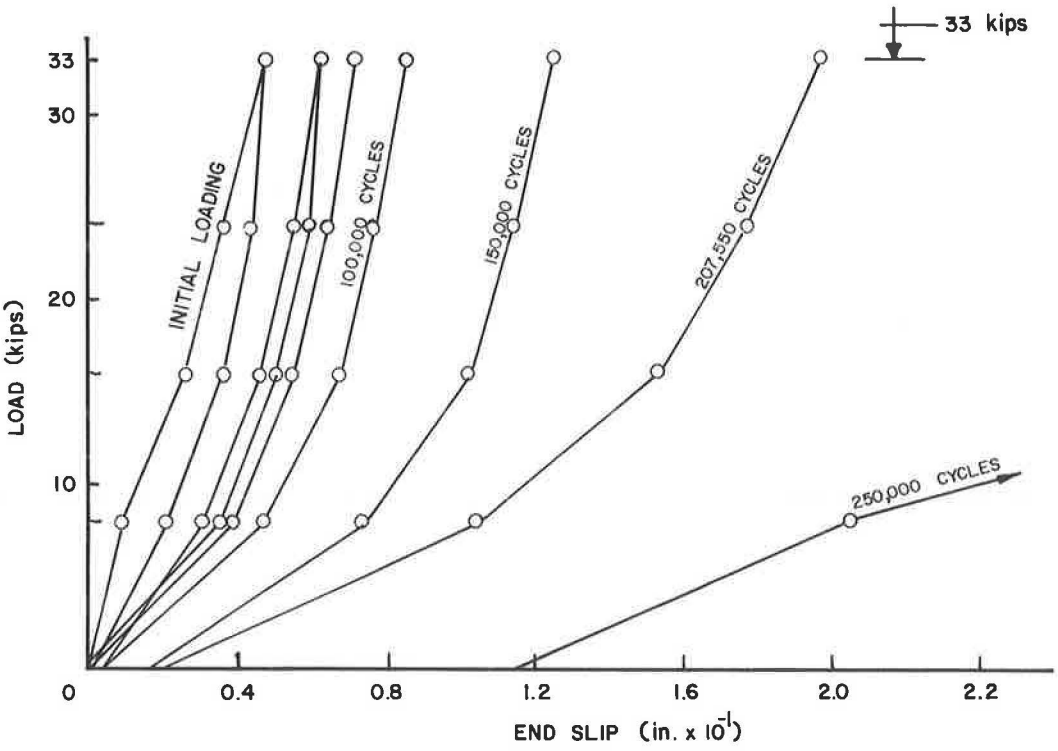


Figure 21. End slip vs load for specimen 1-C.

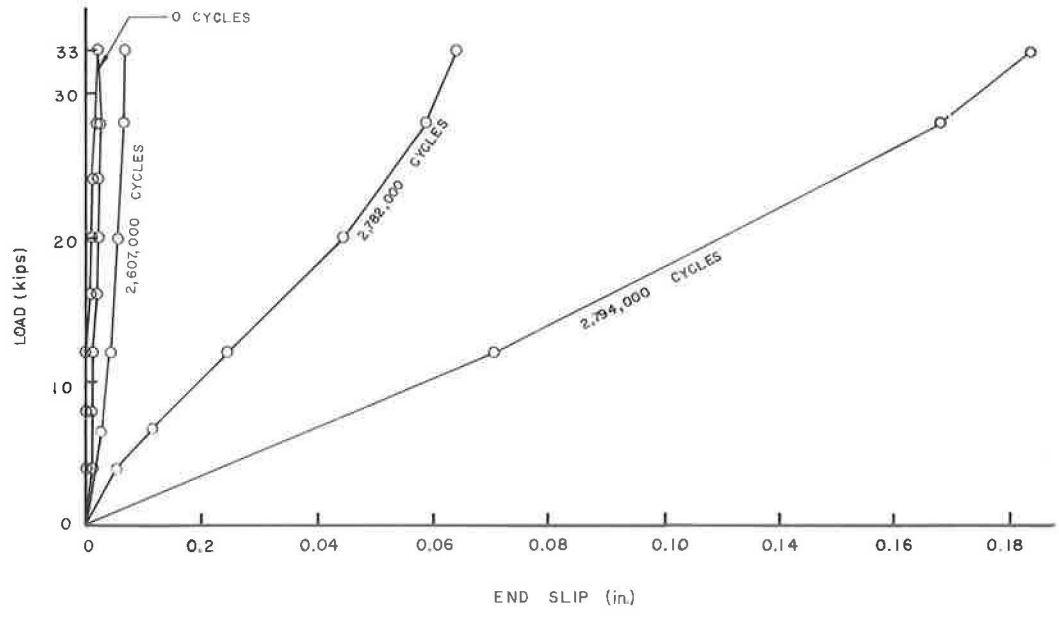


Figure 22. End slip vs load for specimen 1-D.

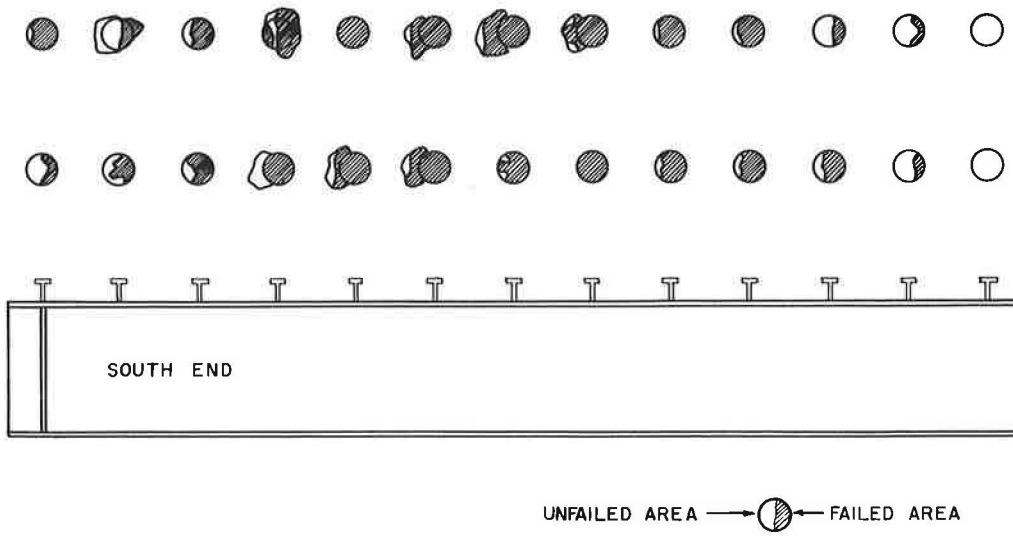


Figure 23. Representations of stud failures for specimen 1-C.

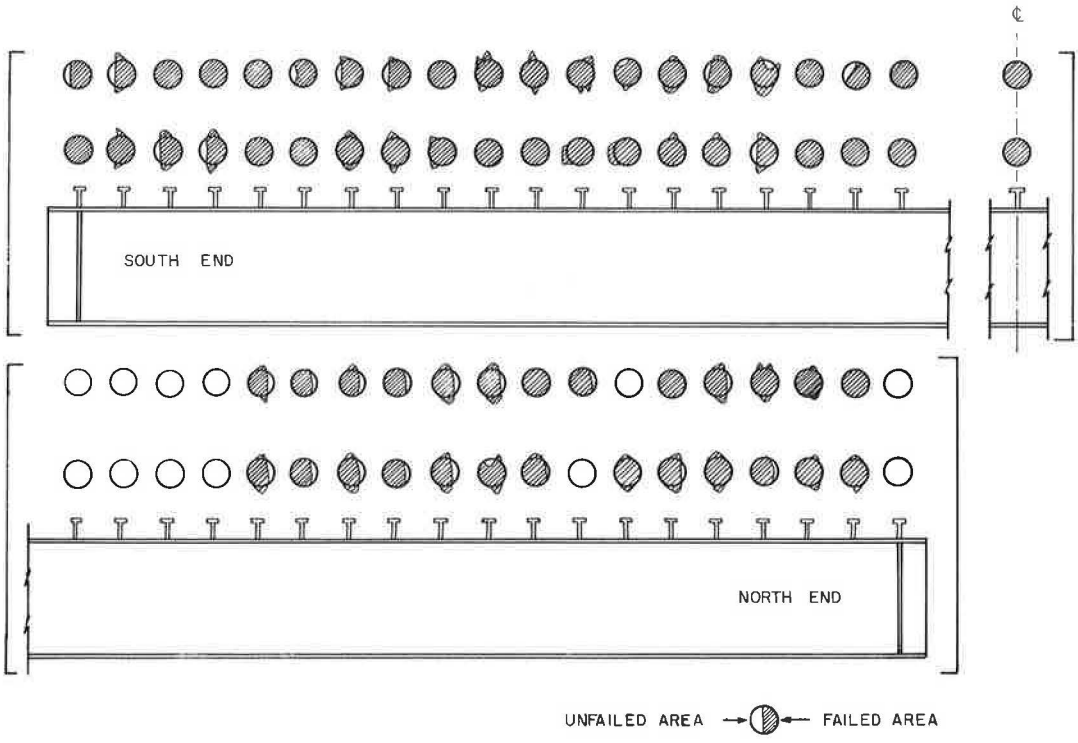


Figure 24. Representations of stud failures for specimen 1-D.

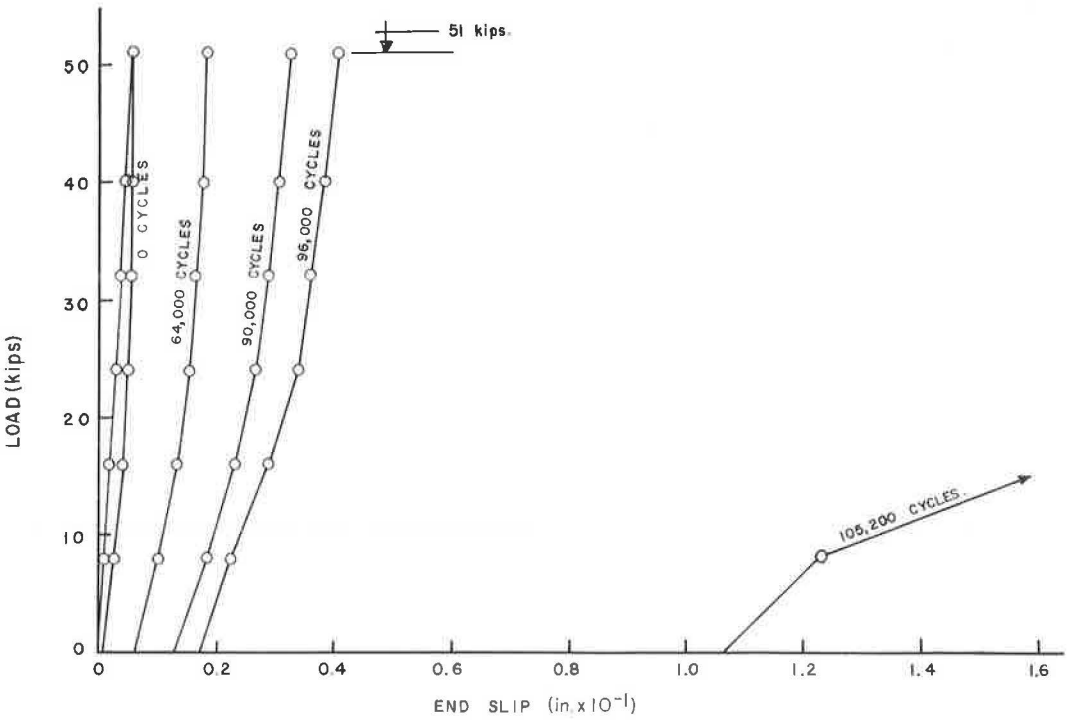


Figure 25. End slip vs load for specimen 1-A.

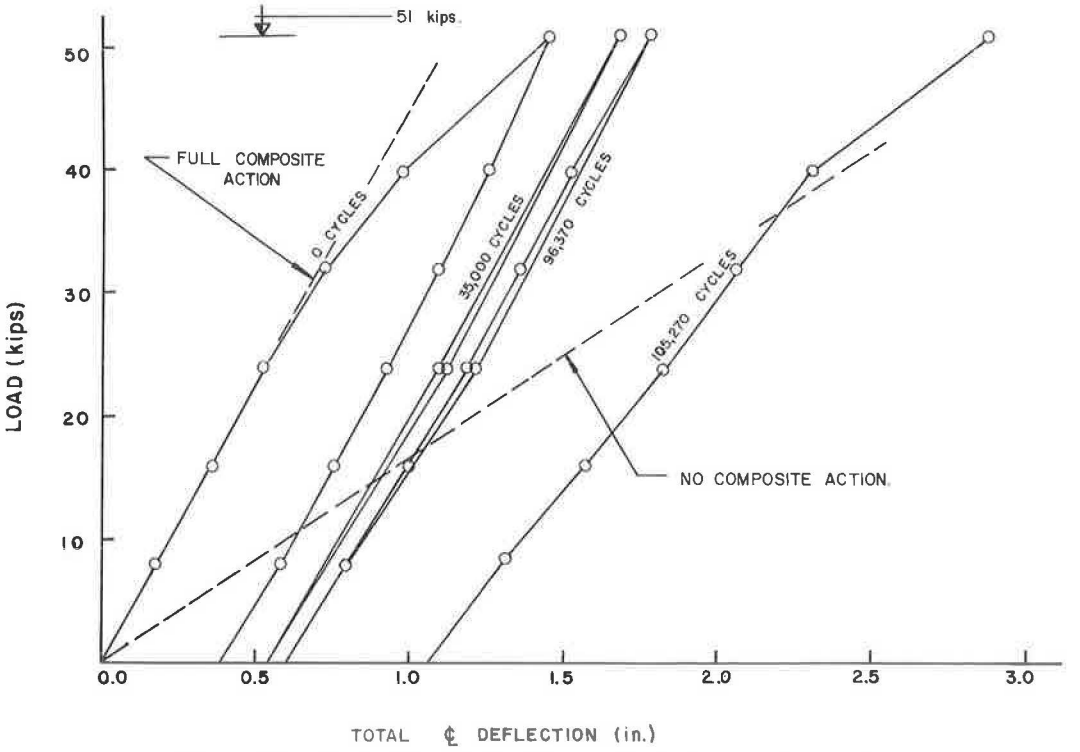


Figure 26. Centerline deflection vs load for specimen 1-A.

1-D had a fatigue failure in the tension flange of the steel section at 1,507,000 cycles. Although this failure and the subsequent repairs could have affected the structural integrity of the composite beam, testing was resumed after repairs.

Figures 23 and 24 show the condition of studs and/or flange after the concrete for beams 1-C and 1-D was removed. In both beams the south shear span (rocker end) showed the largest slip. Whereas all the studs of the south end sheared off completely, 12 (about 32 percent) at the north end were without any crack. These two sketches, which are typical, suggest that stud failure starts at or near the reaction point and proceeds toward the load points. In most specimens the pair of studs above the reaction was either without crack or if it had a crack, it was due to a defective weld.

Specimen A.--This beam was in all respects similar to 2-A with two exceptions: (a) its welds were superior and acceptable, and (b) it was subjected to 58 percent heavier loads. The maximum hydraulic cylinder load for beam 1-A was 51 kips vs 33 kips for 2-A. Such a heavy load resulted in yielding at the bottom flange and in shifting of the neutral axis.

The end slip for this beam is given in Figure 25, and Figure 26 shows the centerline deflection with residual deflections. This beam failed after 105,200 cycles.

## ANALYSIS OF RESULTS

The following discussion is a comparison of the results of this study with other investigations and with current design specifications.

### Criteria for Failure

Several criteria could be used in defining the fatigue life (cycles to failure) of a composite beam, including: (a) number of cycles when the first reduction in stud effectiveness occurs, (b) number of cycles when the first stud becomes completely ineffective, (c) number of cycles when the first pair of studs becomes completely ineffective, and (d) the point at which the rate of loss in composite action increases considerably. Of these, the last was chosen in this report for the obvious reason that even though studs failed in a progressive manner, no corresponding progressive increase in deflection or end slip was observed. In fact, end slip and deflection remained fairly constant throughout the test until just before the beam failed completely. Figures 27 and 28 show end slip, midspan deflection, and the neutral axis position as a function of the number of cycles of Group 1 and 2 beams. The neutral axis location was determined from strain readings at mid-span. It should be pointed out here that for specimens 1-D, 2-B, and 2-C, the deflection plotted is simply that measured as the load was increased from zero to the maximum during the static tests. The deflection for the rest of the specimens, however, represents total deflection, which includes residual deflection, from the beginning of the dynamic tests. This accounts partly for the difference in the deflections as plotted for specimens 2-A and 2-B, and 1-B, 1-C and 1-D.

The results as plotted in Figures 27 and 28 indicate that there is a definite point (number of cycles) which can be taken as the failure point and it should be used as the failure criterion instead of any other whose determination is neither easy and practical nor structurally significant.

## S-N CURVE FOR 3/4-IN. STUD CONNECTORS

Loads on shear connectors were determined by applying elastic analysis to the transformed section and computing a total horizontal shear force in each shear span. This total shear force divided by the area of the studs in that particular shear span gave the average stud shear stress.

As a means of comparing the results of the present study with other fatigue tests, an S-N curve was plotted based on the results of Group 1 beams. This curve, shown in Figure 29a, was drawn as the "best fit" line between the four points using the least squares method. A second-order polynomial when fitted to these points indicated the stress at 10 million cycles to be about 13 ksi. (Specimen 1-D is included in these

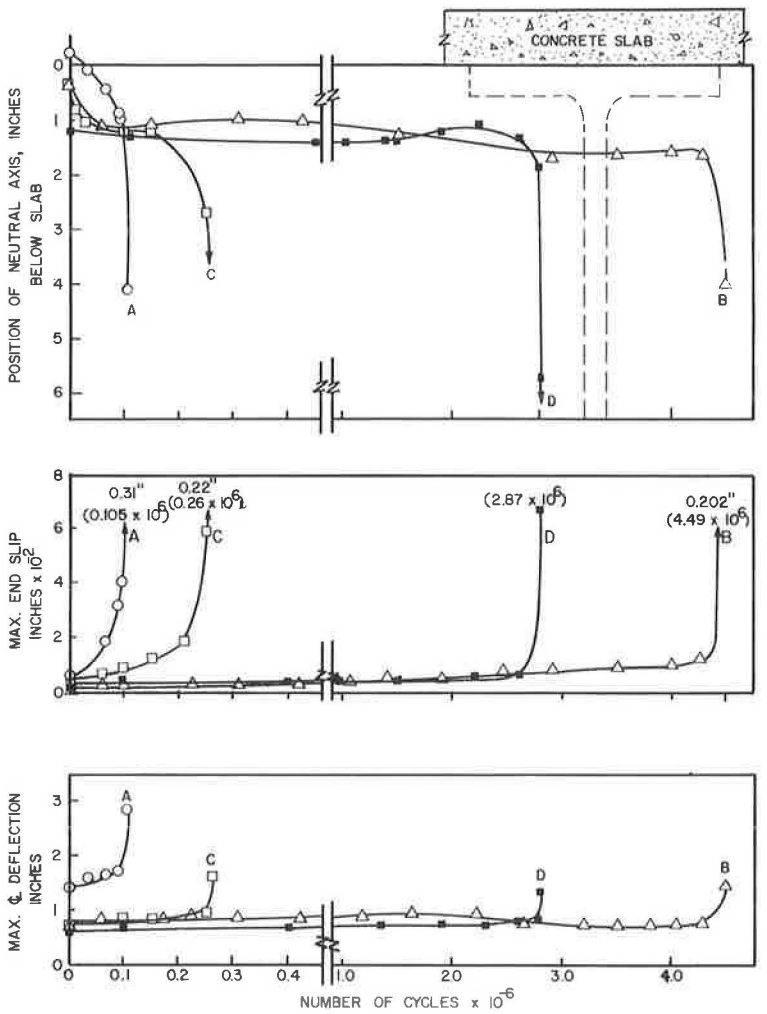


Figure 27. Deflection, end slip, and neutral axis position vs number of cycles—group 1 beams.

results even though its performance indicates that it was affected by the failure in the steel tension flange and by the subsequent operations during repairs. It would have been more logical if this beam were classified as belonging to Group 2.) Further, the curve is rather flat. Between 10,000 and 10 million cycles, the stress varies from about 20 to 13 ksi.

When the results of Group 2 were plotted, it became apparent that only beam 2-A reflected the effect of bad fabrication (defective stud welds). Admittedly, 2-A was the worst of the Group 2 beams. Possibly B and C of this group may not have been as defective as they looked. The S-N curve of Figure 29a is redrawn in Figure 29b and comparisons are made with the results of previous investigations at Lehigh University. The plotted points show that there is a "size effect" when $\frac{1}{2}$- and $\frac{3}{4}$-in. studs are compared, and its magnitude in the 1 to 3 million cycle area seems to be around 3 ksi.

Assuming that the relationship as indicated by the curve is reasonably valid, a comparison of it with the AASHO specifications (8) indicates the factor of safety against fatigue for loading from zero to maximum stress as follows:

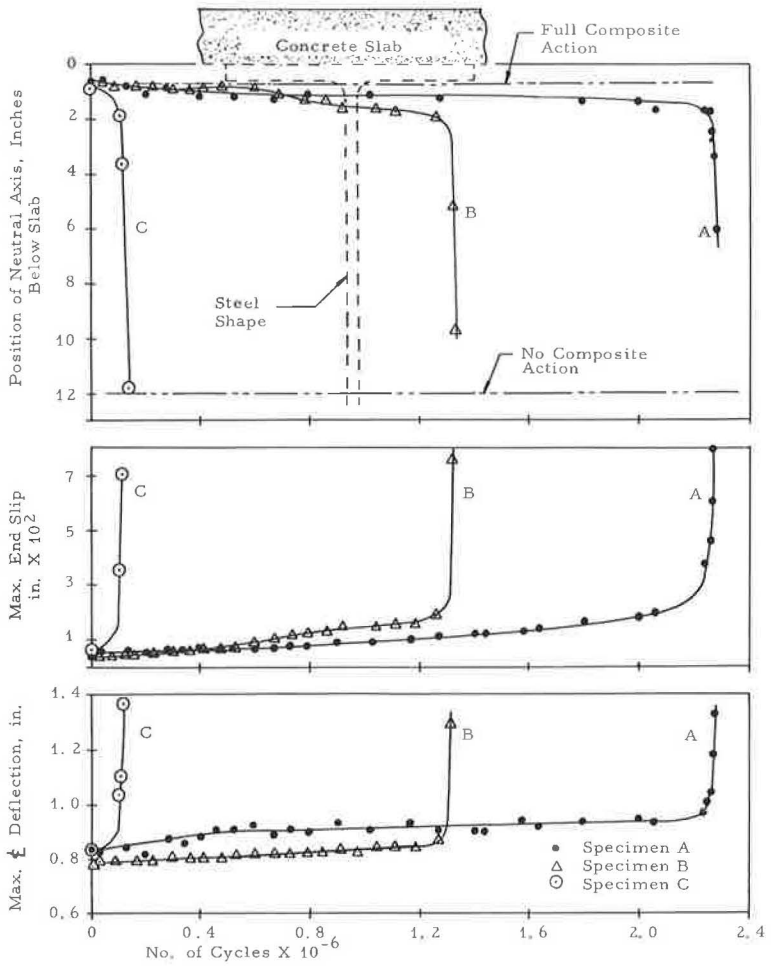


Figure 28. Deflection, end slip, and neutral axis position vs number of cycles—group 2 beams.

Assuming an average factor of safety = 3.70,

$$\text{Useful capacity} = Q_{uc} = 330\,(0.75)^2\sqrt{4400} = 12.3 \text{ kips}$$

$$\text{Allowable load} = 12,300/3.70 = 3,300 \text{ lb/stud}$$

Taking from the S-N curve in Figure 29 the stress value of 13.8 ksi for 2,000,000 cycles, we obtain:

$$\text{Load} = 13,800 \times 0.442 = 6.1 \text{ kips/stud}$$

Thus, the ratio of the load for expected failure at 2,000,000 cycles to the allowable design AASHO load is 6.1/3.3 = 1.85.

If similar calculations are made on the basis of the stress for 10 million cycles, we have the following:

$$\text{Strength of } \tfrac{3}{4}\text{-in. studs for } 10^7 \text{ cycles} = 13.0 \text{ ksi}$$

$$\text{Force per stud} = 13 \times 0.442 = 5.75 \text{ kips}$$

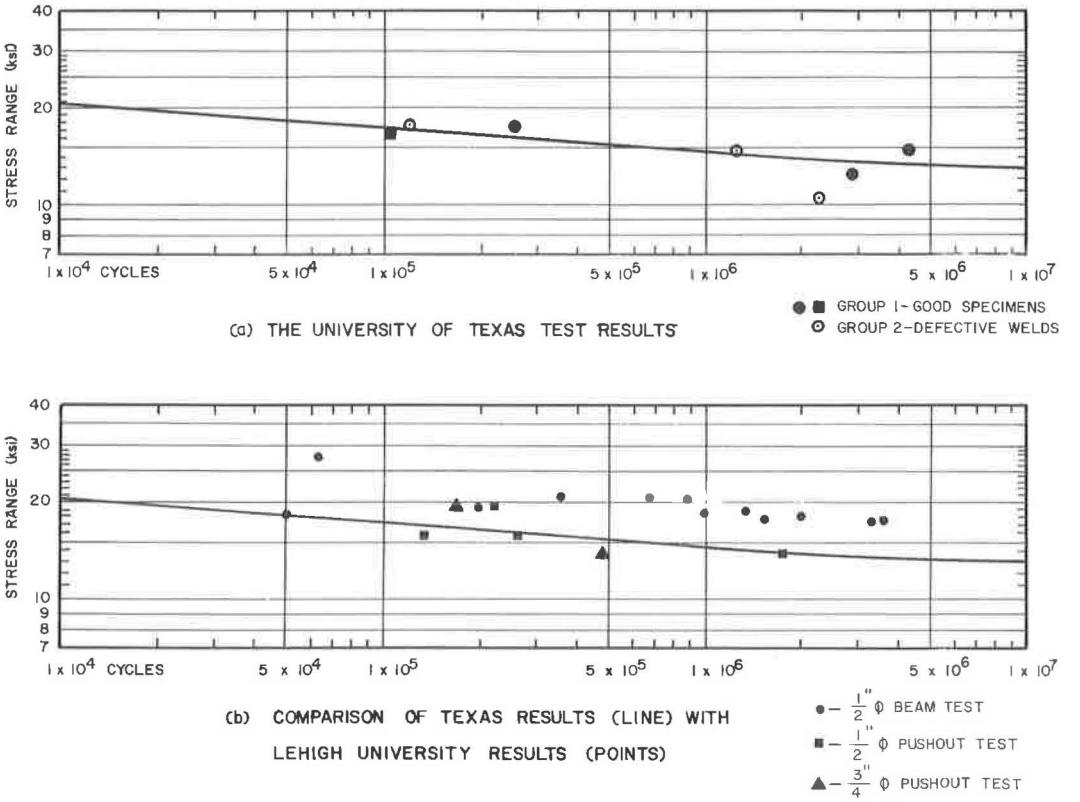


Figure 29. S-N curve for 3/4-in. stud connectors.

The factor of safety based on present AASHO specifications would be then 5.75/3.3 = 1.74. This is a rather high safety factor in view of the fact that even a very defective and totally unacceptable specimen such as beam 2-A was able to sustain 2,282,000 cycles with a stress range of 10.5 ksi. In view of this and if a factor of safety of 1.40 is agreed on, the allowable range of force per stud connector of $\frac{3}{4}$-in. diameter could be set at 4.1 kips.

## CONCLUSIONS AND RECOMMENDATIONS

The small number of specimens tested makes the results of this study tentative in nature. However, augmented by observation reported by Lehigh University, the total body of data is now comparable to that of other investigations which have been used as the basis for design recommendations. Conclusions from this investigation are as follows:

1. The procedure of using strain gages to indicate the effectiveness of individual studs is reliable. It is possible to evaluate the relative effectiveness of individual studs.
2. Stud failure is progressive in nature. Individual studs showed a gradual decrease in effectiveness.
3. End slip and deflection measurements are not sensitive to individual stud failure. Most of the instrumented studs in one shear span always failed before end slip or deflection measurements showed a significant increase.
4. The fatigue life (number of cycles for the same stress) of the beams with $\frac{3}{4}$-in. studs tested in this investigation was shorter than that of the beams with $\frac{1}{2}$-in. diameter

studs of earlier tests. The differences between the two investigations (Texas and Lehigh) are of the order of 3 ksi in stress range.

The question concerning the minimum number of studs required to provide an adequate factor of safety against stud fatigue failure has been partly answered. It seems reasonable that the AASHO specifications should be liberalized with respect to design of studs. Based on the results of the present study, it is recommended that the factors of safety presently used be liberalized.

## ACKNOWLEDGMENTS

This research project was carried out with funds supplied by the American Institute of Steel Construction. The author is thankful for the support and cooperation given by Dr. T. R. Higgins, Director, Engineering and Research, AISC. The interest shown to this project by Dr. Ivan M. Viest is also appreciated.

## REFERENCES

1. Viest, I. M., Fountain, R. S., and Singleton, R. C. Composite Construction in Steel and Concrete. New York, McGraw-Hill, 1958.
2. Viest, I. M. Review of Research on Composite Steel--Concrete Beams. Proc. ASCE, Jour. Struct. Div., June 1960.
3. King, D. C., Slutter, R. G., and Driscoll, G. C., Jr. Fatigue Tests of Composite Beams. Lehigh Univ., Fritz Eng. Lab. Rept. No. 285.3, March 1962.
4. Driscoll, G. C., Jr., Slutter, R. G., and King, D. C. Fatigue Strength of ½ Inch Diameter Stud Shear Connectors. Fritz Eng. Lab., Lehigh Univ. Unpubl. Lab. Rept., June 1963.
5. Türlimann, B. Fatigue and Static Strength of Stud Shear Connectors. Jour. ACI, Vol. 30, No. 12, June 1959.
6. Greer, D. C. (co-signed by A. W. Eatman). Letter from the Texas Highway Dept. concerning inspection of stud welding, Nov. 4, 1963.
7. Construction Bull. C-5. Texas: Texas Highway Dept., Austin.
8. Standard Specifications for Highway Bridges. 8th ed. Washington, D. C., AASHO, 1961.
9. Specification for the Design, Fabrication, and Erection of Structural Steel for Buildings. New York, AISC, 1961.
10. Commentary on the Specification for the Design, Fabrication, and Erection of Structural Steel for Buildings. New York, AISC, 1961.
11. Slutter, R. G., and Driscoll, G. C., Jr. The Flexural Strength of Steel and Concrete Composite Beams. Lehigh Univ., Fritz Eng. Lab. Rept. No. 279.15, 1963.

# Fatigue Strength of ½-Inch Diameter Stud Shear Connectors

D. C. KING, R. G. SLUTTER, and G. C. DRISCOLL, Jr.
Lehigh University, Department of Civil Engineering, Fritz Engineering Laboratory, Bethlehem, Pa.

Composite steel and concrete beams were tested in fatigue at various stress levels. All twelve beams tested had ½-in. diameter welded studs as shear connectors. The beams were designed so that normal working stresses would be achieved at peak loads during repeated loading while the shear stress on connectors was sufficiently high to produce fatigue failure. Fatigue failure of connectors actually occurred in eleven of the beams.

Electrical resistance strain gages were used in eight of the test beams to detect when fatigue cracks were initiated in connectors. The use of such strain gages enabled the investigators to determine the extent of fatigue failure at any time during the testing. This information was compared with end slip and deflection data taken during the tests.

The criterion of failure was taken as the initial cracking of a pair of shear connectors. On this basis an S-N curve was obtained from the results of seven of the beam tests. A statistical analysis of these data was made and the 95 percent confidence limits of the data were obtained. The data on fatigue of stud connectors obtained by other investigators fall generally within these 95 percent confidence limits.

•COMPOSITE STEEL and concrete beams are being extensively used in structures which are subjected to fatigue loading. Various aspects of this problem as related to composite beams have been studied, but the fatigue strength of various types of full-size shear connectors has not been determined by a systematic investigation. For this reason, information on the behavior of shear connectors subjected to fatigue loading is not as extensive as the seriousness of the problem seems to warrant. The magnitude of the factor of safety which design specifications provide against fatigue failure of the concrete slab (1) or a built-up steel section (2) is generally known, but the magnitude of the factor of safety with regard to shear connectors is for the most part unknown.

Before the 1957 revision of the AASHO Standard Specifications for Highway Bridges (3) a considerable amount of research on composite beams was conducted at the University of Illinois (4, 5). Both static and fatigue tests were performed in these investigations involving beams with channel connectors. The AASHO formulas for the useful capacity of shear connectors were derived from the static behavior of beams based on limitations on the amount of slip between concrete slab and steel beam. Tests showed that by placing limitations on the magnitude of slip, fatigue failure of connectors could be prevented.

Most of the full-scale beam tests made before 1962 were conducted to verify the adequacy of the AASHO formulas. However, there has been some evidence that the AASHO specifications do not permit the maximum economy of design possible in com-

Paper sponsored by Committee on Steel Superstructures.

posite construction. Before any revision of specifications can be undertaken, a thorough study of the fatigue strength of various types of shear connectors must be made.

In bridge construction today, the stud shear connector is the most commonly used type, but its fatigue behavior is not well understood. A research program was started in 1961 at Lehigh University to study the behavior of welded stud shear connectors subjected to fatigue loading.

The general objective of this investigation was to determine the fatigue strength of stud shear connectors and to determine if the design of beams could be based on this information. Fatigue tests of 12 composite beams are reported. Two groups of identical beams were tested with the only variable being the magnitude of loading on the beam. The results of these tests establish the fatigue strength of $\frac{1}{2}$-in. diameter studs for one value of minimum stress.

## REVIEW OF PREVIOUS INVESTIGATION

A review of previous testing programs involving the fatigue of stud shear connectors is useful so that this information can be analyzed along with the new test results. The previous tests consist of three approaches to the problem of investigating the fatigue strength of shear connectors. These are fatigue tests of bare studs, of pushout specimens, and of composite beams.

### Tests of Bare Studs and Pushout Specimens

Studs welded to steel plates without being incased in concrete were tested with stress reversal by a load applied perpendicular to the stud (6). These tests were performed with the force applied to the head of a $\frac{3}{4}$-in. diameter by 4-in. long stud. Sufficient results were obtained at various stress levels to establish the S-N curve for this loading condition, given as the upper curve in Figure 1. These results were quite high, and there would apparently be little danger of fatigue failure of stud connectors in composite beams.

Pushout specimens consisting of concrete slabs 6 in. thick attached to the flanges of 8 WF 40 beams by four connectors in each slab were tested (7). The results obtained from these tests are summarized in Table 1. The term hooked refers to studs having a 90 deg bend at the top. The horizontal leg at the top of a $\frac{1}{2}$-in. diameter stud was $1\frac{1}{2}$ in. long. The maximum and minimum shear stresses were obtained by dividing the maximum and minimum loads applied to the specimen by the area of the shear connectors.

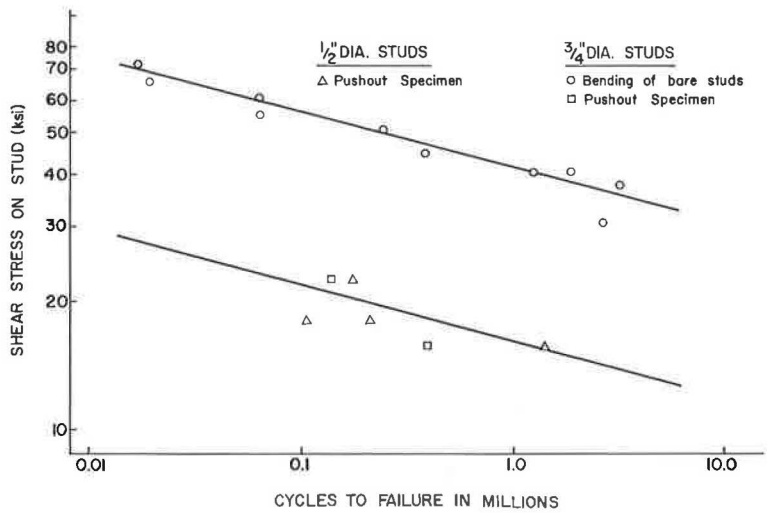


Figure 1. S-N curves for previous tests of stud shear connectors.

TABLE 1

SUMMARY OF FATIGUE TEST RESULTS BY OTHER INVESTIGATORS

| Specimen Number | Reference | Type of Stud Connector | Type of Test Specimen | Minimum Shear Stress on Stud (psi) | Maximum Shear Stress on Stud (psi) | Cycles of Loading | Results |
|---|---|---|---|---|---|---|---|
| 4 | 7 | 1/2" Dia. Hooked | Pushout* | 2900 | 22,300 | 223,200 | Stud Fracture |
| 5 | 7 | 1/2" Dia. Hooked | Pushout* | 2200 | 17,800 | 134,200 | Stud Fracture |
| 6 | 7 | 1/2" Dia. Hooked | Pushout* | 2200 | 17,800 | 261,000 | Stud Fracture |
| 7 | 7 | 1/2" Dia. Hooked | Pushout* | 1900 | 15,600 | 1,748,000 | Stud Fracture |
| 9 | 7 | 3/4" Dia. Headed | Pushout* | 2800 | 22,300 | 169,400 | Stud Fracture |
| 10 | 7 | 3/4" Dia. Headed | Pushout* | 1700 | 15,600 | 474,00~ | Stud Fracture |
| Bridge | 8 | 1/2" Dia. Bent | Beam | 1850 | 15,700 | 256,800 | No Failure |
| B4 | 9 | 1/2" Dia. Bent | Beam | 1500 | 21,000 | 619,000 | No Failure |
| B4 | 9 | 1/2" Dia. Bent | Beam | 1500 | 24,100 | 122,400 | No Failure |

*Concrete slabs on these specimens were 28 inches high by 20 inches wide

The data of Table 1 are plotted in Figure 1. The S-N curve through these points was arbitrarily drawn parallel to the upper curve. A statistical analysis of these data would result in a flatter curve than the one shown. Because only a small amount of data are available and there were several variables involved, the approximate curve shown in Figure 1 was considered acceptable for planning the new test series. The important point to be made concerning Figure 1 is that there is a vast difference between the two curves. It is, therefore, imperative that the correct curve for composite beams be known. The two curves of Figure 1 were taken as the probable upper and lower limits of the test results in planning the tests.

It is of considerable interest in making these tests to determine if pushout test results are comparable to beam test results since the testing of composite beams in fatigue is an expensive and time-consuming process and the pushout test is more easily performed and could be effectively used in extending the research work into other areas of interest.

## Beam Tests

Two composite beams with stud shear connectors were tested in fatigue at Lehigh University (8, 9). The first member consisted of two 18 WF 50 steel beams with a concrete slab 18.0 ft wide by 6 in. thick attached to the top flange by ½-in. diameter studs on one beam and ¾-in. diameter studs on the other beam. This member was tested on a span of 30 ft. The second member having a span of 10 ft consisted of an 8 WF 17 steel section with a concrete slab 4 in. thick and 2 ft wide attached to the top flange with ½-in. diameter studs.

Both of these beams were subjected to fatigue loading, but no failure of connectors occurred during the tests. The results of these tests were limited except to verify that the AASHO design specifications are satisfactory from the point of view of limiting shear connector stresses to values which probably prevent fatigue failure.

The data from the two beam tests are included in Table 1. The maximum and minimum stresses on the studs are calculated stresses. The shear stress on the connector, $f_s$, was calculated by

$$f_s = \frac{VQS}{I_{tr} A_s} \tag{1}$$

where V is the applied shear force at the cross-section, Q is the first moment of the transformed concrete slab area, S is the spacing of studs having a cross-sectional area

of $A_S$, and $I_{tr}$ is the moment of inertia of the transformed composite section. These data have not been plotted on Figure 1 since no failures were obtained. A comparison of the data from the beams with data from the pushout test specimens reveals that the beam test points would plot near the lower curve of Figure 1.

The data contained in Table 1 provide no basis for conclusions concerning the fatigue strength of stud connectors in composite beams. The only conclusion that can be drawn is that beam specimens must be tested at load levels which will produce fatigue failures of connectors. Such tests were conducted and the results are reported and analyzed in the subsequent sections of this report.

## EXPERIMENTAL PROGRAM OF THIS INVESTIGATION

### Scope

The investigation was limited to ½-in. diameter welded stud shear connectors to match the specimen size to the capacity of the available loading equipment. An additional advantage of using ½-in. diameter connectors was that more information was available for this size of connector than for any other. It was assumed that information obtained from these tests could be extrapolated to larger sizes of stud shear connectors, and that these extrapolated values would be verified by later tests.

### Preliminary Beam Tests

Before begining a full-scale series of fatigue investigations, it was decided that some preliminary tests should be made: (a) to produce fatigure failure of connectors in a beam; (b) to develop a method to determine exactly when a connector failed in fatigue; and (c) to develop a more comprehensive instrumentation and testing procedure for future tests.

Description of Specimens.—Each of four beams for the preliminary tests consisted of a 2-ft wide by 3-in. thick concrete slab cast onto an 8 WF 17 steel beam as shown in Figure 2. The shear connection consisted of ½-in. diameter hooked welded stud connectors. The spacing of these connectors is also shown in Figure 2. The section properties of the four specimens are given in Figure 3.

The testing of the specimens took place between 28 and 79 days after pouring. The average concrete strength at the time of testing for BF-A and BF-B was 3,030 psi and that for BF-C and BF-D was 3,500 psi.

Instrumentation.—The instrumentation consisted of electrical resistance strain gages at midspan under the top and bottom flanges of the steel section, a midspan deflection gage, and slip measuring devices at both ends and near the quarter points. The location of the strain gages is as shown in Figure 4. The locations of the deflection gage and four slip gages are shown in Figure 5. The slip gages consisted of 0.001-in. dial gages for the dynamic readings and 0.0001-in. dial gages for the static readings.

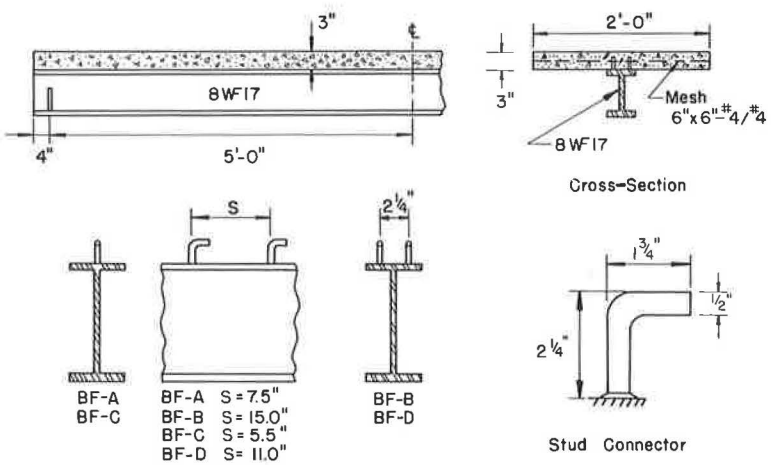


Figure 2. Dimensions of test specimens BF-A through BF-D.

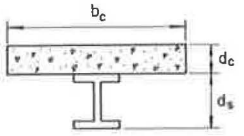


Concrete Slab
$b_c$ = 24 in.
$d_c$ = 3 in.
$f'_{c_{design}}$ = 3,500 psi
n = 10

Steel Beam (8 WF 17)
$d_s$ = 8.00 in.
$A_s$ = 5.00 sq.in.
$I_s$ = 56.4 $in.^4$
$f_{y_{design}}$ = 33,000 psi

Composite Section
$a_{st}$ = 7.48 in.
I = 156.0 $in.^4$

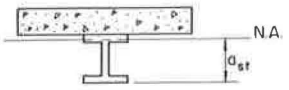


Studs (L-connector)
diameter = ½ in.
height = 2.25 in.
area = 0.196 sq.in.

Figure 3. Section properties for BF-A through BF-D.

Test Procedure.—The specimens were moved to the loading frame and testing was begun after the specimens had been wet-cured for 2 wk and air-cured for a minimum of 2 wk. Each specimen was initially loaded to a static value sufficient to break the bond between beam and slab. The testing arrangement is shown in Figure 5.

While being loaded statically, all strain gage deflection and slip gage readings were taken at intervals of 1.5 kips per jack. After this initial static test each specimen was loaded dynamically at 250 cycles/min. Static tests were taken at intervals until failure occurred. Periodically, dynamic end slip and deflection readings were taken.

## Primary Beam Tests

In the preliminary beam tests stud fatigue failures could be produced for the first time in a beam specimen. However, these tests supplied only four points for plotting the S-N curve for ½-in. diameter stud connectors. Obviously, many more points would be required firmly to establish the position of the S-N curve.

Also, even after the conclusion of the preliminary beam tests, a method had not been perfected for determining when a connector actually failed in a beam under a fatigue loading. The points taken as failure were determined on the basis of a visual observation that vertical movement of the slab with respect to the beam was taking place. However, it was observed that at the number of cycles designated as failure, several shear connectors were actually fractured.

As a result of these problems the primary beam tests concentrated on obtaining additional points for the S-N curve and on perfecting a method by which the initial failure of a connector in a beam could be determined.

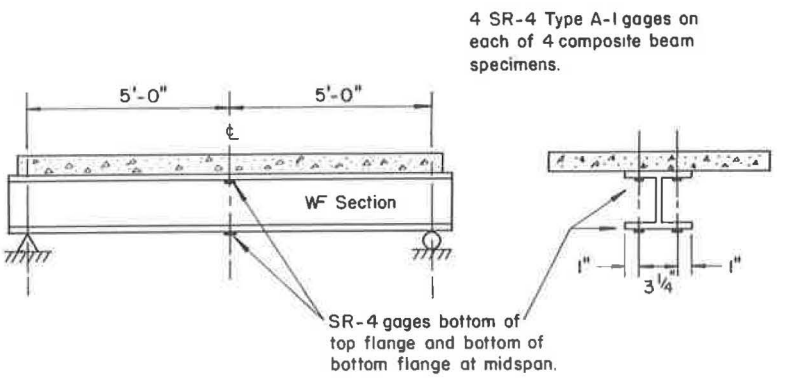


Figure 4. Strain gage locations for BF-A through BF-D.

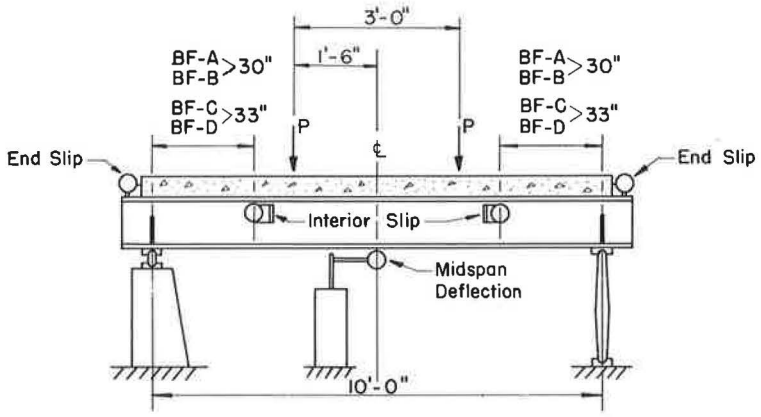


Figure 5. Test setup for BF-A through BF-D.

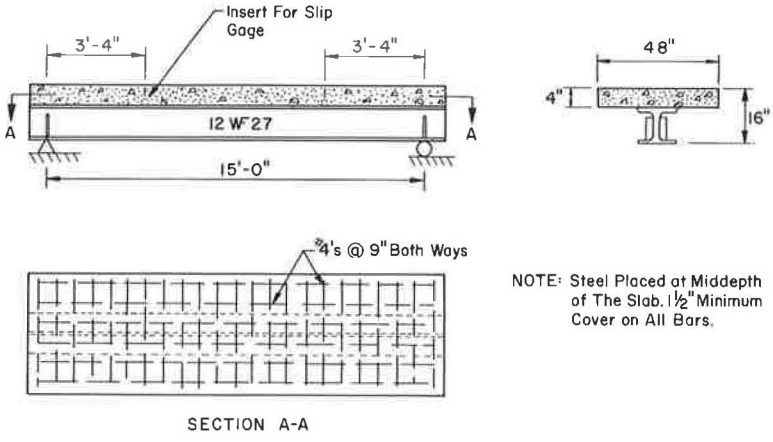


Figure 6. Typical beam fatigue specimens BF-1 through BF-8.

Description of Specimens.—The primary test program included eight identical steel and concrete composite beams. Each beam consisted of a concrete slab 4 ft wide and 4 in. thick connected to a 12 WF 27 steel beam by means of ½-in. diameter welded stud shear connectors. The rolled section was of ASTM A7 steel. The concrete slabs were cast at Fritz Engineering Laboratory using transit-mixed concrete proportioned for a 28-day compressive strength of 3,000 psi. Four test cylinders were poured with each test beam.

The shear connectors were ½-in. diameter headed studs which varied in length after welding from 2 in. to 2⅛ in. The studs were welded by a stud-welding process at a local fabrication shop. The welding was typical of general shop welding in quality. Connectors were arranged in pairs on the eight test beams. Details of the specimens are shown in Figure 6. The concrete slab reinforcement consisted of No. 4 bars at 9 in. center-to-center in both the longitudinal and transverse directions. The transverse slab reinforcement was supported 1½ in. from the bottom of the slab, and the longitudinal reinforcement was supported by the transverse steel. The arrangement of the 40 shear connectors, identical in all eight test members, is shown in Figure 7. Section properties and design strengths of the composite beams are given in Figure 8.

In the selection of the size of the test specimens, it was desirable to choose a size of member such that the dynamic loading correction would not become appreciable

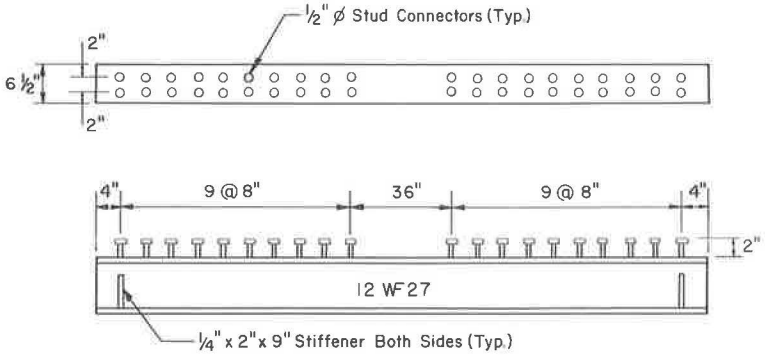


Figure 7. Stud shear connector arrangement for BF-1 through BF-8.

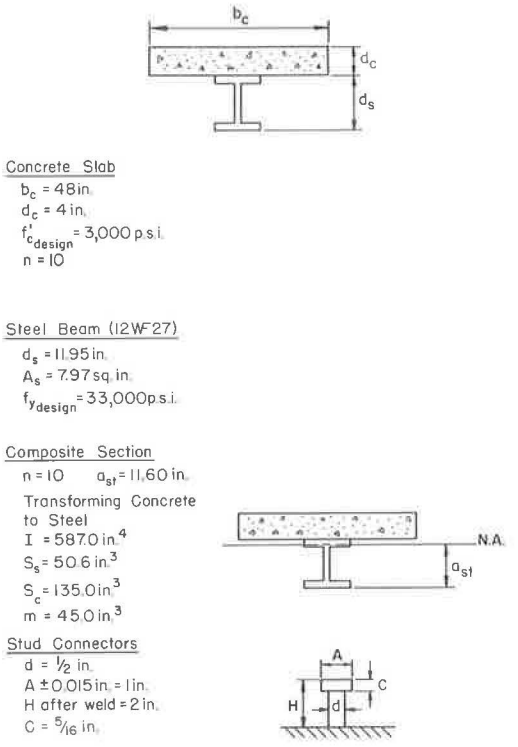


Figure 8. Section properties for BF-1 through BF-8.

during the test even though the effective stiffness of the member might decrease. This was an important consideration since it was desirable to test some of the beams until there was little or no composite action remaining. The size of the member made it necessary to use ½-in. diameter connectors to have a sufficient number so that the change in properties of the beam with cycles of load would be gradual and could, therefore, be studied carefully.

No studs were placed between the loading points because the loading points were placed close enough together so that the hydraulic jacks being used to apply the test load were sufficient to prevent separation of the slab and beam. This was done so that at all times it could be determined exactly which connectors were effective in transferring shear stresses. In the preliminary beam tests, it had been observed that connectors located between loading points were being forced to carry shear by means of the slab reinforcing steel. The effectiveness of these connectors in transferring shear was difficult to evaluate. Actually it probably varied depending on the magnitude of slip and the condition of the connectors near the ends of the member.

The number of connectors supplied in these test members was sufficient to develop the static ultimate moment capacity of the member. It had been established in a previous investigation of the static strength of composite beams that this minimum amount of shear connection should be provided to avoid reduction of the ultimate moment capacity by shear connector failure (10). The magnitude of the bottom flange steel stresses was limited to magnitudes less than the yield stress so that fatigue failure of the steel section would not occur.

Instrumentation.—The instrumentation consisted of dial gages at midspan to measure deflection and at both ends and 3 ft 8 in. from each end to measure slip, as well as numerous electrical resistance strain gages. The dial gages located at the ends and at

midspan for measurement of deflection were 0.001-in. gages. The other two dial gages were 0.0001-in. gages. The location of electrical resistance strain gages varied from test to test, depending on the data required.

The midspan deflection gage was used in adjusting the dynamic load at the beginning of each test. Since the bending stiffness of the beam changes because of bond failure at the beginning of the test, the magnitude of the applied load changes. The dynamic loading correction also changes as bending stiffness varies. Therefore, the midspan deflection was held constant until bond failure was complete, generally by 5,000 cycles, determined by visual inspection. After complete bond failure, the load was held constant and the midspan deflection was allowed to vary as the test continued. The change in deflection with cycles became an indication of loss of interaction in the member. The change in deflection was difficult to detect with a 0.001-in. dial gage until after a substantial number of connectors had failed. A more sensitive gage could not be used because of the necessity of disconnecting the instrument during dynamic loading.

Electrical resistance strain gages were placed on the bottom of both the top and bottom flanges at midspan on all beams. Two methods of determining initial connector failure by electrical resistance strain gages were studied during the testing of beam BF-1. The first method consisted of instrumenting cross-sections of the beam on each side of a pair of connectors. Although connector failure could be detected by comparing data from these gages, the method was not satisfactory because the magnitude of the changes in strain due to connector failure were too small.

A second method of detecting connector failure was based on the assumption that the connector forces caused local bending stresses in the top flange of the beam as indicated in Figure 9. This method proved to be quite sensitive to changes in the condition of connectors, and could be used to detect the initial growth of a fatigue crack. The best location for these gages was determined experimentally, and is indicated in Figure 10 which shows the location of all strain gages used in the tests.

The slip gages were used to measure the movement of the slab relative to the steel beam and to serve as a general indication of connector failure. The slip gages also indicated when connector failure began seriously to affect interaction. The interior gages were removed during dynamic testing. The stems of end dials were isolated from contact with the specimen during dynamic tests, but these dials were not removed from the member.

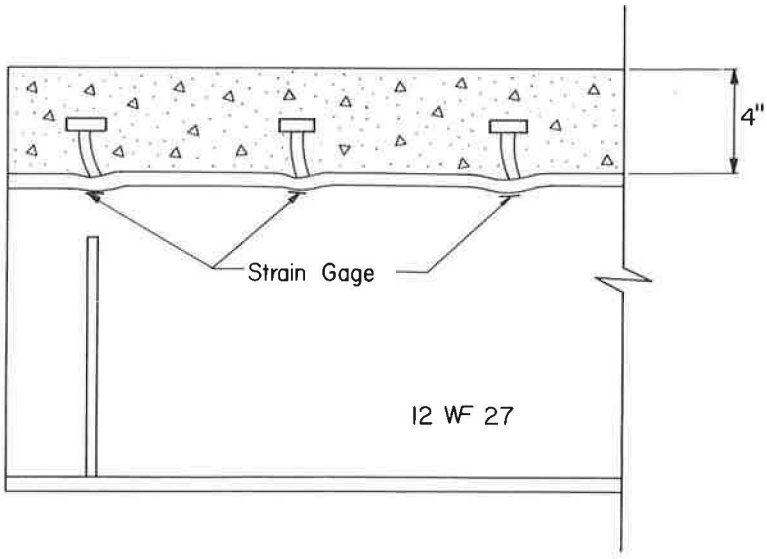


Figure 9. Distortion of top flange of steel beam due to shear connector load.

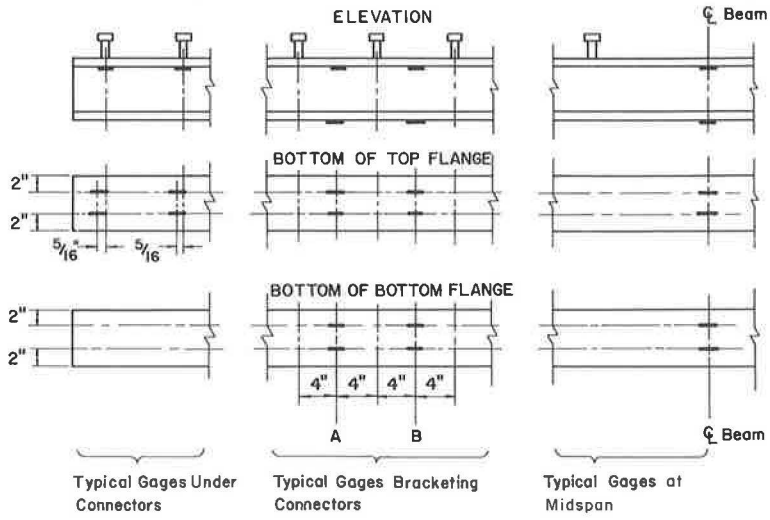


Figure 10. Typical strain gage locations for BF-1 through BF-8.

TABLE 2

INSTRUMENTATION USED WITH EACH SPECIMEN

| Specimen | End Slip Gages | Interior Slip Gages | Midspan Deflection Gage | Number of Electrical Resistance Strain Gages Used | | |
|---|---|---|---|---|---|---|
| | | | | Midspan | Opposite Connector | Bracketing Connector |
| BF-A | x | x | x | 4 | | |
| BF-B | x | x | x | 4 | | |
| BF-C | x | x | x | 4 | | |
| BF-D | x | x | x | 4 | | |
| BF-1 | x | x | x | 4 | 4 | 14 |
| BF-2 | - | - | x | 4 | 10 | - |
| BF-3 | x | x | x | 4 | 8 | - |
| BF-4 | x | x | x | 4 | 8 | - |
| BF-5 | x | - | x | 4 | 8 | - |
| BF-6 | x | - | x | 6 | 8 | 24 |
| BF-7 | x | - | x | 4 | 17 | - |
| BF-8 | x | - | x | 4 | 8 | - |

For members BF-1 through BF-4, strain gages with a gage length of $^{13}/_{16}$-in. were used. Starting with member BF-5, strain gages with a gage length of $^{1}/_{4}$-in. were tried for measuring the local stresses near connectors. These were found to be slightly more sensitive than the larger gages. Local stresses being measured were found to be confined to an area having a diameter only about twice that of the connectors.

Once the behavior of the strain gages opposite connectors was determined, it was not necessary to use as many gages to detect initial failure of connectors. After tests of a few members were completed it was found that the slip and deflection data were not as significant as the strain gage data in studying the behavior of individual connectors. The interior slip gages were omitted in some tests. The major difficulty with these gages is the fact that the sensitivity of a 0.0001-in. dial gage is required to detect the minute

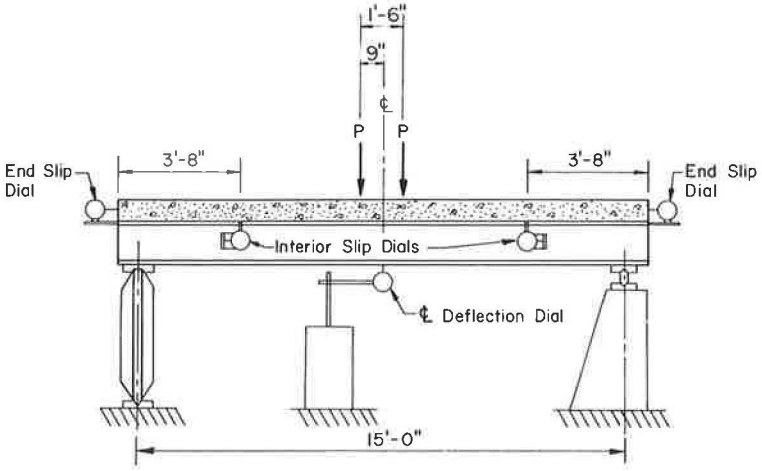


Figure 11. Test setup for BF-1 through BF-8.

TABLE 3

CONCRETE AGE AND STRENGTH AT TIME OF TESTING

| Beam | Concrete Age at Start of Test | $f'_c$ (psi) |
|---|---|---|
| BF-A | 28 | 3030 |
| BF-B | 30 | 3030 |
| BF-C | 36 | 3500 |
| BF-D | 45 | 3500 |
| BF-1 | 33 | 3330 |
| BF-2 | 33 | 3290 |
| BF-3 | 39 | 3350 |
| BF-4 | 39 | 3490 |
| BF-5 | 37 | 3310 |
| BF-6 | 58 | 3108 |
| BF-7 | 70 | 4060 |
| BF-8 | 84 | 3980 |

changes in slip caused by cracking of connectors, but these gages are too delicate to be used during dynamic loading.

The instrumentation used on each of the eight test beams is summarized in Table 2. The general arrangement of electrical resistance strain gages is shown in Figure 10. The locations of slip and deflection dial gages are shown in Figure 11.

Test Procedure.—Each beam was simply supported on a span of 15 ft and loaded by hydraulic jacks located 9 in. on each side of the centerline. The arrangement for testing of members is shown in Figure 11. Testing was started at least 28 days after the concrete slabs were cast. In some cases the concrete was older than 28 days when testing began. Concrete slabs were moist-cured for 7 days and then air-cured until time of testing. The concrete strength and age of the eight specimens are given in Table 3. Four concrete test cylinders were poured with each beam. Two of these cylinders were tested when dynamic loading was started. The other two were tested at the end of the test. The concrete strength given in Table 3 is the average of the four cylinders tested.

Initially each specimen was loaded statically to the maximum load to be applied dynamically. None of the members were overloaded statically. If the bond between the steel beam and the concrete slab was broken throughout the length of the member due to the initial static test, the deflection measurements were used to determine the correct dynamic load. If the bond was not broken by the initial static test, cycling was begun using a theoretically determined load until bond was completely broken.

The maximum load to be maintained during dynamic testing was determined from previous results. A second static test was made as soon as bond failure was complete. Generally it required about 5,000 cycles to break bond, but on one member 7,000 cycles were required. The midspan deflection was measured on the second static test and was

used in adjusting the dynamic loading equipment for the correct jack load. Thereafter, the loading equipment settings were held constant and deflection of the member was allowed to change.

Throughout an entire test, static tests were run at regular intervals. During each static test, the member was loaded in increments of 2 kips per load point to the maximum test load. All dial gages and electrical resistance gages were read at each load increment whenever it was judged from the behavior of the specimen that the data would be significant. In some of the tests, complete readings were taken only at zero load and maximum load.

All specimens were loaded at the rate of 250 cycles/min. The minimum load was the smallest that could be applied without separation of beam and loading jack at any time during the load cycle. Generally this minimum load was approximately 10 percent of the maximum load.

After the completion of each test, the concrete slab was removed from the steel beam and a visual inspection of the connector failures was made. Photographs were made of connector failures and cracked connectors. The final visual inspection was used as a check on the information gained from electrical resistance strain gage data. In several instances, this final inspection verified strain gage data which were in doubt at the completion of the test. These inspections were important in establishing confidence in the technique used to detect connector failures.

## RESULTS OF BEAM TESTS

During the course of the preliminary and primary beam tests, it was possible to obtain data for eleven points with which to establish an S-N curve for ½-in. diameter studs. The S-N curve obtained was derived using only data from seven of the eight primary beam tests in which fatigue failure of connectors occurred. This curve was obtained by a regression analysis of the data using the following mathematical model:

$$\log N = A + B\ (S_{max.} - S_{min.}) \qquad (2)$$

in which

A, B = empirical constants,
$S_{max.}$ = maximum shear stress,

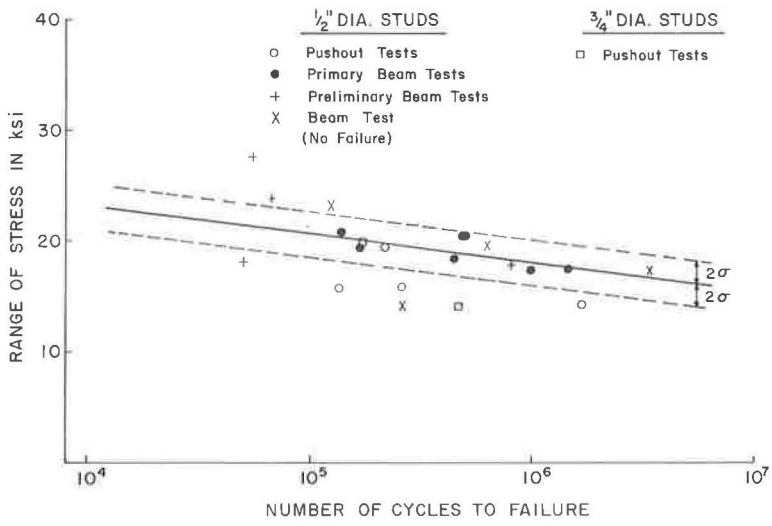


Figure 12. S-N curve for primary beam tests.

$S_{min.}$ = minimum shear stress, and
N = number of cycles to failure.

The resulting curve is plotted in Figure 12 with the range of stress as ordinate and the number of cycles to failure as abscissa. Data points from all beam and pushout tests are shown. The failure criterion for determining the value of N differs for each group of tests. That for pushout specimens was complete failure of connectors on one or both flanges. The failure criterion for the preliminary beam tests and primary beam tests is described in the following sections. A statistical analysis of the seven data points from the primary beam tests resulted in an unbiased standard deviation of $\sigma = 1.027$ ksi. The 95 percent confidence limits of the data are shown in Figure 12.

Data points from pushout tests are shown along with other test results in Figure 12. Generally the pushout test results fall below the curve, but the curve is much closer to the pushout results than it is to the results obtained from tests of bare studs as can be seen by comparison of Figure 12 with Figure 1. It appears that pushout tests can be used in evaluating the fatigue strength of shear connectors.

Although Figure 12 presents the general results of the tests, much of the additional data taken and many of the visual observations made during the tests are of interest. The additional information has considerable bearing on the interpretation of the results given in Figure 12 and will be presented before making a complete evaluation of the S-N curve. The results of the preliminary beam tests are considered separately. The subsequent sections of the report are concerned mostly with the primary beam tests but some of the information pertains to the preliminary tests also.

## Preliminary Beam Tests

The details of these test specimens have been already presented, and section properties are given in Figure 3. The behavior of these members as fatigue failure of connectors took place was similar to the behavior of composite beams with channel shear connectors tested at the University of Illinois (5). The most difficult problem in connection with performing these tests was to determine when a connector somewhere on the specimen first developed a fatigue crack or when it became completely fractured.

In all members, failure began with the end pair of connectors at the expansion end of the member. Shortly thereafter failure occurred at the opposite end of the member. Failure of connectors then progressed rather gradually from both ends toward the center. From the start of a test until a sufficient number of connectors had failed so that a noncomposite member remained, there was no sudden change in applied loads, strains, slip, or deflection.

The most complete data were obtained on specimen BF-D because the shear connector stress on the other three test specimens was higher and failure took place before very much data were obtained. Beam BF-D was loaded so that the maximum stress on the connectors was equal to the useful capacity of this type of connector as specified in Section 1.9.5 of the 1961 AASHO specifications (3).

The test results of preliminary and primary beam tests are summarized in Table 4. The minimum stress on the connectors was always approximately 10 percent of the maximum stress, and hence the S-N curve of Figure 12 is actually based on data from tests in which the stress range was approximately 90 percent of the maximum stress.

As each member was cycled between the minimum and maximum loads given in Table 4, the first obvious indication of failure was an audible banging of the slab on the steel section. For the preliminary beam tests, this determined the number of cycles to failure recorded in Table 4. This is also the failure criterion used in plotting the preliminary beam test data points in Figure 12.

The visual inspection method of detecting failure is not precise, and an analysis of data on slip, strains, and deflection was also used in attempting to determine N. Since N could only be determined approximately by using all of the information available, a failure zone was defined as being the probable range of N within which failure occurred. A failure zone for beam BF-D is indicated in Figures 13 and 14. The left edge of the failure zone was determined by the first indication of failure which could be discerned from the data, and the right edge was established by the first positive proof that failure had occurred.

TABLE 4

SUMMARY OF TEST RESULTS

| Specimen | Minimum (kips/jack) | Maximum (kips/jack) | Calculated Stud Stress* Minimum | Calculated Stud Stress* Maximum | Static Test Interval (kc) | Cycles to Failure† (kc) | Total Number of Cycles during Test (kc) |
|---|---|---|---|---|---|---|---|
| BF-A | 1.6 | 13.5 | 5730 | 23,900 | 50.3 | 50.3 | 50.3 |
| BF-B | 1.3 | 11.5 | 4900 | 32,600 | 50.3 | 55.4 | 63.9 |
| BF-C | 1.1 | 11.0 | 3600 | 27,700 | 100.0 | 78.0 | 198.5 |
| BF-D | 0.7 | 7.0 | 2160 | 20,100 | 100.0 | 820.0 | 2,008.0 |
| BF-1 | 1.2 | 14.2 | 1880 | 22,200 | 50.0 | 490.0 | 880.0 |
| BF-2 | 1.2 | 14.2 | 1880 | 22,200 | 50.0 | 480.0 | 680.0 |
| BF-3 | 1.2 | 12.4 | 1880 | 19,400 | 100.0 | 980.0 | 1,556.0 |
| BF-4 | 1.4 | 12.4 | 2190 | 19,400 | 100.0 | -- | 3,315.0 |
| BF-5 | 1.2 | 14.5 | 1880 | 22,600 | 50.0 | 140.0 | 354.0 |
| BF-6 | 1.2 | 13.5 | 1880 | 21,100 | 50.0 | 168.5 | 1,009.0 |
| BF-7 | 1.2 | 13.0 | 1880 | 20,300 | 50.0 | 450.0 | 1,344.0 |
| BF-8 | 1.2 | 12.5 | 1880 | 19,500 | 50.0 | 1,445.0 | 3,522.0 |

*For BF-A to BF-D, shear stress was determined by dividing the compressive force in the slab at midspan by the number of connectors in the shear span. For BF-1 to BF-8, shear stress was determined by Eq. 2.1

† Failure for BF-A to BF-D was based upon slip and deflection data, but failure of BF-1 to BF-8 was based on the average number of cycles to produce fatigue crack in a pair of studs

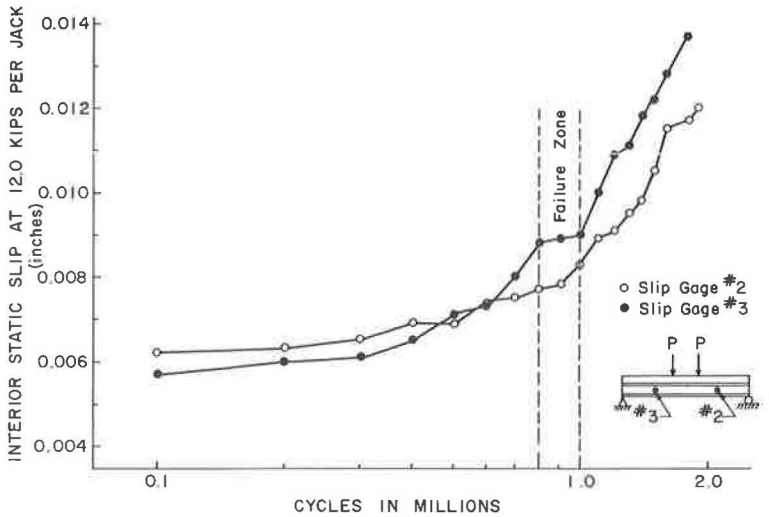


Figure 13. Interior static slip vs cycles for BF-D.

Failure of connectors in specimen BF-D was observed at 820,000 cycles. A plot of maximum slip measured at the two interior slip gages (see Fig. 5) vs cycles of loading from start to completion of the test is shown in Figure 13. This maximum slip was measured in a static test with a load of 12 kips per jack on the beam, which was the maximum static load applied in all of the static tests on beams of this series. The failure point does not correspond closely with any definite change in the slope of the two

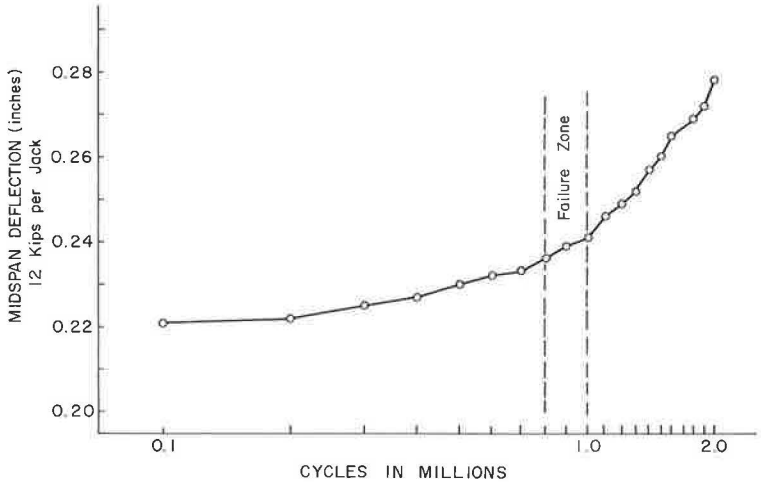


Figure 14. Midspan deflection vs cycles for BF-D.

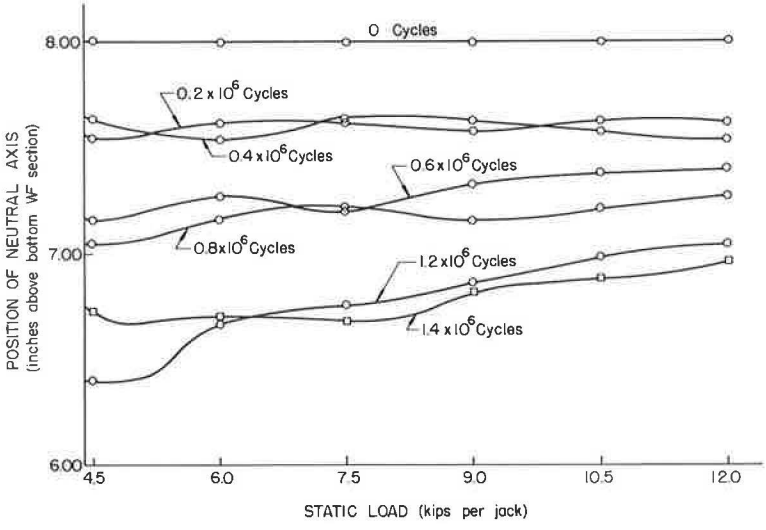


Figure 15. Movement of neutral axis under static load as fatigue failure progresses for BF-D.

curves. Figure 13 shows that the slip increased gradually as cycling progressed before failure of connectors as well as after failure. The magnitude of slip obtained in a static test was dependent on the length of time which the beam was allowed to rest before making the static test. For this reason the point-to-point curves are not smooth. This is also one of the reasons why the slip data were not considered to be very conclusive in determining failure of connectors.

A plot of the position of the neutral axis vs applied load at various numbers of cycles for specimen BF-D is given in Figure 15. These curves indicate a loss of interaction throughout the test, but a gradual shift of the neutral axis. Even when a curve was plotted for each static test, the point of failure of connectors could not be determined with any degree of certainty. There was a large shift in the neutral axis between zero cycles and the next static test because of failure of bond, and this was typical for all specimens.

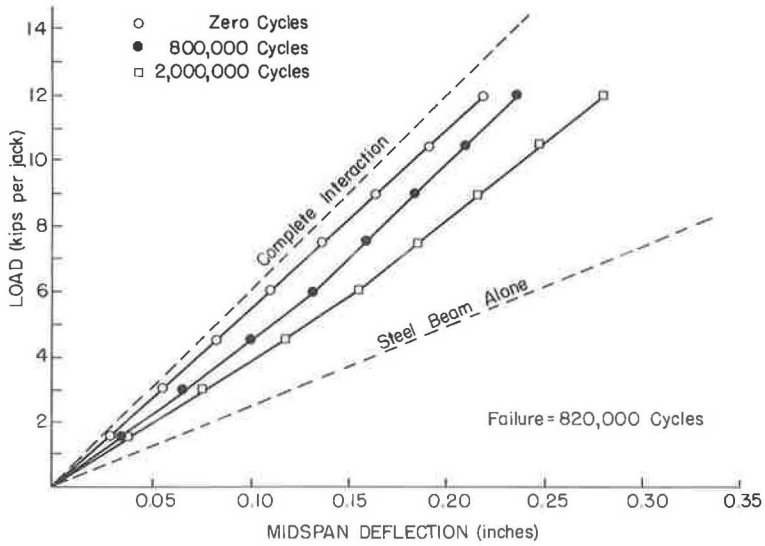


Figure 16. Load vs deflection curves for BF-D.

The static deflection at a load of 12 kips per jack obtained in each static test is plotted in Figure 14 vs the number of cycles of loading plotted on a log scale. There is no distinct change in the slope of this curve in the vicinity of 820,000 cycles. It would not have been possible to determine when failure occurred from this curve alone.

The load vs deflection curves of specimen BF-D at the start of the test, at 800,000 cycles, and at the end of the test are shown in Figure 16 along with the theoretical curves for a composite beam with complete interaction and the steel beam alone. The departure of the initial curve from the theoretical curve for complete interaction is due to the fact that these members were designed with a weak shear connection to insure that failure would take place in the shear connection rather than in the bottom flange of the steel beam. The number of shear connectors was about 57.5 percent of that required to develop the static ultimate strength of the member. The plotting of load vs deflection curves at intervals of 100,000 cycles was not useful in pinpointing the initial failure of connectors because of the gradual loss of interaction throughout the test.

After two million cycles of loading the test was stopped. As can be seen in Figure 16 the final load vs deflection curve for specimen BF-D is situated about midway between the two theoretical limits of complete interaction and bare steel beam. The concrete slab was removed and it was discovered that six of the eight shear connectors per shear span were fractured at one end and seven were fractured at the opposite end of the member. Some of these were actually broken when the slab was removed, but only about 10 percent of the cross-sectional area of these studs remained uncracked after fatigue loading. It is interesting to note that the fracture of about 80 percent of the total shear connector cross-sectional area in the shear spans resulted in approximately an 18 percent increase in deflection as compared with the original curve, whereas complete loss of interaction would result in an increase of 105 percent in deflection.

One of the reasons why it may have been difficult to determine when a connector failed was the fact that shear connectors between the load points carried some of the horizontal shear forces after the end connectors failed. Presumably, as connectors failed, connectors near midspan carried more and more of the horizontal force. This explains why BF-D performed somewhat like a composite beam after 2 million cycles even though only about 20 percent of the shear connector area in the shear spans remained effective.

In specimens BF-A, BF-B, and BF-C, the concrete actually cracked across the full width of the slab in each shear span near the load points. These members then performed as a member with a composite section between load points and a bare steel beam in the shear spans.

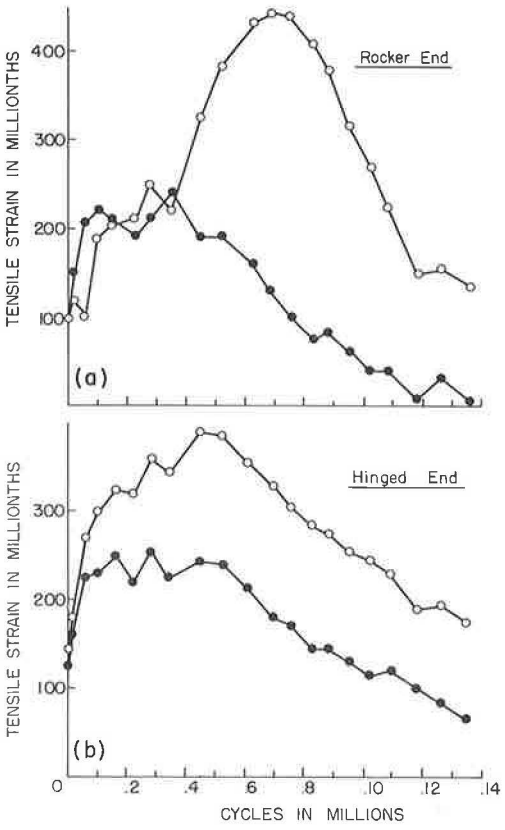


Figure 17. Strain readings of distortion gages at maximum load vs cycles for end pairs of connectors of BF-7.

The primary beam tests were planned to avoid the major difficulties encountered in the preliminary tests. The primary test specimens were designed with a knowledge of stress which would cause fatigue failure of connectors. It was also known that very little difference in stress range would be required to obtain a failure at 1 million cycles as compared to that required to produce a failure in 100,000 cycles from the S-N curve plotted using the preliminary test results.

The primary beams were designed with no connectors between load points so that there would be no difficulty in determining the stress on connectors at any time during the tests. It was felt that designing the members without connectors between load points would reduce scatter in the data obtained from the tests.

It was concluded from the preliminary tests that a better means of determining connector failure than the measurement of strains at midspan, slip, and deflection must be found to obtain suitable test results in the primary beam tests. The magnitude of slip measured in the tests led to the conclusion that the shear force transmitted by the connector must cause considerable bending stresses in the top flange of the steel beam. This notion led to the method of determining when failure of connectors took place described earlier and in the following section.

## Instrumentation for Determination of Connector Failure

The tests of the primary beams were started before a method of determining connector failure was perfected. Therefore, beam BF-1 was used as an experimental beam, and strain gages were placed at various points on the bottom of the top flange in an effort to measure the effect of the horizontal forces transmitted to the top flange of the steel beam by the shear connectors. Strain gages directly under connectors and gages on the cross-section on each side of a connector were used as shown in Figure 10. The latter method was not successful because of the small difference in strain between the two cross-sections.

The strain gages placed directly under the connector produced very satisfactory results. Usually the gages were placed on the side of the connector nearest the end of the beam to record tensile strains. If the gages were mounted on the opposite side, compressive strains were recorded.

During a test, readings on these strain gages were taken at each load increment of a static test. As the test proceeded, the strain readings at the maximum static load was plotted as ordinate and the number of cycles of loading was plotted as abscissa. This was done for several connectors at each end of the member. Typical curves obtained from these readings are shown in Figure 17. Curves of strain at the maximum applied static load of 13 kips per jack vs number of cycles for the pair of connectors on each end of BF-7 are shown.

The curves for the end connectors were chosen for the purpose of illustration because the strain in the top flange being measured is due almost solely to the flange dis-

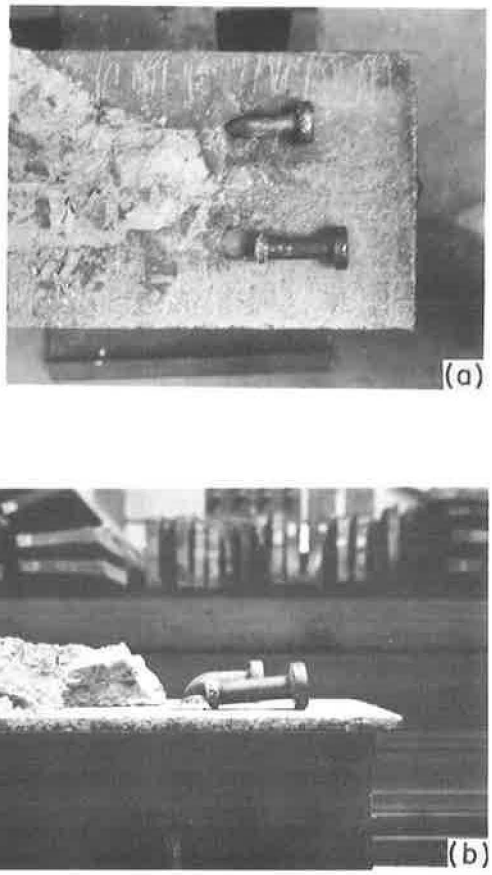


Figure 18. Stud fatigue failure adjacent to uncracked connector.

tortion since the strain gage is actually located between the end of the beam and the support. For studs located nearer midspan, the strain in the top flange will be equal to the strain corresponding to the compressive stress in the top flange due to moment at that point plus the strain due to the flange distortion. In this case, it is necessary to subtract the compressive strain due to bending from the strain readings.

## Interpretation of Local Distortion Strains

Qualitatively the curves of local distortion strains vs number of cycles are not difficult to interpret. The strains begin to decrease after a fatigue crack begins to propagate, and when the strain reading decreases to zero or to the strain due to bending moment at that cross-section the connector has failed completely. Of the four curves shown in Figure 17, only one actually decreased to zero before the test was stopped. Most of the connectors continued to transmit a small amount of horizontal shear even though they were completely fractured because the fracture took place in the base metal and a mechanical connection capable of transmitting some horizontal load existed after failure of the connector.

Inspection of beams by removal of the concrete slab after the test checked the validity of this interpretation. Inspection also revealed that the strain reading on the downward portion of the curve divided by the maximum recorded strain was approximately equal to the proportion of uncracked shear connector area. It was possible to determine the percentage of shear connector area which remained uncracked in a shear span if the connectors had distortion gages by making a static test.

One occurrence particularly proved the validity of the distortion readings. The strain readings under the end studs of specimen BF-3 indicated that one connector had completely failed and the other stud of the pair was still 100 percent effective. The concrete was broken away to check this result because it did not seem possible. However, inspection verified the findings from the distortion strain readings as shown in Figure 18. One stud was completely fractured and the other stud could be completely bent over with a hammer without cracking the stud. This example, along with the other inspections of beams after testing, caused complete confidence in the use of the distortion gages for the prediction of shear connector failures.

The curves of Figure 17 were typical of most of those obtained. The strain readings increased to a maximum before decreasing. The curves in Figure 17b are typical for connectors which began to fail very early in the test, but most strains increased considerably above the initial reading before decreasing. It was observed that the increase of strain above the initial reading was less if the concrete in the slab was older. This increase in strain would seem to be due to inelastic deformation of the concrete around connectors so that the horizontal force was applied to the top flange primarily as a shear force initially but with more and more bending action as the test proceeded. The magnitude of distortion strain often decreased on these gages if the specimen was allowed

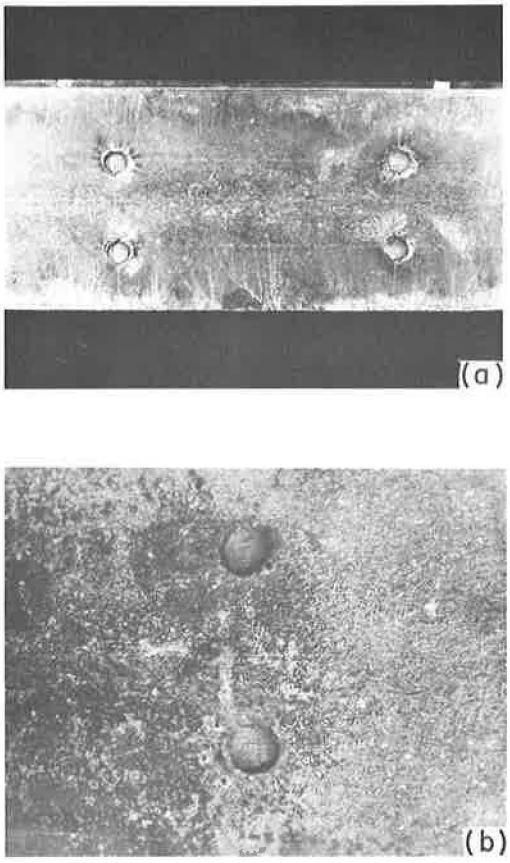


Figure 19. Typical stud fatigue failures in heat-affected zone of base metal.

TABLE 5

NUMBER OF CONNECTORS FRACTURED AT END OF TEST

| Specimen | Number of Connectors completely fractured at expansion end | Number of Connectors completely fractured at fixed end |
|---|---|---|
| BF-A | 7 | 7 |
| BF-B | 6 | 6 |
| BF-C | 9 | 8 |
| BF-D | 7 | 6 |
| BF-1 | 14 | 14 |
| BF-2 | 12 | 0 |
| BF-3 | 1 | 0 |
| BF-4 | 0 | 0 |
| BF-5 | 14 | 20 |
| BF-6 | 16 | 16 |
| BF-7 | 2 | 12 |
| BF-8 | 8 | 10 |

to rest. This suggests that the creep properties of the concrete and the method of conducting the tests may be important factors in the fatigue strength of connectors.

## Typical Study Failures

The distortion strain readings reached a magnitude of 700 μin./in. tension in some members. Usually the maximum compressive strains were somewhat smaller. This corresponds to a stress of nearly 21 ksi on the bottom of the top flange. Presumably a similar stress exists on the top surface. This magnitude of stress in the base metal, combined with a shear stress of similar magnitude on the stud, may help to explain why a typical stud failure was a failure along the heat-affected zone in the base metal. Typical failures are shown in Figures 18 and 19.

In all cases checked, fatigue failure was initiated at the side of the connector toward the end of the beam, which would seem to be the wrong side for a failure to start. This mode of failure is the main reason why the position of the distortion gage shown in Figure 10 was found to be the most sensitive location for detecting failure of the connector.

Some connectors were found to have fatigue cracks on both sides and sound portions near the center. In these cases, the crack toward the end of the beam was equal to or larger than the other one. An explanation of why the fatigue fracture begins apparently on the wrong side of the connector was not developed in this program; however, shrinkage of the concrete slab which initially stresses the connectors in the opposite direction to the applied load could be the cause. As a result of shrinkage, the flange stress range on the outside face of the stud could be tension so that the distortion caused by loads resulted in fluctuating tensile rather than compressive stresses.

Of the 141 studs which failed in fatigue in the primary beam tests, all except two failed as shown in Figure 19. The near end of the beam is to the left in Figure 19. In Figure 19a the portion of the shear connectors which failed statically when the slab was removed is visible in the right-hand pair of connectors. Two studs failed in fatigue through the heat-affected zone of the stud above the bead of the weld. It is not known which side of these studs was cracked initially. Failures of the type shown in Figure 19 were also experienced in the preliminary beam tests. However, because some of the welds were observed to be porous along the failure zone, it was felt that

the welds might be of inferior quality. Analysis of the steel of the preliminary beams revealed that the chemical composition of the base metal was not ideal for good stud welding. By comparison with the results of the primary tests, the preliminary beam test results seem to be satisfactory as regards both the type of failure and the general test results.

In Table 5, the number of shear connectors completely fractured due to fatigue loading is reported for each shear span of the member. Most of the tests were continued until a substantial number of connectors had failed. Many other connectors were partially cracked. In the case of specimen BF-3, the test was stopped to check instrumentation as soon as a fractured connector was detected. Beam BF-4 was the only member in which none of the connectors failed, and inspection of this beam after removal of the slab did not reveal any fatigue cracks.

## Failure of End Connectors

In both the preliminary and primary beam tests, all connectors which failed first were located in the vicinity of the end of the beam. Usually the end pair of connectors failed first, but occasionally the failure took place first in the second pair of connectors from the end of the beam.

There seem to be several factors inherent in the testing procedure which may be partially responsible for the fact that connectors near the end of the member fail first. In several members, torsional vibration of the specimen occurred due to slight eccentricities in either the specimen or the loading. This difficulty could be corrected so that no visible torsional vibration took place, but end shear connectors may still have been overstressed by the tendency for the member to twist on each cycle of load.

Bond failure took place in the first 5,000 to 10,000 cycles of loading. This failure started at the end of the member and progressed toward midspan. End shear connectors, therefore, were the first to undergo an increase in stress due to bond failure.

Strain measurements made on specimen BF-6 showed that end shear connectors are stressed higher than interior connectors after bond failure was complete as well as during the time that bond failure was taking place. The variation of load per stud along the length of the member was studied by placing strain gages at cross-sections on each side of two pairs of connectors. Connectors located at 24 and 64 in. from one end of the member were chosen because each pair was located a sufficient distance from local stress conditions at the support and load point.

The force transmitted by a pair of these connectors was determined by calculation of the compressive force in the concrete slab on each side of the pair of connectors being considered. The force on a pair of studs was determined as the difference between the magnitude of the compressive force on each side of the connectors. The strain gage readings were used to calculate the compressive force in the slab at each point required, including the cross-section at midspan.

The average force per connector was taken as the compressive force in the slab at midspan divided by the number of connectors in half of the length of the member. A comparison of the results of this investigation of BF-6 is given in Table 6. The average stress on connectors was obtained by calculating the compressive force in the concrete slab at midspan from strain gage readings with the assumption that this force was dis-

TABLE 6

STUD STRESS AT TWO SELECTED POINTS OF BF-6

| Cycles | Stud Stress (ksi) 24 inches from Beam End | Stud Stress (ksi) 64 inches from Beam | Average Stud Stress (ksi) $= \frac{\text{force in slab at } \mathbb{Q}}{\text{area of studs}}$ |
|---|---|---|---|
| 9,000 | 21,400 | 15,300 | 17,900 |
| 49,000 | 23,100 | 16,700 | 18,500 |
| 415,000 | 21,500 | 19,300 | 18,600 |
| 667,000 | 19,200 | 22,800 | 18,900 |

tributed uniformly over the area of all connectors in the shear span. In considering the information contained in Table 6, it must be realized that the bond was only partially destroyed at 9,000 cycles and that the first crack in an end stud occurred at 49,000 cycles.

From the comparison of the measured and theoretical stud stress, it will be realized that although the conventional elastic design assumptions may be satisfactory from a design point of view, these assumptions are as much as 25 percent in error for the prediction of the actual stress on studs near the end of a member. It seems worthwhile to consider that this 25 percent error exists with the most elementary loading condition, and that the magnitude of error may be even larger with a more complicated loading condition.

The important fact concerning the results presented in Table 6 is that the difference between the stress on connectors near the end and near the center is not due to friction or bond. Since the results are obtained from strain measurements on the cross-section, any shear transfer due to friction or bond would merely be included in the apparent force per connector. Hence, the total shear force transferred per pair of connectors is higher near the end of the beam. This is also verified by the fact that slip readings are higher near the ends than near midspan on such a member. Higher stresses on end connectors are likewise predicted by the theory of incomplete interaction (4).

## Rate of Loss of Interaction

Another important observation made on the performance of composite beams is the rate at which loss of interaction between concrete slab and steel beam occurs. The first decrease in interaction takes place as a result of bond failure. As cycling continues, slip at the ends of the beam tends to increase.

It is necessary to be cautious in considering the condition of incomplete interaction with regard to fatigue tests. It appears that a time effect exists due to repeated loading, and that a portion of the increase in slip is due to inelastic deformation of concrete around shear connectors. This is undoubtedly the case since rather high bearing stresses exist. Slip and deflection, therefore, increase as cycling continues. However, these increases are not indicative of connector failure or changes in the stresses in the cross-section at midspan. Loss of interaction will be discussed only in terms of changes in the compressive force in the concrete slab at midspan.

It has been found that after bond failure, a composite beam loses interaction at the same rate as the rate of decrease in the total stud area. The measure of the effectiveness of the composite beam in this case is the magnitude of the total compressive force in the concrete slab at midspan. If this total force after some number of cycles is only 90 percent of its value at 0 cycles (when there is almost complete interaction or 100

TABLE 7

AVERAGE STUD SHEARING STRESS FOR BF-6

| Cycles | Total Force in Slab at ℄ (kips) | Effective Number of Studs | Average Shearing Stress (psi) |
|---|---|---|---|
| 49,000 | 72.5 | 20.0 | 18,500 |
| 156,000 | 69.7 | 19.8 | 18,000 |
| 266,000 | 68.9 | 19.4 | 18,100 |
| 370,000 | 68.7 | 19.0 | 17,900 |
| 415,000 | 68.4 | 18.7 | 18,600 |
| 470,000 | 68.1 | 18.3 | 19,000 |
| 564,000* | 65.1 | 17.3 | 19,100 |

*Only the first 564,000 cycles are given because of lack of reliable data beyond this point

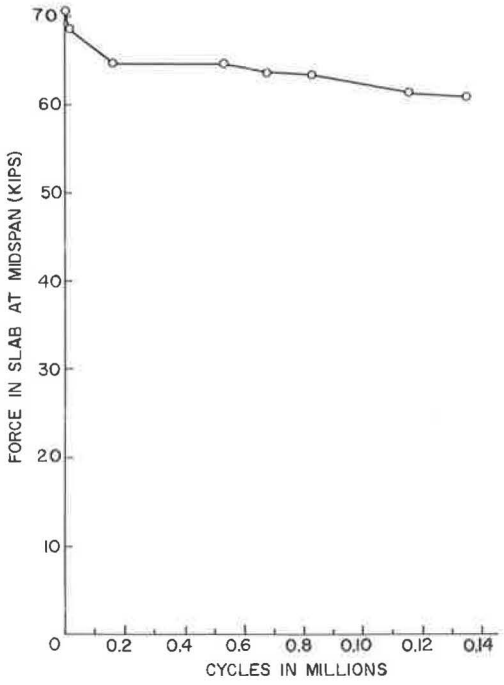


Figure 20. Force in slab at midspan vs cycles for BF-7 at maximum load.

percent effectiveness), then the composite beam is considered to be only 90 percent effective as a composite beam.

It was possible to determine from strain readings, in a manner which has been described, the amount of stud area that remained uncracked at any number of cycles. When 10 percent of the total stud cross-sectional area was gone, leaving 90 percent of the total stud area, the compressive force in the slab was also only 90 percent as large as it was before stud failure. That this is true can be shown in the following manner. For a given composite beam (specimen BF-6 in this case) the total force in the slab at the midspan was calculated from strain readings after the member had been cycled for different lengths of time. At the same number of cycles that this force was calculated, the effective stud area (total stud area minus cracked area) was also calculated from distortion strain readings. If the effectiveness of the slab and the studs decreases at the same rate, then the total force in the slab divided by the effective stud area should remain constant, regardless of the number of cycles. The result of such a calculation is shown in Table 7. The compressive force in the slab at midspan is given for various values of N, and the effective area of studs as determined by strain gage readings is given in terms of the number of studs for corresponding cycles of loading. The average shear stress given in this table was calculated as in Table 6 by dividing the compressive force in the slab at midspan by the unfractured shear connector area in the shear span. The amazing fact is that this average stress is nearly constant throughout the test. The differences which do occur are of smaller magnitude than the probable error in determining the results.

The loss of interaction as determined by measurement of the compressive force in the concrete slab at midspan was found to be directly proportional to the loss of the effective area of shear connectors. Since the stress on the uncracked area of the shear connectors did not increase during the test, the loss of interaction in a member was a gradual process. The rate of decrease of the compressive force in the slab vs cycles of loading is shown in Figure 20 for specimen BF-7. From Figure 17 it appears that the first stud became cracked at about 350,000 cycles and the fourth at about 720,000 cycles. However, at 1,400,000 cycles the force in the slab is still approximately 86 percent of its original magnitude.

## Progressive Failure of Studs

It has been illustrated in Figure 20 that the rate of loss of interaction and, therefore, the rate of stud failure is very gradual. However, with the addition of corrosion effects in the field, the rate of stud failure could be increased. For this reason the determination of the initial failure is significant, and our attention must be focused on initial failure as a design criterion.

Of the eight members tested in the primary beam tests, connectors failed in seven beams. The rate of failure of connectors was gradual. From Table 4 it can be seen that the stress range on specimen BF-7 was about the average value of stress range among the seven beams with connector failure. Thus, the rate of failure of connectors illustrated by Figure 20 is about the average rate for the seven beams.

The tests demonstrated that if one pair of connectors failed in a member, failure of all connectors would eventually result if loading were continued. It has been shown that the average stress on the uncracked connectors remains nearly constant. However, this does not mean that the stress on one particular stud remains constant. In Table 6 the stress on the pair of studs located 64 in. from the end of the beam is shown to increase as failure of end connectors proceeds. The data in Table 6 indicate that the stress on connectors in the shear span becomes more uniform as the loading proceeds. This may be the reason why the reduction in the stiffness of the beam with fatigue loading progresses slowly.

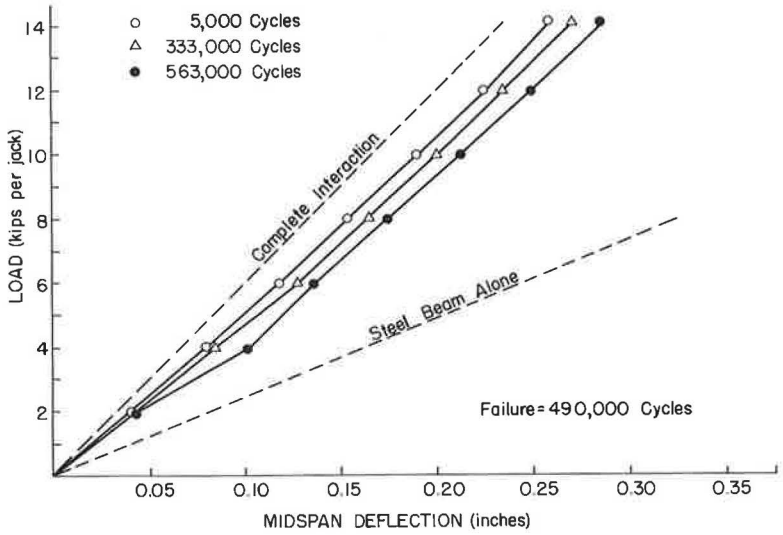


Figure 21. Load vs deflection curves for BF-1.

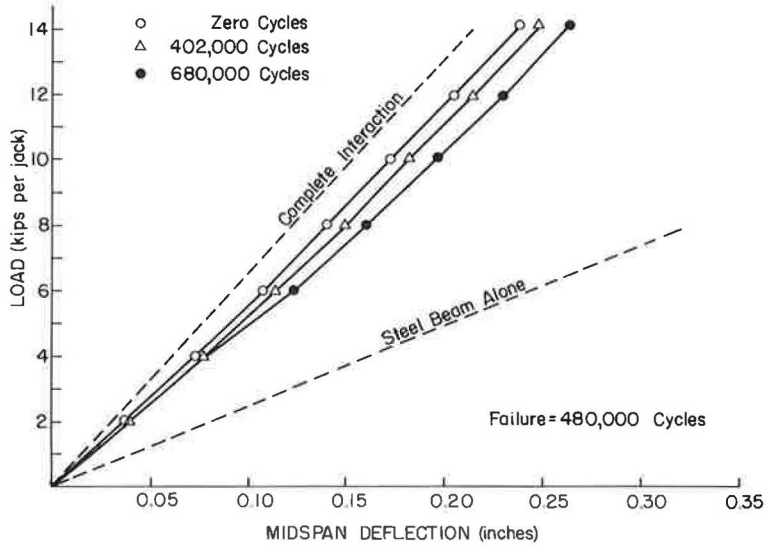


Figure 22. Load vs deflection curves for BF-2.

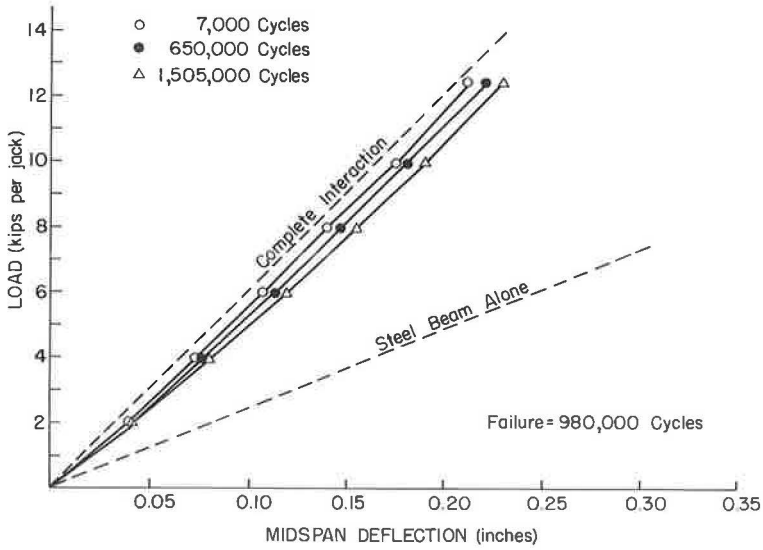


Figure 23. Load vs deflection curves for BF-3.

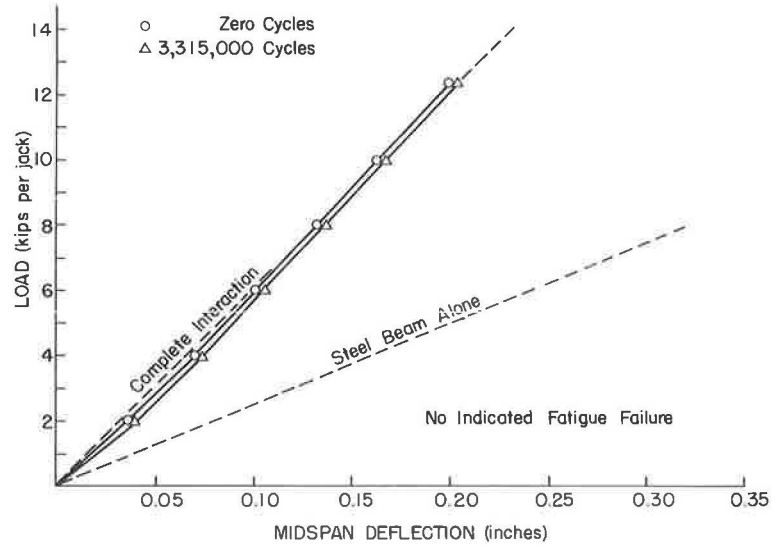


Figure 24. Load vs deflection curves for BF-4.

## Deflection of Members

The deflection of members at maximum cycling load increased from the first cycle to the completion of the test in the primary beam tests in about the same manner as that shown for specimen BF-D in Figure 15. In the early stages of loading, the increase in deflection would seem to be due to bond failure and polishing of the slip plane due to movement of the slab with respect to the steel beam on each cycle. A second stage of deflection increase might be due to inelastic deformation of concrete around connectors. Finally, the increase in deflection becomes due to failure of connectors. It is not possible to separate these stages on a curve such as Figure 15.

A comparison of the load-deflection curves from static tests of the primary beam specimens is of interest. In Figures 21 through 28 are shown load vs deflection curves

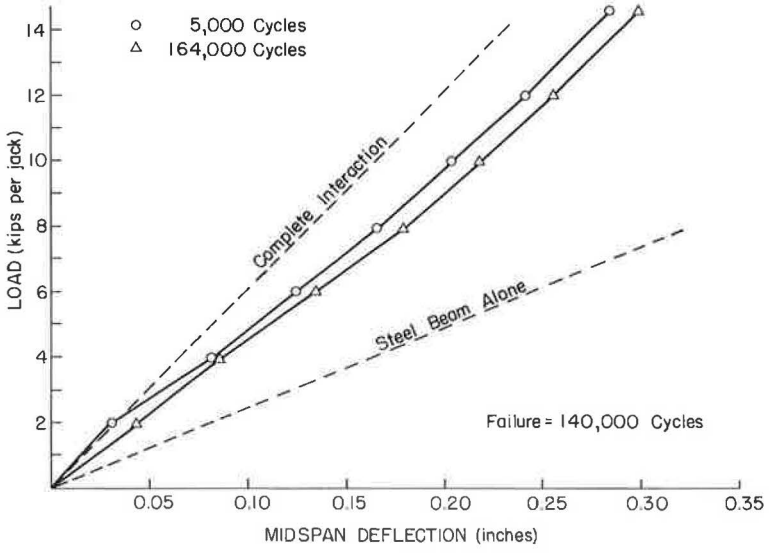


Figure 25. Load vs deflection curves for BF-5.

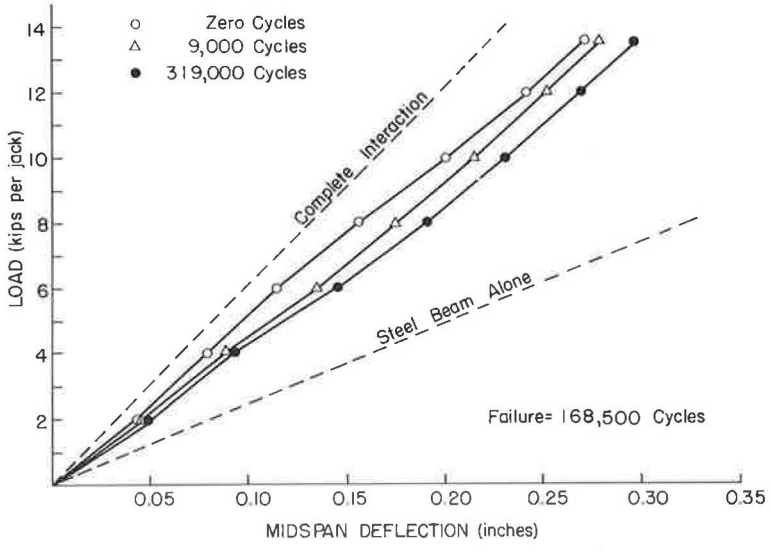


Figure 26. Load vs deflection curves for BF-6.

taken at various numbers of cycles of loading. On each figure two dotted lines are shown for the limits of composite action. The upper dotted line represents complete interaction and the lower dotted line represents the steel beam alone. Deflection due to shear has been taken into account in establishing the upper dotted line. The criterion for establishing the number of cycles to failure shown is discussed in the following section of the report. The curves shown in Figures 21 through 28 represent only a portion of the load vs deflection data taken during the tests.

Comparison of the eight sets of curves in Figures 21 through 28 shows some correlation between deflection data and fatigue failure. The change in deflection curves between the zero cycle curve and a curve before failure is less for members in which connector failure takes place after a larger number of cycles. In Figure 24, for in-

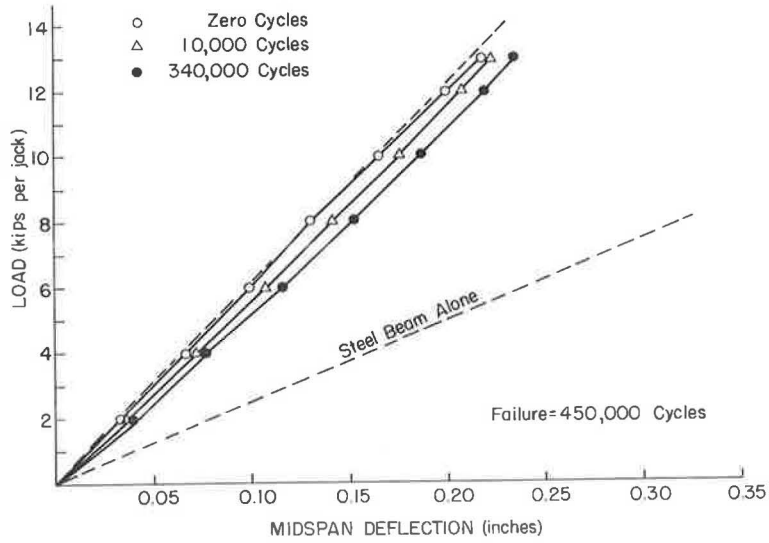


Figure 27. Load vs deflection curves for BF-7.

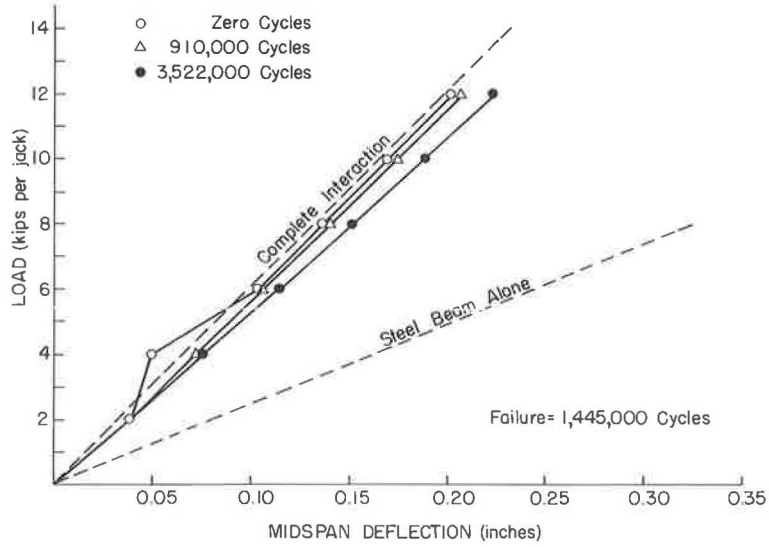


Figure 28. Load vs deflection curves for BF-8.

stance, there was hardly a measurable change in the various load-deflection curves from start to finish of the test, and in this member none of the connectors failed.

The amount which the initial curve departs from the theoretical curve for complete interaction was different for various members. In the case of the two members with the best fatigue endurance, the initial and theoretical load-deflection curves nearly coincide. A study of these curves reveals that the increase in deflection which takes place after failure of connectors is not significant. In several members, the deflection increase with cycles of loading is about the same before failure as it is after failure.

The data obtained from slip readings seem to have a significance equal to that of the load-deflection data. The relationship of connector failure, slip, and deflection is shown for beam BF-6 in Figure 29. Significant changes in the slope of the slip and

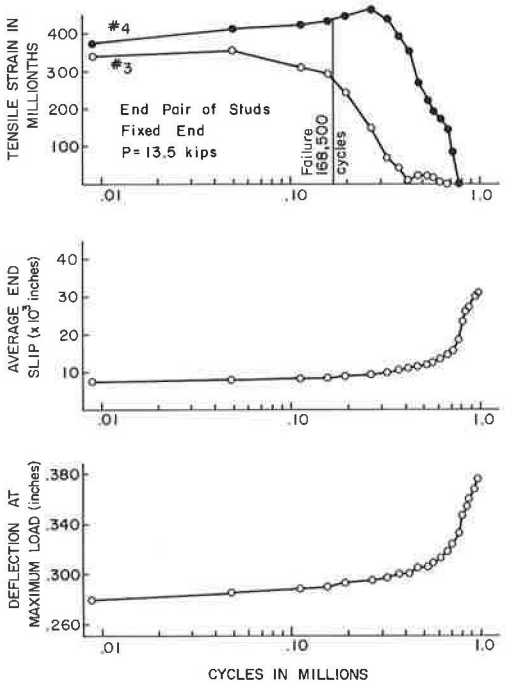


Figure 29. Slip, deflection, and distortion gage readings for BF-6.

deflection curves occurred after the beginning of connector failure, but the changes in slope of these curves were not large and were found to be time dependent. If one had only the slip and deflection curves as evidence it would be impossible to determine initial failure in many of the tests.

## S-N Curve for ½-In. Diameter Stud Connectors

The points on the S-N curve of Figure 12 for the preliminary beam tests and push-out tests had to be plotted using the number of cycles to failure as observed. It is realized from a careful study of the results of the primary beam tests that the method of observation of connector failure in these early tests is not precise. Therefore, the apparently large amount of scatter in the test data may be partly due to the lack of precision in observation. For this reason, the S-N curve of Figure 12 was drawn by considering only the primary beam tests.

Even the use of the distortion gages for the detection of shear connector failure does not completely simplify the plotting of an S-N curve because of the nature of the failure. A decision was necessary on whether the number of cycles to failure should be based on first cracking of a connector, first complete failure of a connector, or some other basis. After study of the data, it was decided that the value of N should be based on the average number of cycles for cracking of the first pair of connectors. This basis is rather arbitrary, but it seemed to provide the best basis for the following reasons:

1. Up to the point of failure, the beam should be capable of developing the static ultimate strength;
2. Complete failure of a connector or pair of connectors was not considered satisfactory because usually many connectors were cracked before the first pair to become cracked finally failed;
3. Cracking of connectors was detected more positively and before any change in slip or deflection; and
4. The cracking of a single connector may not be significant, but the cracking of a pair of connectors seemed to indicate that the member will fail completely in the shear connection if loading continues.

The values of stress plotted in Figure 12 and recorded in Table 4 are those calculated by the elastic formula for horizontal shear stress, as previously stated. The actual average shear stress on connectors was determined at failure by computing the compressive force in the concrete slab at midspan from strain gage readings and dividing this value by the area of shear connectors in half of the beam. These computed values of average stress were found to differ from the value recorded in Table 4 by less than 5 percent in the majority of members. A maximum difference of 10.8 percent was found in member BF-7. Both theoretical and measured values along with the percentage difference are given in Table 8 for all of the primary beam tests. As shown previously, the actual shear stress on an individual connector in these members may exceed the value in Table 4 by more than 10 percent.

The S-N curve of Figure 12 contains all published data on the fatigue strength of ½-in. diameter stud connectors. The authors feel confident that this curve adequately

TABLE 8

COMPARISON OF THEORETICAL AND MEASURED STUD STRESS AT BEGINNING OF TEST

| Specimen | Average Shear Stress $b\frac{VQ}{I}$ (psi) | Average Shear Stress from Strain Measurements at Midspan (psi) | Percent Difference |
|---|---|---|---|
| BF-1 | 22,200 | 21,300 | 4.1 |
| BF-2 | 22,200 | 21,000 | 5.0 |
| BF-3 | 19,400 | 19,200 | 1.0 |
| BF-4 | 19,400 | 19,500 | 0.5 |
| BF-5 | 22,600 | 21,700 | 4.0 |
| BF-6 | 21,100 | 20,300 | 3.8 |
| BF-7 | 20,300 | 18,100 | 10.8 |
| BF-8 | 19,500 | 19,100 | 2.1 |

TABLE 9

BOTTOM FLANGE STEEL STRESS

| Specimen | Initial Bottom Flange Stress (psi) | Average Bottom Flange Stress (psi) | Number of Cycles at this Stress |
|---|---|---|---|
| BF-1 | 22,500 | 24,000 | 880,000 |
| BF-2 | 21,800 | 22,800 | 680,000 |
| BF-3 | 19,900 | 19,500 | 1,556,000 |
| BF-4 | 18,400 | 19,500 | 3,315,000 |
| BF-5 | 25,600 | 27,000 | 354,000 |
| BF-6 | 21,000 | 22,800 | 1,009,000 |
| BF-7 | 18,600 | 19,500 | 1,344,000 |
| BF-8 | 19,300 | 19,800 | 3,522,000 |

represents the fatigue strength of ½-in. diameter connectors in beams for design purposes. Some of the variables which affect the fatigue strength of connectors, such as the effect of minimum stress, rate of loading, flange thickness, and concrete strength, have not been thoroughly investigated and should be the subject of future investigations.

From Figure 12, the failure stress would be greater than 15.9 ksi or 3.12 kips per connector for 97.5 percent of the specimens. The AASHO useful capacity of ½-in. diameter studs in 3,000 psi concrete is 4.51 kips per connector. Since fatigue strength and useful capacity are unrelated terms, different values are to be expected. It is interesting to note, however, that the useful capacity is not a conservative approximation of the fatigue strength. Therefore, it is not advisable to modify present shear connector design procedure by merely using a more liberal value of the factor of safety which is used in deriving allowable connector loads from the useful capacity.

The magnitude of the failure stress serves to point out that fatigue failure of connectors is a severe problem. It is important that S-N curves such as Figure 12 be obtained for other sizes of connectors. These results also indicate that the design of connectors should undoubtedly be based on range of stress rather than on maximum stress as in the case of present specifications.

### Bottom Flange Stress

The primary test specimens were designed in such a way that fatigue failure would not take place except in the shear connection. However, the members were also designed so that the bottom flange steel stress would be equal to or greater than 18 ksi throughout all tests. Stresses in the concrete slab were sufficiently low that data on the slab did not provide any worthwhile information regarding fatigue failure. However, bottom flange steel stresses were high enough during some of the tests that the data are worth including in the report.

The magnitude of the bottom flange stress changed during any one test as the compressive force in the concrete slab decreased. For this reason both the initial bottom flange stress and the average bottom flange stress are given in Table 9.

There were no fatigue failures observed in the bottom flange of the test specimens. The most severe fatigue loading condition from the point of view of possible failure of the bottom flange was in beams BF-1 and BF-5. Beam BF-1 endured 880,000 cycles with an average maximum bottom flange stress of 24 ksi, and beam BF-5 endured 354,000 cycles with the average maximum flange stress at 27 ksi.

## CONCLUSIONS

The information obtained from tests of composite beams containing ½-in. diameter stud connectors leads to the following conclusions concerning fatigue failure of connectors and the effect of connector failure on the performance of a composite beam:

1. The average shear stress at which ½-in. stud connectors failed in fatigue at 1,000,000 cycles of loading was 18.2 ksi;
2. Fatigue failure of connectors was progressive in nature and began at connectors near the ends of the member;
3. A composite member can be considered effective long after initial cracking of studs, but complete failure will eventually occur if a pair of connectors becomes cracked;
4. Fatigue failure of ½-in. diameter studs with good welds usually occurred in the base metal of the beam to which they were attached;
5. Measurements indicate that end connectors were stressed approximately 25 percent higher than the average connector stress when connectors are designed elastically; and
6. The occurrence of fatigue cracks in shear connectors can be detected by using electrical resistance strain gages mounted near connectors on the bottom of the top flange.

## ACKNOWLEDGMENTS

This study is part of a research project on fatigue of composite beams being carried out at the Fritz Engineering Laboratory, Department of Civil Engineering, Lehigh University. The investigation was sponsored by the American Institute of Steel Construction and the Nelson Stud Welding Division of Gregory Industries. Guidance for the project was the responsibility of the AISC Committee on Composite Design, T. R. Higgins, Chairman.

Test specimens for the investigation were fabricated and donated by the Lehigh Structural Steel Co., Allentown, Pa. The authors wish to express their thanks to Joseph A. Corrado, Dorothy Fielding, and Ronald Weiss for their assistance.

## REFERENCES


1. Assimacopoulos, Basil M., Warner, Robert F., and Ekberg, Carl, Jr. High Speed Fatigue Tests on Small Specimens of Plain Concrete. J. Prestressed Concr. Inst., Vol. 4, Sept. 1959.
2. Specifications for Welded Highway and Railway Bridges. 6th ed. Amer. Welding Soc., New York, 1963.
3. Standard Specifications for Highway Bridges. AASHO, Washington, D. C., 1961.
4. Siess, C. P., Viest, I. M., and Newmark, N. M. Studies of Slab and Beam Highway Bridges, Part III: Small Scale Tests of Shear Connectors and Composite T-Beams. Univ. of Illinois, Eng. Exp. Sta. Bull. 396, 1952.
5. Viest, I. M., Siess, C. P., Appleton, J. H., and Newmark, N. M. Full-Scale Test of Channel Shear Connectors and Composite T-Beams. Univ. of Illinois, Eng. Exp. Sta. Bull. 405, 1952.
6. Sinclair, G. M. Fatigue Strength of $^{3}/_{4}$-Inch Welded Stud Shear Connectors. Nelson Stud Welding, Lorain, Ohio, Engineering Test Data, Sept. 1955.
7. Thurlimann, Bruno. Fatigue and Static Strength of Stud Shear Connectors. ACI Jour., Vol. 30, June 1959.
8. Thurlimann, Bruno. Composite Beams with Stud Shear Connectors. Highway Research Board Bull. 174, pp. 18-38, 1958.
9. Culver, Charles, and Coston, Robert. Tests of Composite Beams with Stud Shear Connectors. Proc. ASCE, Jour. Struct. Div., Vol. 87, No. ST2, Feb. 1961.
10. Slutter, Roger G., and Driscoll, George, C., Jr. Ultimate Strength of Composite Members. Proc. Conf. on Composite Design in Steel and Concrete for Bridges and Buildings, Struct. Div. ASCE, March 1962.

# Design of Langer Girder Bridge with Inclined Hangers

SHIGEHIKO NAGAI, Bridge Engineer, Hyogo Prefecture,
HIROYUKI KOJIMA, Lecturer, Tokushima University, and
MASAO NARUOKA, Professor, Nagoya University, Japan

The structure of arch-type bridges with inclined hangers was studied by the deformation method. The Abo bridge, the first Langer girder bridge with inclined hangers in Japan, was designed by the authors and construction is under way. Compared with bridges having vertical hangers, a weight saving of about 10 percent has been obtained with inclined hangers.

•THE STATICAL behavior of the Langer girder, the tied arch, and the Lohse girder bridges with inclined hangers has been under extensive investigation in the Scandinavian countries. These bridges are usually called Nielsen system bridges. The Fehmarnsund bridge recently constructed in West Germany was the first bridge of this kind outside the Scandinavian countries, and it has been reported that the chief advantage of this type of bridge is the saving in the amount of steel used in the construction. The authors have been studying the structure of the arch-type bridges with inclined hangers by the deformation method, and have set up a computer program. The Abo bridge, the first Langer girder bridge with inclined hangers built in Japan, has been designed by the authors and construction is under way. This report presents the computing procedure relative to the designing of this type of bridge.

## SOLUTION BY DEFORMATION METHOD

The static equilibrium in each joint of the planar structures is expressed as shown in Eq. 1 by the deformation method:

$$\begin{bmatrix} a & b & c \\ b' & \bar{a} & \bar{c} \\ c' & \bar{c}' & d \end{bmatrix} \begin{bmatrix} u \\ v \\ \theta \end{bmatrix} = \begin{bmatrix} \bar{P} \\ \bar{Q} \\ \bar{M} \end{bmatrix} \quad \text{or} \quad KU = S \qquad (1)$$

where

- $b'$, $c'$, $\bar{c}'$ = transposed matrices of b, c, and $\bar{c}$, respectively;
- u, v, $\theta$ = column matrices of $u_i$, $v_i$, and $\theta_i$ elements, respectively, where $u_i$, $v_i$, and $\theta_i$ are the displacements of each joint in x and y directions and joint rotation;
- $\bar{P}$, $\bar{Q}$, $\bar{M}$ = column matrices of $\bar{P}_i$, $\bar{Q}_i$, and $\bar{M}_i$, where $\bar{P}_i$ and $\bar{Q}_i$ are the external forces in x and y directions at each joint, and $\bar{M}_i$ is the external moment acting at each joint; and
- K = stiffness matrix.

The submatrices contained in K are defined as follows:

Paper sponsored by Committee on Steel Superstructures.

$$a = \begin{bmatrix} \nwarrow \Sigma a & -a \\ -a & \searrow \end{bmatrix}, \quad \bar{a} = \begin{bmatrix} \nwarrow \Sigma \bar{a} & -\bar{a} \\ -\bar{a} & \searrow \end{bmatrix}, \quad b = \begin{bmatrix} \nwarrow \Sigma b & -b \\ -b & \searrow \end{bmatrix}$$

$$c = \begin{bmatrix} \nwarrow \Sigma c & c \\ c & \searrow \end{bmatrix}, \quad \bar{c} = \begin{bmatrix} \nwarrow \Sigma \bar{c} & \bar{c} \\ \bar{c} & \searrow \end{bmatrix}, \quad d = \begin{bmatrix} \nwarrow 2\Sigma d & d \\ d & \searrow \end{bmatrix} \tag{2}$$

where each $\Sigma$ shows the diagonal elements of the matrices and the other symbols show the antidiagonal elements.

Each of the elements represented by such symbols as a, $\bar{a}$, b, c, $\bar{c}$, and d in Eq. 2 will be determined as follows by using the various dimensions of the members:

$$a_{ij} = \frac{12EI_{ij}}{l^3_{ij}} \frac{(y_j - y_i)^2}{l^2_{ij}} + \frac{EA_{ij}}{l_{ij}} \frac{(x_j - x_i)^2}{l^2_{ij}}$$

$$\bar{a}_{ij} = \frac{12EI_{ij}}{l^3_{ij}} \frac{(x_j - x_i)^2}{l^2_{ij}} + \frac{EA_{ij}}{l_{ij}} \frac{(y_j - y_i)^2}{l^2_{ij}}$$

$$b_{ij} = \left( \frac{EA_{ij}}{l_{ij}} - \frac{12EI_{ij}}{l^3_{ij}} \right) \frac{(x_j - x_i)}{l_{ij}} \frac{(y_j - y_i)}{l_{ij}}$$

$$c_{ij} = \frac{6EI_{ij}}{l^2_{ij}} \frac{(y_j - y_i)}{l_{ij}}$$

$$\bar{c}_{ij} = \frac{6EI_{ij}}{l^2_{ij}} \frac{(x_j - x_i)}{l_{ij}}$$

$$d_{ij} = \frac{2EI_{ij}}{l_{ij}} \tag{3}$$

The sectional forces of each member are determined from the displacements, after computing the inverse matrix of K, as follows:

$$M_i = c_{ij} (u_j - u_i) - \bar{c}_{ij} (v_j - v_i) + d_{ij} (\theta_j + 2\theta_i) \frac{(x_j - x_i)}{|x_j - x_i|}$$

$$N_i = \left\{ a_{ij} \frac{(x_j - x_i)}{l_{ij}} + b_{ij} \frac{(y_j - y_i)}{l_{ij}} \right\} (u_j - u_i) +$$

$$\left\{ b_{ij} \frac{(x_j - x_i)}{l_{ij}} + \bar{a}_{ij} \frac{(y_j - y_i)}{l_{ij}} \right\} (v_j - v_i) +$$

$$\left\{ c_{ij} \frac{(x_j - x_i)}{l_{ij}} - \bar{c}_{ij} \frac{(y_j - y_i)}{l_{ij}} \right\} (\theta_j + \theta_i)$$

$$Q_i = \left\{ b_{ij} \frac{(x_j - x_i)}{l_{ij}} - a_{ij} \frac{(y_j - y_i)}{l_{ij}} \right\} (u_j - u_i) +$$

$$\left\{ \bar{a}_{ij} \frac{(x_j - x_i)}{l_{ij}} - b_{ij} \frac{(y_j - y_i)}{l_{ij}} \right\} (v_j - v_i) -$$

$$\left\{ \bar{c}_{ij} \frac{(x_j - x_i)}{l_{ij}} + c_{ij} \frac{(y_j - y_i)}{l_{ij}} \right\} (\theta_j + \theta_i) \qquad (4)$$

## COMPUTATIONAL PROCEDURE

The block diagram in Figure 1 shows the process of solution of the problem. A number is assigned to each of the joints. If there are 2n joints, the numbers will be 0, 2, 4, . . . , 2n in the lower joints and 1, 3, 5, . . . , 2n - 1 in the upper joints as shown in Figure 2.

The following input data are needed:

1. The projections $(x_j - x_i)$ and $(y_j - y_i)$ of the member $\overline{ij}$ in the x and y directions, respectively;

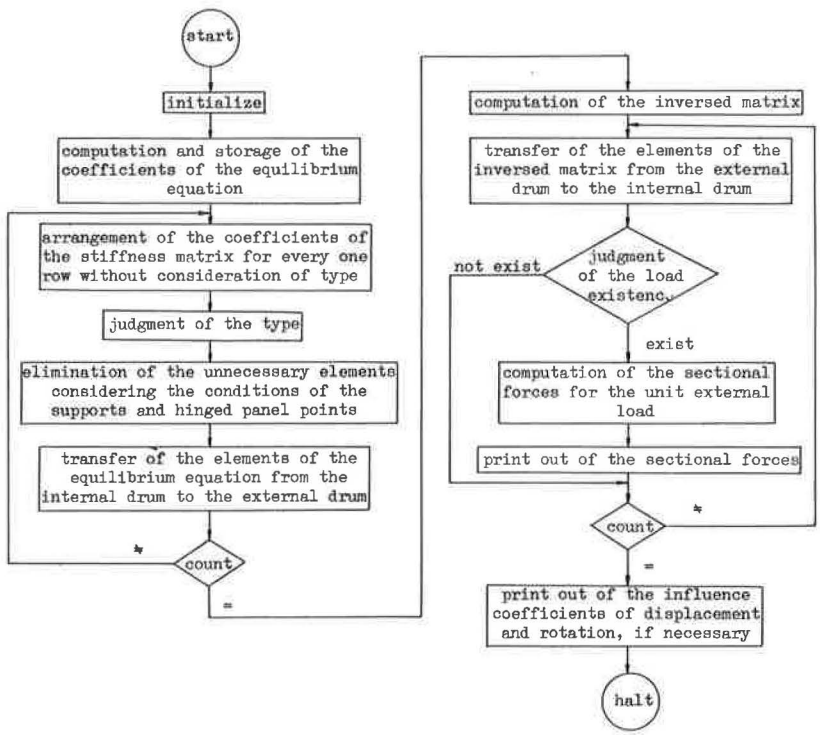


Figure 1. Block diagram for computer analysis.

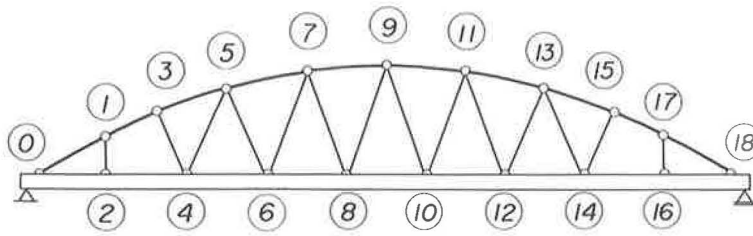


Figure 2. Example of number assignment to panel point.

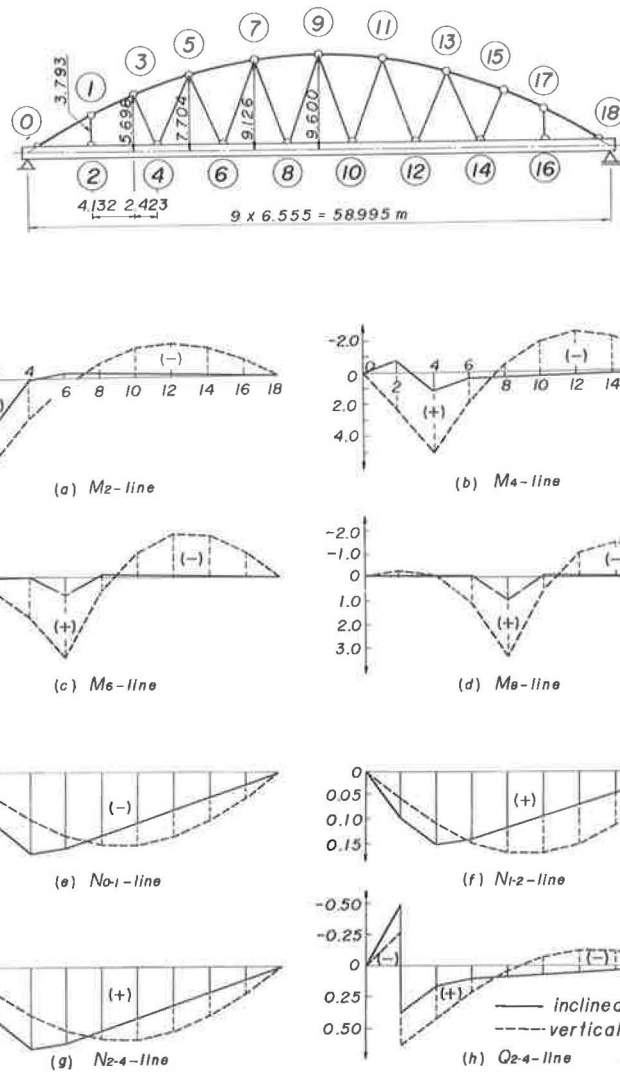


Figure 3. Skelton diagram of Abo bridge and comparison of ordinates of influence lines.

TABLE 1

NORMAL FORCES OF UPPER CHORD MEMBERS AND HANGERS

| Member | Dead Load | Live Load | Impact | Total |
|---|---|---|---|---|
| $N_{01}$ | -123.455t | -51.375t | -9.453t | -183.283t |
| $N_{13}$ | -117.651 | -48.960 | -9.009 | -175.620 |
| $N_{35}$ | -117.839 | -49.038 | -9.023 | -175.900 |
| $N_{57}$ | -117.569 | -49.213 | -9.005 | -175.839 |
| $N_{79}$ | -115.489 | -48.432 | -8.911 | -172.832 |
| $N_{12}$ | 12.601 | 5.244 | 0.965 | 18.810 |
| $N_{34}$ | 11.111 | 4.604 | 0.847 | 16.562 |
| $N_{45}$ | 2.396 | 11.367 | 3.990 | 18.293 |
| | | -7.381 | -2.591 | -7.917 |
| $N_{56}$ | 12.514 | 10.452 | 3.669 | 26.635 |
| | | -6.758 | -2.372 | -0.370 |
| $N_{67}$ | 8.385 | 11.082 | 3.890 | 23.357 |
| | | -5.844 | -2.051 | -2.026 |
| $N_{78}$ | 9.250 | 9.996 | 3.509 | 22.755 |
| | | -6.392 | -2.244 | -2.161 |
| $N_{89}$ | 8.803 | 10.749 | 3.773 | 23.325 |
| | | -6.524 | -2.290 | -2.652 |

TABLE 2

BENDING MOMENTS AND NORMAL FORCES OF STIFFENING GIRDER

| Member | Dead Load | Live Load | Impact | Total |
|---|---|---|---|---|
| (a) Applied Loads Producing Maximum Bending Moment | | | | |
| $M_2$ | 31.293 tm | 40.545 tm | 7.460 tm | 79.298 tm |
| $M_4$ | 36.044 | 27.167 | 4.999 | 68.210 |
| $M_6$ | 15.435 | 16.260 | 2.992 | 34.687 |
| $M_8$ | 12.897 | 15.942 | 2.933 | 31.772 |
| $N_{02}$, $N_{24}$ | 106.858 t | 40.401 t | 7.434 t | 154.693 t |
| $N_{46}$ | 109.997 | 40.523 | 7.456 | 157.976 |
| $N_{68}$ | 112.062 | 25.574 | 4.706 | 142.342 |
| $N_{8-10}$ | 112.345 | 20.065 | 3.692 | 136.102 |
| (b) Applied Loads Producing Maximum Normal Force | | | | |
| $N_{02}$, $N_{24}$ | 106.858 t | 44.468 t | 8.182 t | 159.508 t |
| $N_{46}$ | 109.997 | 45.521 | 8.376 | 163.894 |
| $N_{68}$ | 112.062 | 46.336 | 8.526 | 166.924 |
| $N_{8-10}$ | 112.345 | 46.131 | 8.488 | 166.964 |
| $M_2$ | 31.293 tm | 10.501 tm | 1.932 tm | 43.726 tm |
| $M_4$ | 36.044 | 23.925 | 4.402 | 64.371 |
| $M_6$ | 15.435 | 15.538 | 2.859 | 33.832 |
| $M_8$ | 12.897 | 14.647 | 2.695 | 30.239 |

2. The cross-sectional area $A_{ij}$ and the moment of inertia $I_{ij}$ of each member;
3. Numbers of the members at each joint and the assigned numbers at the other end of each member;
4. Applied loads;
5. Total numbers of the members;
6. Total numbers of the joints including the supports;
7. Total numbers of the pinned joints excluding the supports; and
8. Smallest number assigned at the pinned joints.

The output data consist of the ordinates of the influence lines of bending moment M at all rigid joints, of normal force N and shearing force Q of all rigidly jointed members, and of normal force N of all pin-jointed members.

This computational procedure has been programmed for the NEAC-2203 computer of Nagoya University, and is applicable to the Langer girder, the tied arch, and the Lohse girder with inclined or vertical hangers up to 15 panels. The details have been previously presented (1).

## DESIGN OF ABO BRIDGE

Dimensions of the bridge include span length, 58.995 m; effective width, 6.0 m; specified load, 2nd class of Japan Standard Specification for Steel Highway Bridges (1962); distance between stringers and crossbeams, 2.3 and 6.555 m, respectively; slab, 15 cm thick of reinforced concrete; pavement, 5 cm thick of concrete. The assumed cross-sectional area and moment of inertia of the members are for upper chord members, A = 137 sq cm for 0-1, 17-18, and A = 123 sq cm for the others; for lower chord members, A = 223.7 sq cm and I = 834,865 $cm^4$ for all members; and for hangers, A = 51.2 sq cm for members 1-2 and 16-17 and A = 40.15 sq cm for the others.

Comparison of the influence lines of the sectional forces of certain members is shown in Figure 3. The normal forces of the upper chord members and hangers due to dead loads and live loads are given in Table 1. The bending moments and normal forces of the lower chord members due to dead loads and live loads are given in Table 2.

The quantities of material necessary for the bridge are computed as follows: 26.344 tons for main girder, 16.263 tons for upper chord members, 6.694 tons for hangers, 2.418 tons for portal, 1.472 tons for sway bracings, 9.844 tons for floor beams, 15.258 tons for stringers, 6.048 tons for lateral bracings, and 2.072 tons for shoes, totalling 86.413 tons (240.9 kg/sq m). The steel weight of the same type of bridge with the vertical hangers would be 95.2 tons, and, therefore, a saving of about 10 percent in the weight of steel has been achieved.

## DISCUSSION

Normal stresses of the hangers due to dead loads are always positive. The member stress $N_{34}$ is always positive for live loads, but $N_{45}$ - $N_{89}$ are alternate stresses, even though the negative magnitude is very small except for $N_{45}$. If the negative stresses in the inclined hangers are erased by some means, rods or cable wires may be used as the hanger members. In the Fehmarnsund bridge in West Germany, use of cable hangers is made possible by the additional dead weight of concrete blocks. In Sweden, rod hangers are used without the aid of any dead weight in particular. If the combined stresses become negative in some rod hangers under the dead and live loads, the rod hangers can no longer support the force. Hence, the behavior of the bridge system will change under the corresponding loads, and a special computation will be required. Therefore, pipe members are being used for the inclined hangers of the Abo bridge so that the compressive forces are taken care of by these members as well. That is, a saving in the weight of steel used is expected in the stiffening girder due to the reduction in the bending moment applied to the girder.

According to a Swedish bridge engineer, however, use of the stiff hangers instead of flexible hangers will change the characteristics of the Nielsen system bridge because the hangers will then function for any kind of load, which is not the case with the original Nielsen system.

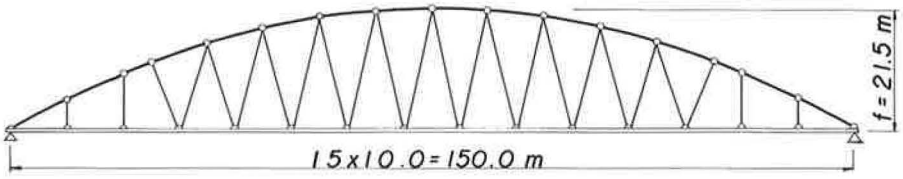


Figure 4. Skelton Diagram of Shitoku bridge.

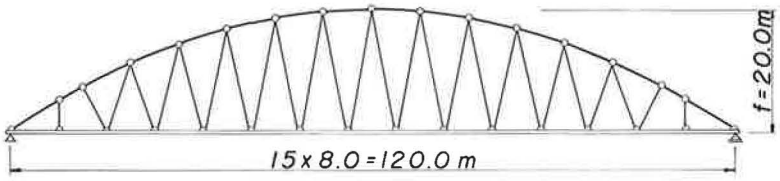


Figure 5. Skelton diagram of Shin-Ishikari bridge.

The span length of the Abo bridge is small, and, therefore, the compressive forces are caused in the inclined hangers. If the span length were longer, the compressive forces would not be caused in the inclined hangers except for $N_{45}$, and in such a case the cable wires or rods would be used. Because this particular bridge is the first Langer girder bridge with inclined hangers to be constructed in Japan, the pipe members have been adopted for the inclined hangers. The authors, however, are inclined to think that the bridge is not a good specimen of this special type of Langer girder bridge.

## DESIGN EXAMPLES

The amount of steel used for a Langer girder bridge (Fig. 4) with a span length of 150 m and an effective width of 5.5 m will be 383.3 tons with the inclined hangers; the same bridge with the vertical hangers will require 432.8 tons of steel. The saving in the steel used in the case of the former will amount to about 11 percent.

A total of 237.2 tons of steel will be needed for a Langer girder bridge (Fig. 5) with a span length of 120 m and an effective width of 8.0 m with inclined hangers for upper and lower chord members, and hangers. With vertical hangers, the amount required would be 258.1 tons. The saving in the amount of materials by use of inclined hangers is apparent.

## CONCLUDING REMARKS

As already stated, the authors have demonstrated the automatic computational process by the deformation method for the analysis of the Langer girder bridge and also have shown the several comparative designs of the various bridges. A weight saving of about 10 percent has been obtained for the bridges with inclined hangers compared with those having vertical ones.

The computer program is also applicable without any difficulty to the Lohse girder, the Vierendeel girder, and the tied arch with the inclined or vertical hangers.

## REFERENCE

1. Kojima, Hiroyuki and Naruoka, Masao. Analysis of Nielsen System Bridge by Digital Computer. Prelim. Pub., 7th Cong. Int. Assoc. for Bridge and Struct. Eng., pp. 65-74, 1964.